CANCER IMAGING WITH

FLUCICLOVINE (^{18}F)

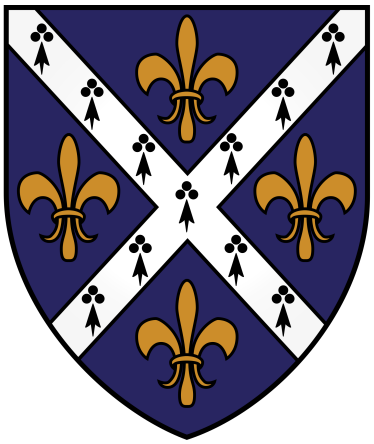

Thesis submitted by:

Eugene Jueren Teoh

St Hugh's

For the degree of:

Doctor of Philosophy

Department of Oncology

Hilary Term 2018

University of Oxford

Supervisors:

Professor Adrian L. Harris

Professor Fergus V. Gleeson

ABSTRACT

[^{18}F]1-amino-3-fluorocyclobutane 1-carboxylic acid (^{18}F-fluciclovine) is a synthetic amino acid developed as a PET radiotracer for cancer imaging. Upon project commencement, ^{18}F-fluciclovine was in late phase of pharmaceutical development for recurrent prostate cancer imaging, requiring validation of clinical utility. Growing prospect in targeting of tumour metabolism in breast cancer treatment set the premise to investigate the role of amino acid imaging in this prevalent disease. The aims of this project were to: (1) establish the transport mechanisms of fluciclovine in breast cancer; (2) explore the utility of fluciclovine in early assessment of response to treatments of related metabolic and biological targets; (3) run a clinical study to investigate how ^{18}F-fluciclovine uptake can be used to characterise breast cancer biology; and (4) run a multicentre clinical trial to investigate the impact of ^{18}F-fluciclovine imaging on clinical management of men with recurrent prostate cancer. Fluciclovine transport in breast cancer was found to be predominantly mediated by the high-affinity glutamine transporter ASCT2. Increased fluciclovine uptake was demonstrated in cell lines sensitive to glutaminase inhibition with CB-839 (known to result in build-up of intra-cellular glutamine); and the opposite with bithionol and metformin which are known to reduce intra-cellular glutamine. These results were recapitulated in animal models, and collectively raise the potential for fluciclovine to be used as an imaging biomarker of glutamine pool, in addition to early response assessment in therapies augmenting glutamine metabolism. The FRONTIER study was established to investigate how ^{18}F-fluciclovine can be used to

characterise breast cancer biology and is ongoing. Initial data demonstrate a trend of highest uptake in triple-receptor negative, followed by ER+ then HER2+ tumours, complementing *in vitro* data. The FALCON multicentre trial investigated the impact of ^{18}F-fluciclovine imaging on clinical management of recurrent prostate cancer. In the 32-patient Oxford cohort, 44% of patients had their intended management plan revised following ^{18}F-fluciclovine PET/CT. Initial short term follow-up data demonstrate a higher proportion of short-term responders to ^{18}F-fluciclovine guided radiotherapy (71%, 5/7) compared to standard radiotherapy (53%, 8/15). This encouraging trend will require ratification with trial-wide data. Across the trial, interim analysis found management was revised post-scan in 52/85 (61%) patients, exceeding a pre-set criteria for overwhelming effectiveness (45/85), leading to early closure.

LIST OF PUBLICATIONS RELATED TO THESIS

Teoh EJ, McGowan DR, Schuster DM, Tsakok MT, Gleeson FV, Bradley KM. Bayesian penalised likelihood reconstruction (Q.Clear) of ^{18}F-fluciclovine PET for imaging of recurrent prostate cancer: semi-quantitative and clinical evaluation. Br J Radiol. Published online 22 Jan 2018. doi:10.1259/bjr.20170727

Teoh EJ, Tsakok MT, Bradley KM, Hyde K, Subesinghe M, Gleeson FV. Recurrent Malignant Melanoma Detected on ^{18}F-Fluciclovine PET/CT Imaging for Prostate Cancer. Clin Nucl Med. 2017;42(10):803-04.

Teoh E, Morotti M, Bridges E, Jones D, Miar A, Wigfield S, et al. Fluciclovine (^{18}F) is a marker for high-affinity glutamine transporter ASCT2-mediated amino acid transport in breast cancer. J Nucl Med. 2017;58(S1):1028. [abstract]

Teoh EJ, Bridges EM, Morotti M, Zois CE, Lord SR, Gleeson FV, et al. Fluciclovine is a potential imaging biomarker of glutamine utilisation in breast cancer. Eur J Nucl Med Mol Imaging. 2017;44(2):633. [abstract]

Teoh EJ, Bottomley DM, Scarsbrook A, Payne H, Afaq A, Bomanji J, et al. The FALCON trial: Impact of ^{18}F-fluciclovine PET/CT on clinical management choices for men with biochemically recurrent prostate cancer. J Clin Oncol. 2018;36(6_suppl):165-65. [abstract]

Teoh E, Bottomley D, Scarsbrook A, Payne H, Afaq A, Bomanji J, et al. Impact of ^{18}F-fluciclovine PET/CT on Clinical Management of Patients with Recurrent Prostate Cancer: Results from the Phase 3 FALCON Trial. Int J Radiat Oncol Biol Phys. 2017;99(5):1316-17. [abstract]

ACKNOWLEDGMENTS

I thank my supervisors, Prof. Adrian Harris and Prof. Fergus Gleeson, for patiently guiding me throughout the doctorate with sage advice, encouragement to maintain high standards and inspiring me to always think outside the box.

I thank both past and present members of the team at Blue Earth Diagnostics Ltd, who have collectively supported this work from inception, and from whom I have learnt a great deal in working on FALCON. Several have become close acquaintances.

I thank all past and present members of Prof. Harris' laboratory at the WIMM for allowing me to learn from and work alongside them. Several have directly supported my work for which I am very grateful. I also thank members of the OIRO Imaging Core, Gouverneur group and OCHRe who have supported my work.

I thank the many patients, clinical staff and investigators I have worked with on FALCON and FRONTIER, within Oxford and throughout the UK. It has been an incredibly formative experience working with such a diverse group of individuals, all of whom have made contributions to these studies.

I thank several individuals, who have given me advice and encouragement during my doctorate. Thank you for sharing your wisdom and experiences with me.

Undertaking this doctorate has been one of the most challenging and enriching times of my life. While the many aforementioned people were pivotal to my work, I absolutely could not have reached this stage without the loving, patient support of my wife Suliana, and the sweet distraction by my two patient children Nathanael and Naomi. I have found deeper love and appreciation for them during the course of this project, and will treasure them always. My parents have provided me with immense support as well, and I am so grateful for their loving encouragement throughout. I sincerely hope to be able to support my children to similar depths in the future.

Finally, I am grateful to God who has, through all the experiences over the past few years, reminded me of His faithfulness.

LIST OF ABBREVIATIONS

AAT	Amino acid transporter
ACTB	ß-actin
ADT	Androgen deprivation therapy
AE	Adverse event
AI	Aromatase inhibitor
AMPK	5' adenosine monophosphate-activated protein kinase
ASCT2	Alanine-serine-cysteine transporter 2
AUC	Area under the curve
BCH	2-Amino-2-norbornanecarboxylic acid
BCR	Biochemical recurrence of prostate cancer
BPL	Bayesian penalised likelihood
BPTES	Bis-2-(5-phenylacetamido-1,3,4-thiadiazol-2-yl)ethyl sulphide
BSA	Bovine serum albumin
CD1	Cluster of differentiation 1
CI	Confidence interval
CoA	Coenzyme A
CT	Computed tomography
DCIS	Ductal carcinoma in situ
DMEM	Dulbecco’s modified Eagle medium
DNA	Deoxyribonucleic acid
EAU	European Association of Urology
ECOG	Eastern Cooperative Oncology Group

EDTA	Ethylenediaminetetraacetic acid
ER	Oestrogen receptor
FACBC	1-amino-3-fluorocyclobutane 1-carboxylic acid
FCS	Foetal calf serum
FDG	Fluorodeoxyglucose
GLUT1	Glucose transporter 1
GMD	Geometric mean diameter
GPNA	L-Glutamic acid γ-(p-nitroanilide)
HEPES	4-(2-hydroxyethyl)-1-piperazineethanesulfonic acid
HER2	Human epidermal growth factor receptor 2
HIF	Hypoxia inducible factor
HIFU	High intensity focused ultrasound
HRP	Horseradish peroxidase
IC_{50}	Half maximal inhibitory concentration
ICC	Intra-class coefficient
IHC	Immunohistochemistry
IMP	Investigational medicinal product
IMRT	Intensity modulated radiotherapy
IMS	Industrial methylated spirit
Km	Michaelis constant
LAT1	L-type amino acid transporter 1
LC-MS	Liquid chromatography-mass spectrometry
LND	Lymphadenectomy
MAPK/ERK	Mitogen-activated protein kinase
MBq	Megabequerel

MeAIB	α-(Methylamino)isobutyric acid
MRI	Magnetic resonance imaging
mRNA	Messenger ribonucleic acid
mTOR	Mammalian target of rapamycin
mTORC1	Mammalian target of rapamycin complex 1
NAC	Neoadjuvant chemotherapy
NEM	N-Ethylmaleimide
NICE	National Institute for Health and Care Excellence
OR	Odds ratio
OSEM	Ordered subset expectation maximisation
PBS	Phosphate-buffered saline
PCa	Prostate cancer
pCR	Pathological complete response
PERCIST	Positron Emission Tomography Response Criteria in Solid Tumours
PET	Positron emission tomography
PI3K	Phosphoinositide 3-kinase
PSA	Prostate-specific antigen
PSA_{dt}	PSA doubling time
PSA_{vel}	PSA velocity
PSF	Point spread function
PSMA	Prostate specific membrane antigen
qPCR	Quantitative polymerase chain reaction
REC	Research ethics committee
RIPA	Radioimmunoprecipitation assay

RP	Radical prostatectomy
RPMI	Roswell Park Memorial Institute
RRT	Radical external beam radiotherapy
SBR	Signal-to-background
SBRT	Stereotactic beam radiotherapy
SD	Standard deviation
SEM	Standard error of mean
siRNA	Small interfering RNA
SLC1A5	Solute carrier family 1 member 5
SLC7A5	Solute carrier family 7 member 5
SNAT2	Sodium-dependent neutral amino acid transporter 2
SNR	Signal-to-noise
SPECT	Single photon emission computed tomography
SRT	Salvage radiotherapy
SUSAR	Suspected unexpected serious adverse reaction
SUV	Standardised uptake value
SUV_{max}	Maximum standardised uptake value
SUV_{peak}	Peak standardised uptake value
SUV_{mean}	Average standardised uptake value
SUV_{dev}	Standard deviation of standardised uptake value
TBS	Tris-buffered saline
TCA	Tricarboxylic acid
TLG	Total lesion glycolysis
TN	Triple receptor negative
ToF	Time of flight

TRUS	Transrectal ultrasound
VOI	Volume of interest
WOCBP	Women of child bearing potential

TABLE OF CONTENTS

ABSTRACT 2

LIST OF PUBLICATIONS RELATED TO THESIS 4

ACKNOWLEDGMENTS 6

LIST OF ABBREVIATIONS 8

TABLE OF CONTENTS 13

LIST OF FIGURES 21

LIST OF TABLES 26

Chapter 1 : Introduction 28

1.1 Overview of ^{18}F-fluciclovine 29

1.1.1 Known transport mechanisms 29

1.2 Overview of diagnostic work-up and salvage therapies in recurrent prostate cancer 32

1.2.1 Initial diagnosis and treatment 32

1.2.2 Diagnosis of BCR 33

1.2.3 Conventional Imaging in BCR 33

1.2.4 ^{18}F-FDG PET-CT Imaging in BCR 34

1.2.5 Choline PET/CT 34

1.2.6 Conventional and emerging radical salvage options in BCR 38

1.3 Rationale for accurate imaging in BCR 40

1.3.1 ^{18}F-Fluciclovine imaging in prostate cancer 40

1.3.2 The next step for defining clinical utility of ^{18}F-fluciclovine in recurrent prostate cancer imaging 43

1.4 Advanced PET image reconstruction 44

1.4.1 Overview 44
1.4.2 Rationale for tracer-specific optimisation 46
1.5 Amino acid metabolism as an imaging and therapeutic target in breast cancer 47
1.5.1 Rationale for focus on breast cancer 47
1.5.2 ASCT2 and LAT1 expression are associated with poor prognosis in breast cancer 48
1.5.3 Majority of cell mass is derived from amino acids 52
1.5.4 Glutamine metabolism and its aberration in cancer 52
1.5.5 Glutamine targeted therapies in cancer 53
1.5.6 Involvement of ASCT2 and LAT1 in mTOR signalling 55
1.5.7 Hypoxia and amino acid metabolism 56
1.6 Imaging in personalised medicine and early treatment response assessment in cancer 57
1.6.1 Rationale 57
1.6.2 Performance and limitations of ^{18}F-FDG as an early treatment response marker 58
1.7 Experience of ^{18}F-fluciclovine in breast cancer 61
1.7.1 Preclinical experience 61
1.7.2 Clinical experience 62
1.8 Summary and aims 64
1.8.1 Summary 64
1.8.2 Aims 64
Chapter 2 : Materials and methods 66
2.1 FALCON TRIAL 67

2.1.1 Objectives and endpoints 67
2.1.2 Study design 68
2.1.3 Regulatory approval 69
2.1.4 Inclusion criteria 69
2.1.5 Exclusion Criteria 71
2.1.6 Baseline measures 71
2.1.7 ^{18}F-Fluciclovine PET/CT imaging protocol 72
2.1.8 ^{18}F-Fluciclovine PET/CT image interpretation 72
2.1.9 Revised management plan 72
2.1.10 PSA follow-up 73
2.1.11 Statistical analysis 73
2.1.12 BPL substudy: Aim 73
2.1.13 BPL substudy: Image reconstruction 74
2.1.14 BPL substudy: Semi-quantitative analysis 74
2.1.15 BPL substudy: Statistical analysis 75
2.1.16 BPL substudy: Clinical evaluation – reconstruction and visual analyses 75
2.2 PRE-CLINICAL WORK 76
2.2.1 Cell culture 76
2.2.2 Drugs 76
2.2.3 Baseline expression of AATs in cell line panel 77
2.2.4 RNA extraction and quantitative PCR 77
2.2.5 Protein extraction and Western blotting 78
2.2.6 ASCT2 and LAT1 knockdown using siRNA transfection 79
2.2.7 Proliferation assays 80

2.2.8 Measurement of fluciclovine uptake in vitro 80
2.2.9 Competitive inhibition of ^{14}C-FACBC uptake 81
2.2.10 Hypoxia work 82
2.2.11 In vivo experiments 83
2.2.12 ^{18}F-fluciclovine synthesis for in vivo imaging 83
2.2.13 ^{18}F-Fluciclovine PET/CT in vivo imaging protocol 83
2.2.14 ^{18}F-Fluciclovine PET/CT in vivo image analysis 85
2.2.15 Bithionol experiment 85
2.2.16 Metformin experiment 86
2.3 FRONTIER: An open-labelled study to characterise Fluciclovine (^{18}F) uptake measured by positron emission tomography in breast cancer 86
2.3.1 Objectives and endpoints 86
2.3.2 Study design 87
2.3.3 Regulatory approval 88
2.3.4 Inclusion criteria (version 3.0) 89
2.3.5 Exclusion Criteria (version 3.0) 89
2.3.6 Baseline measures 90
2.3.7 Blood samples 90
2.3.8 ^{18}F-Fluciclovine PET/CT imaging protocol 91
2.3.9 Image analysis 92
2.3.10 Tissue sample collection 93
2.3.11 Metabolomic analysis of tumour samples 93
2.3.12 Immunohistochemistry techniques for FRONTIER 94
2.3.12.1 Generation and sectioning of cell pellets 94
2.3.12.2 Immunohistochemistry protocol 95

2.3.12.3 Antibody validation overview 96
2.3.12.4 Validation of ASCT2 antibody 96
2.3.12.5 Validation of LAT1 antibody 96
2.3.12.6 Validation of SNAT2 antibody 97
2.3.12.7 pS6 staining 97
2.3.13 Statistical analysis 99
Chapter 3 : ^{18}F-Fluciclovine PET/CT has an impact on the clinical management of recurrent prostate cancer 101
3.1 Introduction 103
3.2 Results 103
3.2.1 Patients 103
3.2.2 ^{18}F-fluciclovine PET/CT findings 103
3.2.3 Clinical impact 104
3.2.4 Clinicopathological factors influencing scan positivity 108
3.2.5 BPL substudy – Semi-quantitative analysis 112
3.2.6 BPL substudy – Clinical evaluation 117
3.3 Discussion 118
3.4 Conclusion 127
Chapter 4 : Fluciclovine uptake is mediated by high-affinity glutamine transporter ASCT2 128
4.1 Introduction 129
4.2 Heterogeneity of amino acid transporter expression in breast cancer 129
4.3 Optimisation of an *in vitro* fluciclovine uptake assay 132
4.3.1 Concentration 132

4.3.2 Time course 134
4.4 Mechanisms of fluciclovine uptake in breast cancer 135
4.4.1 Heterogeneity of fluciclovine uptake across a panel of breast cancer cell lines 135
4.4.2 Fluciclovine uptake correlates with ASCT2 but not LAT1 expression in breast cancer 136
4.4.3 High affinity natural amino acids for ASCT2 but not LAT1 inhibit fluciclovine uptake in breast cancer 137
4.4.4 siASCT2 confirms ASCT2 as the dominant transporter of fluciclovine in breast cancer 140
4.5 Discussion 142
Chapter 5 : Fluciclovine is a biomarker of early response to modulation of glutamine metabolism 144
5.1 Introduction 145
5.2 Optimisation of ^{18}F-fluciclovine imaging in vivo 147
5.2.1 Scan acquisition timing 147
5.2.2 Fasting improves tumour uptake of ^{18}F-fluciclovine 148
5.2.3 Tumour uptake of ^{18}F-fluciclovine is highly dependent on size 149
5.2.4 Test re-test variability of ^{18}F-fluciclovine uptake 151
5.3 Fluciclovine as a biomarker of early response to treatment 151
5.3.1 Increase in fluciclovine uptake predicts response to glutaminase inhibition in sensitive breast cancer cell lines 152
5.3.2 Decrease in fluciclovine uptake predicts response to metformin in sensitive breast cancer cell lines in vitro 156

5.3.3 Baseline fluciclovine uptake potentially predicts response to metformin at the outset 159
5.3.4 Early changes in ^{18}F-fluciclovine uptake predicts sensitivity to metformin in vivo 162
5.3.5 Bithionol treatment of breast cancer cell lines are associated with decreased fluciclovine uptake in vivo 165
5.3.6 mTORC1 inhibition does not alter fluciclovine uptake 169
5.3.7 Fluciclovine uptake is non-predictive of sensitivity to, and unaltered following glutamine deprivation 172
5.3.8 Fluciclovine uptake is unaltered in hypoxia 175
5.4 Discussion 178
Chapter 6 : Initial insights from FRONTIER: A clinical study to characterise ^{18}F-fluciclovine uptake in breast cancer 186
6.1 Introduction 187
6.2 Patients 188
6.3 Definition of ^{18}F-fluciclovine tumour uptake 188
6.4 ^{18}F-Fluciclovine uptake stratified by molecular type and grade 190
6.5 Initial metabolomics insights 191
6.6 Axillary lymph node involvement 194
6.7 Discussion 195
6.8 Conclusion 199
Chapter 7 : Final discussion 200
7.1 Overview 201
7.2 The positive impact of ^{18}F-fluciclovine PET/CT in management of recurrent prostate cancer 201

7.3 The potential implications of ASCT2-mediated transport of ^{18}F-fluciclovine in breast cancer 202
7.4 Characterising tumour biology with ^{18}F-fluciclovine: the tasks ahead 204
REFERENCES 206

LIST OF FIGURES

Figure 1.1: Chemical structure of 18F-fluciclovine compared to leucine and glutamine. ……. 30

Figure 1.2: ^{18}F-Fluciclovine biodistribution. …… 44

Figure 1.3: ^{18}F-FDG PET images reconstructed with different reconstruction algorithms. …… 47

Figure 1.4: Association between ASCT2 and LAT1 with survival in breast cancer patients. ……... 50

Figure 1.5: ASCT2 (SLC1A5) and LAT1 (SLC7A5) mRNA expression across different breast cancer subtypes in the METABRIC breast cancer microarray dataset. ……. 51

Figure 1.6: Targeting of glutamine metabolism in cancer. ……... 55

Figure 2.1: Summary flow chart of FALCON study design. ……. 70

Figure 2.2: Chemical structure of ^{14}C-FACBC. …….. 81

Figure 2.3: Summary flow chart of FRONTIER study design. ……..89

Figure 2.4: ASCT2 staining of HCC1806 cell pellets, with siRNA knockdown of ASCT2. ……..99

Figure 2.5: LAT1 staining of HCC1806 cell pellets, with siRNA knockdown of LAT1. ……99

Figure 2.6: SNAT2 staining of HCC1806 and MCF7 cell pellets. ……..100

Figure 2.7: pS6 staining of HCC1806 and MCF7 cell pellets. ……100

Figure 3.1: FALCON case example. ……..106

Figure 3.2: Incidental findings on ^{18}F-fluciclovine PET/CT. ……107

Figure 3.3: FALCON case example. ……..108

Figure 3.4: Pie charts demonstrating the distribution of response type in patients who underwent salvage radiotherapy. ……109

Figure 3.5: Graphs of PSA, PSA kinetics and BCR-free survival dichotomised by scan positivity. ……..112

Figure 3.6: Graphs of ^{18}F-fluciclovine scan positive detection rate stratified by Gleason score, T stage and surgical margin status. ……113

Figure 3.7: Axial images of different PET reconstructions at the level of the pubic symphysis. ……114

Figure 3.8: Graphs of lesion SUVmax, SBR and SNR across different PET reconstructions. ……..115

Figure 3.9: Graphs of organ SUVmean across different PET reconstructions. ……..……. 116

Figure 3.10: Graphs of organ SUVdev across different PET reconstructions. ……...117

Figure 3.11: Graphs of organ SNR across different PET reconstructions. ……...118

Figure 3.12: Maximum intensity projection images of a patient demonstrating small foci of disease recurrence, rendered more conspicuous on the BPL β300 reconstruction compared to OSEM. ……125

Figure 4.1: LAT1 mRNA expression is higher than ASCT2 across several breast cancer cell lines. ……131

Figure 4.2: Protein expression of LAT1 and ASCT2 across the breast cancer cell line panel. ……132

Figure 4.3: Correlation between mRNA and protein expression of ASCT2 and LAT1 across the breast cancer cell line panel. ……132

Figure 4.4: Linear increase in ^{14}C-FACBC uptake with increasing ^{14}C-FACBC concentration. ……135

Figure 4.5: Linear increase in ^{14}C-FACBC uptake up to 15 minutes in the 'low' (BT474) and 'high' (HCC1806) uptake cell lines. ……136

Figure 4.6: ^{14}C-FACBC uptake across a panel of breast cancer cell lines under baseline conditions. ……..137

Figure 4.7: ^{14}C-FACBC uptake correlates with ASCT2 protein expression but not LAT1. ……138

Figure 4.8: Competitive inhibition of ^{14}C-FACBC uptake by natural amino acids in HCC1806. ……139

Figure 4.9: Competitive inhibition of ^{14}C-FACBC uptake by MeAIB compared to GPNA. ……..……141

Figure 4.10: Effects of si-ASCT2 (1 nM) and competitive inhibition by 1 mM GPNA on ^{14}C-FACBC uptake in 3 representative breast cancer cell lines...142

Figure 4.11: Effect of si-LAT1 (1 nM) ± competitive inhibition by 1 mM GPNA on ^{14}C-FACBC uptake in 3 representative breast cancer cell lines. …….143

Figure 5.1: Time activity curves from analysis of tumour and organs in a HCC1806 xenograft model. ……149

Figure 5.2: ^{18}F-Fluciclovine uptake in HCC1806 xenografts is higher in fasted mice. ……150

Figure 5.3: Representative ^{18}F-Fluciclovine PET/CT axial images of CD1-nude mice bearing HCC1806 xenografts, fasted and non-fasted pre-tracer administration. ……..……150

Figure 5.4: Time course of ^{18}F-Fluciclovine uptake in HCC1806 xenografts. ……...151

Figure 5.5: Dose response graphs for HCC1806, MCF7 and BT474 treated with CB-839 for 5 days. ……155

Figure 5.6: Growth of HCC1806, MCF7 and BT474 treated with CB-839 at 2 and 5 days. ……156

Figure 5.7: ^{14}C-FACBC uptake after 2 days of CB-839 treatment. ……157

Figure 5.8: Growth of MDA-MB-468, MCF7 and MDA-MB-231 treated with metformin. ……...158

Figure 5.9: ^{14}C-FACBC uptake after 2 days of metformin treatment. ……...159

Figure 5.10: Growth of a panel of breast cancer cell lines cell lines treated with a range of concentrations of metformin. ……161

Figure 5.11: Correlation of ^{14}C-FACBC uptake with growth effect of metformin. ……..162

Figure 5.12: ^{18}F-Fluciclovine uptake ratios in sensitive MDA-MB-468 xenografts compared to relatively resistant HCC1806 xenografts. ……...164

Figure 5.13: In vivo response to metformin in sensitive MDA-MB-468 and resistant HCC1806 xenografts. ……...165

Figure 5.14: Representative ^{18}F-Fluciclovine PET/CT axial images of CD1-nude mice bearing MDA-MB-468 xenografts from the control and metformin treatment groups. ……..166

Figure 5.15: Decrease in ^{18}F-Fluciclovine uptake ratios after a short course of bithionol treatment predicts subsequent response in HCC1806 xenografts. ……...168

Figure 5.16: Representative ^{18}F-Fluciclovine PET/CT axial images of CD1-nude mice bearing HCC1806 xenografts from the control and bithionol treatment groups. ……..169

Figure 5.17: ^{14}C-FACBC uptake in the HCC1806 cell line after 7 days of bithionol treatment. ……170

Figure 5.18: Growth of MCF7, BT474 and HCC1806 treated with everolimus over 5 days. ……171

Figure 5.19: ^{14}C-FACBC uptake after 2 days of everolimus treatment. ……172

Figure 5.20: pS6 does not correlate to ^{14}C-FACBC uptake. ……..173

Figure 5.21: Effect of glutamine deprivation on proliferation of the breast cancer cell line panel. ……175

Figure 5.22: ^{14}C-FACBC uptake at neither baseline nor following glutamine deprivation correlate with sensitivity to glutamine deprivation.……...176

Figure 5.23: ^{14}C-FACBC uptake after 2 days of glutamine deprivation. ……176

Figure 5.24: Effect of different levels of hypoxia on ^{14}C-FACBC uptake. ….177

Figure 5.25: Competitive inhibition of ^{14}C-FACBC uptake by MeAIB compared to GPNA. ……178

Figure 5.26: Proposed schematic of fluciclovine as an imaging biomarker of intracellular glutamine levels. ……..180

Figure 6.1: ^{18}F-Fluciclovine breast tumour uptake in the first 5 FRONTIER participants. ……190

Figure 6.2: ^{18}F-Fluciclovine breast cancer uptake in the FRONTIER cohort. ……..192

Figure 6.3: Total ion count on LC/MS analysis of tumour and adjacent “normal” stroma samples. ……193

Figure 6.4: Coefficients of correlation between tumour 18F-fluciclovine uptake and metabolites. ……194

LIST OF TABLES

Table 1.1: Summary of evidence to support ASCT2 involvement in cellular internalisation of fluciclovine. …… 31

Table 1.2: Summary of evidence to support LAT1 involvement in cellular internalisation of fluciclovine. …… 32

Table 1.3: Summary of evidence to support minor SNAT2 and B0 involvement in cellular internalisation of fluciclovine. …..…… 32

Table 1.4: Publications reporting LAT1 in breast cancer. …… 52

Table 2.1: FALCON trial objectives and endpoints pertaining to this thesis. 68

Table 2.2: Scoring system applied to the four image quality parameters in the visual analysis. ……77

Table 2.3: Primer sequences used for qPCR. ……79

Table 2.4: Antibodies used for Western blotting. ……... 80

Table 2.5: Amino acid / inhibitor used for competitive inhibition experiments. …… 83

Table 2.6: FRONTIER study objectives and endpoints. ……..…..88

Table 2.7: Blood sample processing protocol for FRONTIER. ……92

Table 2.8: Tumour sample handling protocol in FRONTIER. ……...94

Table 3.1: Patient demographics of Oxford FALCON trial participants. ……...105

Table 3.2: Positive detection rate of ^{18}F-fluciclovine PET/CT stratified by PSA. ……..……105

Table 3.3: Nature of revised management classified by scan outcome. ……...106

Table 3.4: PSA, PSA kinetics and BCR-free survival of patients with positive and negative scans. ……..110

Table 3.5: Primary pathological variables in patients with positive and negative scans. ……..110

Table 3.6: Multi- and uni-variate binary logistic regression analysis of factors predicting ^{18}F-fluciclovine scan positivity. ……..111

Table 3.7: Scores of image quality parameters in the visual analysis. …….119

Table 5.1: Test re-test reproducibility metrics of 18F-fluciclovine uptake in various organs. ……..152

Table 6.1: Demographics of FRONTIER participants. ……189

Table 6.2: Diagnostic performance of ^{18}F-fluciclovine for detection of axillary nodal involvement. ……196

Chapter 1 : Introduction

1.1 Overview of ^{18}F-fluciclovine

[^{18}F]1-amino-3-fluorocyclobutane 1-carboxylic acid (^{18}F-FACBC / ^{18}F-fluciclovine) is a synthetic amino acid developed by Shoup et al. as a PET radiotracer for visualising malignant tumours [1]. The concept of using radiolabelled amino acids for the imaging of cancer is based on the increased metabolic demand of tumour cells, with enhanced channelling of amino acids into select metabolic pathways and increased expression of amino acid transporters to acquire these substrates.

1.1.1 Known transport mechanisms

^{18}F-Fluciclovine has been described to be structurally analogous to leucine (Figure 1.1), has been shown in prostate cancer and glioma cell lines to be taken up predominantly by amino acid transporters (AATs) ASCT2 and LAT1 (,), and is not metabolised upon internalisation [2]. ASCT2 is a high-affinity transporter of glutamine, alanine, serine, cysteine and threonine, and LAT1 is a high affinity transporter of leucine. Both transporters are anti-porters – in order to transport a molecule in one direction, exchange of a molecule in the opposite direction is required. Competitive inhibition experiments point to the minor contribution of other AATs, including B^0 and SNAT2 (), the latter being another high-affinity glutamine transporter.

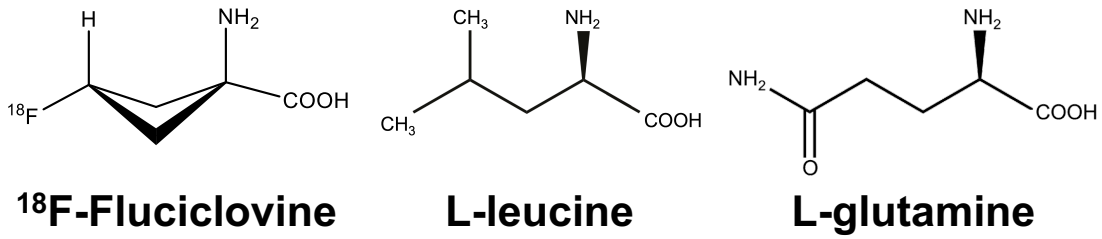

^{18}F-Fluciclovine **L-leucine** **L-glutamine**

Figure 1.1: Chemical structure of ^{18}F-fluciclovine compared to leucine and glutamine.

The uptake of fluciclovine is rapid, demonstrated to plateau between 3-12 minutes *in vivo* [3], and 5-15 minutes *in vitro* [4]. For the purposes of whole body PET imaging, this is an ideal property as it permits early imaging following administration, during which excretion of tracer into the urinary tract is minimal. This is particularly important for evaluation of the retroperitoneum.

Since commencement of this doctorate, over 1,000 patients have been imaged with ^{18}F-fluciclovine. The majority of the clinical experience with ^{18}F-fluciclovine has been in imaging of recurrent prostate cancer, for which it received regulatory approval in the USA and Europe [5, 6] during the course of this doctorate.

Table 1.1: Summary of evidence to support ASCT2 involvement in cellular internalisation of fluciclovine.

Evidence	Cell type	Paper
ASCT2 knockdown results in a 30-40% decrease in fluciclovine uptake	DU145	Okudaira et al. 2011 [2]
Na^+ deprivation results in a 70-80% decrease (DU145, PC-3) and 98.5% decrease (LNCaP) in fluciclovine uptake	DU145, PC-3, LNCaP	Oka et al. 2012 [4]
Competitive inhibition with glutamine results in a 80-90% decrease in fluciclovine uptake	DU145	Oka et al. 2012 [4]
Competitive inhibition with phenylalanine/proline results in <50% decrease in fluciclovine uptake (cross specificity with glutamine with exception of system ASC and y^+L. The role of y^+L is insignificant as there is minimal efflux of fluciclovine in presence of arginine, a substrate of y^+L)	DU145	Oka et al. 2012 [4]
Exposure to glutamine causes >95% efflux of intracellular fluciclovine (also implicates anti-porting mechanism of transport)	DU145	Oka et al. 2012 [4]
ASCT2 transported fluciclovine with Km values of 92.0 ± 32.3 μM	*Xenopus laevis* oocytes	Okudaira et al. 2013 [7]

Table 1.2: Summary of evidence to support LAT1 involvement in cellular internalisation of fluciclovine.

Evidence	Cell type	Paper
Na^+ deprivation and BCH (system L competitor) results in decrease in FACBC uptake to basal levels.	DU145	Okudaira et al. 2011 [2]
In Na^+ deprivation, BCH compared to NEM results in decrease in fluciclovine uptake of 40%. (cross-specificity apart from LAT1-BCH & y^+-NEM. The role of y^+ is insignificant as there is minimal change in uptake when competing with arginine, a substrate of y^+, in Na^+ deprivation)	PC-3	Oka et al. 2012 [4]
In Na+ deprivation, fluciclovine uptake increases in a lower pH environment (activity of system L is increased in lower pH)	DU145	Oka et al. 2012 [4]
In Na+ deprivation and BCH, there is 85% efflux of intracellular fluciclovine	DU145	Oka et al. 2012 [4]
LAT1 transported fluciclovine with Km values of 230.4 ± 184.5 μM	*Xenopus laevis* oocytes	Okudaira et al. 2013 [7]

Table 1.3: Summary of evidence to support minor SNAT2 and B^0 involvement in cellular internalisation of fluciclovine.

Evidence	Cell type	Paper
SNAT2: SNAT2 knockdown results in a 17% decrease in FACBC uptake	DU145	Okudaira et al. 2011 [2]
SNAT2: Fluciclovine uptake decreases in a lower pH environment (activity of system N is decreased in lower pH, while system ASC is stable)	DU145	Oka et al. 2012 [4]
SNAT2: Competitive inhibition with glutamine results in a 80-90% decrease in fluciclovine uptake	DU145	Oka et al. 2012 [4]
SNAT2: SNAT2 transported fluciclovine with Km values 222.0 ± 29.3 μM.	*Xenopus laevis* oocytes	Okudaira et al. 2013 [7]
B^0: With BCH, in presence and absence of Na+, change in FACBC uptake differs by 9-15%.	DU145, LNCaP	Okudaira et al. 2011 [2]

1.2 Overview of diagnostic work-up and salvage therapies in recurrent prostate cancer

Prostate cancer (PCa) is the commonest cancer in males in the UK, accounting for 26.1% of total malignancies in men in 2016, with an age-standardised incidence of 173.7 per 100,000 males [8]. It is the second commonest cause of male cancer deaths [9] with a recurrence rate of 20-30% in patients who have received primary radical treatment [10].

1.2.1 Initial diagnosis and treatment

The diagnosis of PCa is often made following the detection of elevated prostate-specific antigen (PSA) and / or an abnormal digital rectal examination, with confirmation of diagnosis by prostate biopsy. Serum PSA measurement forms the basis for prostate cancer screening, which has seen a recent shift from recommendations against routine screening, towards advocating individual informed decisions on periodic screening in men between 55-69 years [11]. This followed demonstration of a small benefit in metastatic disease prevention in this age group (3 men per 1,000 screened), and prostate cancer-related mortality (1.28 men per 1,000 screened), from systematically reviewed randomised controlled trial data [11]. PSA is also used as a tumour marker and its levels are positively correlated with the risk of metastatic disease or subsequent disease progression.

The primary treatment of PCa can be divided into radical and non-radical treatment, the former applicable to patients with localised non-invasive disease. Radical primary treatment options include radical prostatectomy

(RP), radical external beam radiotherapy (RRT) and brachytherapy, with adjuvant androgen deprivation therapy. Following radical treatment, patients undergo surveillance via PSA measurement.

1.2.2 Diagnosis of BCR

Detection of PSA post radical therapy (at least 6 weeks post treatment in the case of RP), or an initially falling and then rising PSA are evidence of biochemical disease relapse, BCR. Various definitions of BCR exist and differ between the mode of primary treatment. In the context of RP, the European Association of Urology defines BCR as two consecutive PSA rises ≥0.2 ng/mL [12]. In the context of RRT, the most widely known is the ASTRO-Phoenix criteria which defines BCR as a PSA rise by 2 ng/mL or more above the nadir PSA [13].

Depending on clinical factors and local practice, patients may undergo imaging, usually a bone scan and/or pelvic MRI, to confirm the sites and extent of disease relapse.

1.2.3 Conventional Imaging in BCR

Standard imaging investigations are an isotope bone scan to evaluate for bony metastatic disease [14] and MRI / CT to assess for local / nodal recurrence [15]. However, BCR after RP or RRT precedes clinical metastases by 7-8 years on average, rendering the diagnostic yield low in asymptomatic patients [16]. European Association of Urology (EAU) guidelines recommend these tests only be performed in patients with BCR who have a high baseline

PSA (> 10 ng/mL) or a high PSA velocity (> 0.5 ng/mL/month) or in patients with symptoms of bone disease. The positive detection rate of these investigations are poor below these thresholds [17, 18]. In a large cohort of 443 patients with PSA < 20 ng/mL, Mcarthur et al. [19] found only 3% of patients to have positive bone scans. Studies have shown CT to be positive in only 11–14% of men with BCR after RP [18, 20]. The diagnosis of nodal involvement on conventional cross-sectional imaging (CT / MRI) is based primarily on nodal size, which is known to be inaccurate, with pooled sensitivities of 39% and 42% for MRI and CT respectively and pooled specificities of 82% in both modalities [21]. As such, the utility of imaging and type of investigation in BCR varies across the UK.

1.2.4 ^{18}F-FDG PET-CT Imaging in BCR

The uptake of fluorodeoxyglucose (^{18}F-FDG) is low in prostate cancer and its use as an imaging agent in PET-CT in prostate cancer has been shown to be of limited value [22, 23]. Several radionuclide tracers have been developed for clinical use in prostate cancer. The most well-established tracers in clinical use within the U.K. are choline-based PET radiotracers.

1.2.5 Choline PET/CT

The concept of using radiolabelled choline in the imaging of prostate cancer is based on the overexpression of choline kinase by prostate cancer cells, a property shared with other tumour types [24]. Two different forms of radiolabelled choline are in current use, ^{11}C-choline and ^{18}F-fluorocholine. With the latter, two chemically variant compounds are commercially available,

^{18}F-fluoromethylcholine and ^{18}F-fluoroethylcholine. No *in vivo* studies directly comparing the different forms of radiolabelled choline have been published. A single retrospective study of variation in physiological distribution between these three tracers has reported statistically significant differences in degree of uptake by several organs, but with no difference in visceral localisation. Areas of pathological uptake were not evaluated [25].

Choline PET/CT has better diagnostic performance in detecting sites of recurrent prostate cancer than conventional imaging and ^{18}F-FDG PET/CT. Evangelista et al. [26] pooled data from 2 studies (n=89) comparing ^{11}C-choline to ^{18}F-FDG PET/CT in detecting prostate cancer metastases. In ^{11}C-choline and ^{18}F-FDG PET/CT scans respectively, they reported pooled sensitivities of 65.1% (95% C.I. 53.8–75.2%) and 39.8% (95% C.I. 29.2–51.1%), and pooled specificities of 83.3 % (35.9–99.6%) and 83.3% (35.9–99.6%). von Eyben et al. [27] pooled data from 7 studies (n=280) comparing choline PET/CT to bone scintigraphy. Choline PET/CT yielded positive results for more patients [127 (45%) vs. 46 (16%), odds ratio (OR) 2.8, 95% C.I. 1.9–4.1]. In a cohort of 109 BCR patients with negative conventional imaging (transrectal US, MRI, abdominopelvic CT, bone scintigraphy), Giovacchini et al. reported positive ^{11}C-choline PET/CTs in 11% [28].

The adoption of choline PET/CT has also been shown to have clinical impact. In a recent retrospective multicentre study, Ceci et al. [29] reported ^{11}C-choline PET/CT led to a major clinical impact change in management in 18% of patients, with an overall management change in 46.7%. Von Eyben et al.

pooled data from 15 studies (n=938) evaluating the impact of choline PET/CT on changing treatment in prostate cancer [16]. They reported 41% of patients undergoing a change in treatment. Based on a secondary pooled analysis restricting this cohort to patients with BCR, 40% underwent a change in treatment [27]. Furthermore, patients with negative choline PET/CT results had better BCR-free, disease-free and treatment-free survival rates than those with positive findings. Choline PET/CT positivity/negativity was the only significant predictor of treatment-free survival.

In the same meta-analysis, PSA response following a change in treatment based on choline PET/CT results was evaluated using pooled data from 10 studies (n=404) [27]. This demonstrated 25% of patients having a complete PSA response. Treatments included salvage lymphadenectomy (LND) and pelvic radiotherapy.

Despite better diagnostic performance compared to conventional imaging, choline PET/CT still suffers from suboptimal sensitivity. Whenever choline-PET/CT identifies a suspected lesion, almost twice as many metastases are demonstrated [30], an observation reflected in data from recent meta-analyses. Von Eyben et al. [27] pooled data from 11 studies (n=609) evaluating the performance of choline in detecting lymph node metastases in BCR – with histological correlation. Pooled sensitivity was 59% (51%–66%) and specificity was 92% (89%–94%). Hence, choline cannot adequately characterise the extent of nodal disease in BCR.

In the context of primary prostate cancer, Evangelista et al. [31] pooled data from 10 studies (n=441) evaluating the performance of choline in detecting lymph node involvement. This also yielded a relatively poor pooled sensitivity of 49.2% (95% C.I., 39.9-58.4%), with a higher specificity of 95% (95% C.I., 92-97.1%).

While it performs better than conventional imaging counterparts, the detection rate of choline PET/CT remains poor in the setting of relatively low PSA and slow PSA kinetics. Husarik et al. and Castellucci et al. reported a moderate and low detection rate in case of PSA value <2 ng/mL and <1.5 ng/mL (71.4% and 28%), respectively [32, 33]. The detection rate of metastases has been described to range between 20% and 36% in patients with PSA <1 ng/mL, compared to 63%-83% where PSA levels exceed 3 ng/mL [33, 34]. In a cohort of 109 BCR patients with negative conventional imaging (TRUS, MR, abdominopelvic CT, bone scintigraphy), Giovacchini et al. reported a higher rate of positive ^{11}C-choline PET/CTs with higher PSA [28]. Imaging was positive in 3 of 65 (5%), 4 of 26 (15%) and 5 of 18 patients (28%) with PSA between 0.2 and 1, between 1 and 2, and greater than 2 ng/ml, respectively.

As with other diagnostic tests, choline PET/CT is liable to produce false positive findings. This is reflected in the aforementioned diagnostic performance parameters and has been described in a number of entities. These included increased choline uptake within: the prostate in benign prostatic hypertrophy (BPH) [35], lymph nodes due to inflammation [36, 37],

the prostate bed due to post-surgical scarring and inflammation post-RP/RRT [38], bones due to degenerative change or recent fractures [39].

The two different forms of radiolabelled choline, ^{11}C-choline and ^{18}F-fluorocholine, have individual drawbacks. ^{11}C-choline exhibits early accumulation in small bowel limiting pelvic analysis [40]. The short 20-minute half-life of ^{11}C limits the use of ^{11}C-choline to centres with an on-site cyclotron and radiopharmacy facilities. Its short half-life also limits the scope for obtaining delayed acquisitions to improve tumour-to-background ratio. The latter can be performed with ^{18}F-fluorocholine, which has a longer half-life of 110 minutes. This also makes it a more widely distributable tracer. However, high urinary tract activity and excretion of ^{18}F-fluorocholine into the urinary bladder limits assessment of the prostate bed [41].

1.2.6 Conventional and emerging radical salvage options in BCR

The options for radical salvage therapy (with curative intent) in BCR remain controversial [15]. In the context of prior RP, the main option is salvage radiotherapy (SRT) to the prostate bed. In patients with intact prostates, having had prior primary RRT or brachytherapy, a wider range of options for salvage therapy with curative intent are available. These include salvage radical prostatectomy, salvage cryotherapy, salvage brachytherapy and salvage high intensity focused ultrasound (HIFU) [15].

The described therapies are local treatments, directed at the prostate / prostate bed. Based on current mainstream practice, the presence of disease

outside the prostate bed precludes radical salvage therapy. Paradoxically, current NICE guidelines recommend against the use of conventional imaging in patients being considered for radical salvage therapy [14], unless symptomatic. This may be rationalised by the observation of more favourable outcomes from radical salvage therapy at low PSA levels, particularly SRT [42], and foreknowledge of the poor diagnostic performance of conventional imaging at such PSA levels. While this in itself underpins the need for an imaging test to accurately detect extra-prostatic disease and thus prevent unnecessary radical salvage treatment, there is an emerging role for salvage treatment of limited nodal disease, with several reports of promising clinical endpoints based on early results. This has been described in the form of salvage pelvic LND or targeted pelvic radiotherapy, the latter afforded by the advent of more sophisticated techniques, namely intensity modulated radiotherapy (IMRT) and stereotactic beam radiotherapy (SBRT).

Rigatti et al. [43] evaluated the effect of salvage LND in 72 patients with BCR post-RP, who had choline-positive lymph nodes on PET/CT. They reported a complete PSA response in 56.9% of patients and 5-year recurrence-free and cancer-specific survival of 24% and 75% respectively. The mean PSA in this cohort was 1.5 ng/mL. In 47 patients with BCR and a history of RP or RRT and choline-positive nodal disease, Jilg et al. [44] evaluated the impact of salvage LND (with adjuvant radiotherapy in a subset). Similar outcomes were reported, a complete PSA response in 46% and 5-year recurrence-free and cancer-specific survival of 25.6% and 77.7% respectively.

Alongi et al. [45] described an overall response rate of 82% (over a median follow-up of 195 days) to SBRT of isolated lymph node metastases in 34 patients with previously radically treated PCa. In a cohort of 24 patients with BCR and up to 3 synchronous bone or nodal metastases treated with SBRT, Berkovic et al. [46] reported a median delay in commencing ADT of 38 months (95% C.I. 18–58 months). In another cohort of 34 patients with BCR and isolated disease recurrence (in various sites) on imaging, robotic SBRT resulted in a progression-free survival of over 40% at 30 months, and complete PSA response in over 60% treated with SBRT alone [47].

1.3 Rationale for accurate imaging in BCR

As mentioned previously, the presence of disease outside the prostate bed precludes radical salvage therapy based on mainstream practice. In addition, more favourable outcomes from salvage therapy are observed at low PSA levels [42], when the diagnostic performance of current imaging options is poor. Conversely, the presence of a high PSA is associated with an increased risk of metastatic disease [48], the presence of which precludes the option of radical salvage therapy. Herein lies the ongoing need for an imaging test to detect sites of recurrent disease earlier and with greater accuracy, to aid clinical management in patients with BCR.

1.3.1 ^{18}F-Fluciclovine imaging in prostate cancer

In 2007, Schuster et al. first described the use of fluciclovine (^{18}F) PET/CT in PCa in 15 patients with either primary disease or BCR [49]. This yielded promising findings of accurate nodal staging and identification of disease sites

in patients with proven recurrence. This group have gone on to expand their work in a single centre study, evaluating the diagnostic performance of ^{18}F-fluciclovine PET/CT compared to that of ^{111}In-capromab pendetide SPECT/CT in BCR. The latter is a radionuclide tracer licenced and established as standard of care for PCa imaging in the USA, but has been shown to have low sensitivities, with dismal detection of bone metastases [50].

Based on their latest published results in May 2014 from a cohort of 93 patients [51], ^{18}F-fluciclovine PET/CT demonstrated a significantly higher accuracy, detecting more prostatic and extra-prostatic disease, and effectively up-staging 25.7% of cases. With specific regards to extra-prostatic disease (n=70), ^{18}F-fluciclovine PET/CT detected disease in 18 more patients compared to ^{111}In-capromab pendetide (22 vs 4). ^{18}F-Fluciclovine PET/CT had 55.0% sensitivity, 96.7% specificity, 72.9% accuracy, 95.7% positive predictive value (PPV) and 61.7% negative predictive value (NPV) compared to ^{111}In-capromab pendetide with 10.0%, 86.7%, 42.9%, 50.0% and 41.9%, respectively. Histological proof was obtained for the majority (96.1%) of the lesions which had ^{18}F-fluciclovine positivity.

In the largest cohort to date of intra-individual comparison of ^{18}F-fluciclovine to ^{11}C-choline PET/CT, Nanni et al. [52] compared diagnostic performance between the two tracers in 50 patients with BCR after RP, in a single-centre study. In the setting of relatively low PSA levels (mean 3.2 ng/mL, range 0.24-15.6), the overall positive detection rate was found to be higher in ^{18}F-fluciclovine compared to ^{11}C-choline PET/CT (34.0% vs 22.0%). This trend

was observed in all PSA categories, including that of PSA <1 ng/mL where the positive detection rate with ^{18}F-fluciclovine was 21%, compared to 14% in ^{11}C-choline. ^{18}F-Fluciclovine PET/CT was positive in an additional 6 patients who had negative ^{11}C-choline PET/CTs. In an interim report on the subset of this cohort, the group also described fewer false positive findings for ^{18}F-fluciclovine PET/CT [53]. Increased choline uptake by liver angiomatosis and several inflammatory inguinal lymph nodes were fluciclovine-negative.

Compared to its radiolabelled choline counterparts, ^{18}F-fluciclovine also has a more favourable biodistribution (). As described in the beginning of the chapter, this is achievable as tumour uptake of the tracer is rapid following injection [3], allowing a short tracer uptake time prior to commencement of imaging. This results in minimal renal excretion and associated bladder activity, and compared to choline, has lower homogeneous activity in the bowel [3]. As illustrated in , the former characteristic affords improved visualisation of disease within the prostate bed, normally hampered by radioactivity within the urinary bladder. Furthermore, the presence of minimal activity in the urinary tract aids interpretation of disease in the retroperitoneum, another known site of predilection for prostate cancer spread [54]. Finally, being an ^{18}F-labelled tracer, it is a distributable product which does not have to be manufactured on-site.

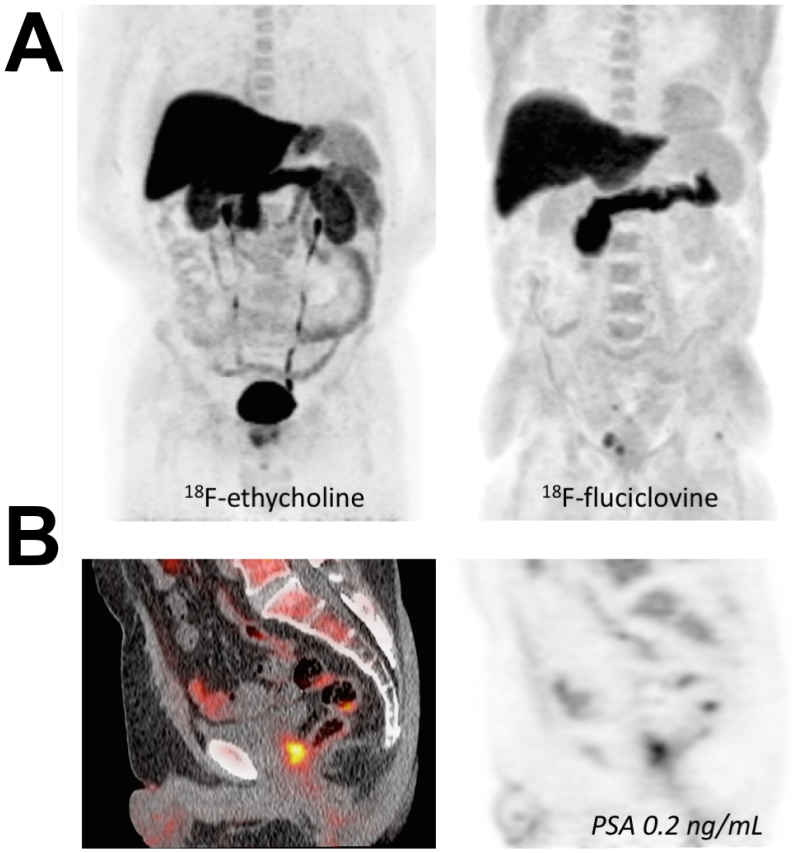

Figure 1.2: ^{18}F-Fluciclovine biodistribution. (A) Two patients imaged in Oxford, demonstrating the differences in tracer biodistribution between 18F-ethylcholine and 18F-fluciclovine. The paucity of radioactivity within the upper urinary tracts and bladder affords improved visualisation of disease around these areas which are common sites of prostate cancer recurrence. (B) 18F-fluciclovine images of a post-prostatectomy patient, PSA 0.2 ng/mL, who took part in the FALCON trial in Oxford. Fluciclovine-avid disease was readily demonstrated in the prostatectomy bed, interposed between the bladder and rectum, aided by the absence of radioactivity within the urinary bladder.

1.3.2 The next step for defining clinical utility of ^{18}F-fluciclovine in recurrent prostate cancer imaging

With a high positive predictive value (95.7%) for extra-prostatic disease, almost entirely confirmed by histology, and a higher detection rate than

choline, ^{18}F-fluciclovine bears hallmarks of a competitively diagnostic agent in BCR. The impact of ^{18}F-fluciclovine PET/CT on clinical management of patients with BCR remains to be defined, as are the PSA level, kinetics and other clinicopathological factors associated with probability of a positive scan. The latter are pertinent to forming appropriate use criteria for this scanning agent, and bar PSA, have not been described in published literature.

In the setting of growing single-centre evidence of superior diagnostic performance of ^{18}F-fluciclovine PET/CT in BCR, we aimed to assess its clinical impact on treatment decisions in a multi-centre study in patients with BCR being considered for radical salvage treatment (with curative intent). In addition, we aimed to assess the effect of clinical parameters on probability of lesion detection, and the possible improvement in outcome of radical salvage treatment based on ^{18}F-fluciclovine PET/CT being included in the assessment.

1.4 Advanced PET image reconstruction

1.4.1 Overview

Ordered subset expectation maximisation (OSEM) reconstruction remains the most widely used image reconstruction method in PET imaging. It is an iterative method, aiming to establish the most representative image from PET data through repeated iterations of possibilities, with each iteration producing an image with a higher probability of representing the acquired data / stronger image signal [55]. The main disadvantage of this technique is that it is not possible to run it to full convergence as the image noise increments with each

iteration, becoming unacceptable for clinical interpretation even before full convergence is achieved [56, 57].

A newer generation of iterative reconstruction methods allow the modelling of the imaging system point spread function into the algorithm, resulting in improved image signal [58]. However, the same penalty of increasing image noise with each iteration applies (Figure 1.3).

In the last five years, a new iterative reconstruction, Bayesian penalised likelihood (BPL), has been developed by GE Healthcare. The optimisation of BPL reconstruction for ^{18}F-FDG whole body oncological PET [59], and its effect on evaluating various clinical entities on ^{18}F-FDG PET/CT has been recently reported [55, 60, 61]. BPL runs to effective convergence and includes point spread function (PSF) modelling while controlling noise through the use of a penalty term (β), which achieves greater noise reduction as β is increased [59]. It has been shown to improve lesion signal-to-noise (SNR) on clinical ^{18}F-FDG PET compared to widely utilised OSEM reconstruction, particularly in small, sub-centimetre abnormalities [55]. The nuclear medicine department in Oxford currently uses BPL reconstructed images (β=400) [59] (Figure 1.3) for the clinical interpretation of all ^{18}F-FDG whole body oncological PET/CT studies.

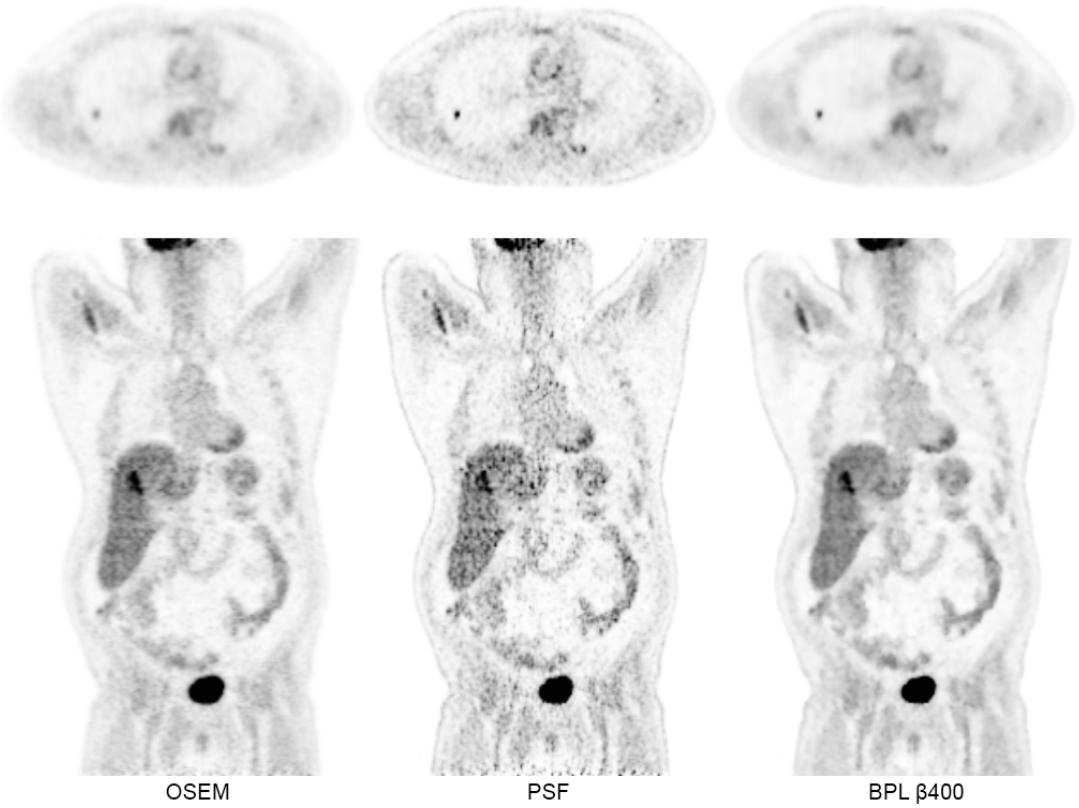

Figure 1.3: ^{18}F-FDG PET images reconstructed with different reconstruction algorithms demonstrating a lung nodule (top panel) and liver metastasis (bottom panel). The limitation of OSEM in signal recovery is best demonstrated in the lung nodule images, where PSF and BPL render the nodule with improved clarity. However, there is a considerable amount of noise in the PSF images. While this is inconsequential to characterisation of the lung nodule, the liver metastasis is relatively well demonstrated against the homogeneous appearance of surrounding liver on the BPL reconstruction. This is in stark comparison to the PSF reconstruction where, despite increased lesion signal, there is a detrimental amount of noise which could even risk false-positive interpretation of small lesions. Adapted from Teoh et al. [59].

1.4.2 Rationale for tracer-specific optimisation

The use of non-FDG oncological PET tracers coupled with progressive adaptation of modern image reconstruction technology requires tracer-specific reconstruction optimisation, due to the inherent variation of physiological distribution and degree of pathological uptake observed between different

tracers. For example, imaging ^{90}Y post-selective internal radiation therapy has been optimised for BPL reconstructions as using β=4000 [62].

Prior to this doctorate, the performance of BPL to standard PET reconstruction of ^{18}F-fluciclovine images and the optimum penalisation factor (β) for clinical use of BPL in ^{18}F-fluciclovine whole body imaging was unknown.

1.5 Amino acid metabolism as an imaging and therapeutic target in breast cancer

1.5.1 Rationale for focus on breast cancer

Breast cancer is the most common cancer in the UK, with 46,083 cases diagnosed in 2015 [63], and a lifetime risk of occurrence in 1 in 8 women [64]. Encouragingly, as a testament to the vast efforts in preclinical and clinical breast cancer research, survival has increased over the past few decades. In the UK, ten-year age-standardised net survival has increased from 40% in the 1970s to a predicted 78% during 2010-2011 [65].

Nonetheless, focus on breast cancer remains a research priority. It is the second most common cause of cancer deaths in women after lung cancer. In 2012, 11,600 women in the UK died from breast cancer [66]. Within 5 years of primary breast cancer treatment, approximately one in 10 patients have disease recurrence [67], indicating that the current arsenal of neoadjuvant, adjuvant and systemic therapies are sub-optimally effective in some patients. Furthermore, as these therapies, particularly cytotoxic agents, carry a non-

negligible side effect profile contributing to morbidity, there is mileage to be gained in potentiating these treatments or counteracting resistance mechanisms by exploiting other targets. In particular, the targeting of cancer metabolism has gained significant interest.

PET imaging affords a better reflection of tumour metabolism, which can be tailored according to the ligand. The uptake of PET tracer by a tumour (and hence the degree of metabolic activity) can be quantified by its standardised uptake value (SUV), which can be generated for comparison across multiple scans. Beyond that of recurrent prostate cancer detection, the ability to image amino acid metabolism and/or amino acid transporter expression with ^{18}F-fluciclovine, may have utility in breast cancer management.

1.5.2 ASCT2 and LAT1 expression are associated with poor prognosis in breast cancer

Bioinformatic analysis of the METABRIC cohort (Molecular Taxonomy of Breast Cancer International Consortium) demonstrates increased expression of both ASCT2 and LAT1 to be associated with poorer overall survival (ASCT2: HR 1.25 (1.09-1.44) p=0.002; LAT1: HR 1.45 (1.26-1.67), $p=2.67x10^{-7}$; ASCT2+LAT1: HR 1.86 (1.53-2.26), $p=3.31x10^{-10}$) (Figure 1.4). Furthermore, there is heterogeneity of LAT1 expression in all subtypes of breast cancer, with highest mRNA expression in triple receptor negative (TN), followed by human epidermal growth factor receptor 2 (HER2) positive breast cancer (), both of which are inherently aggressive subtypes. LAT1 mRNA expression is higher than adjacent normal breast tissue in oestrogen receptor

(ER) positive cancers, but is relatively low compared to TN and HER2+ cancers. This supports the observation of a low rate of LAT1 positivity (15.5%) and intensity in ER+ breast cancers compared to TN and HER2+ (64.0% and 51.2% respectively) on immunohistochemistry (IHC) [68].

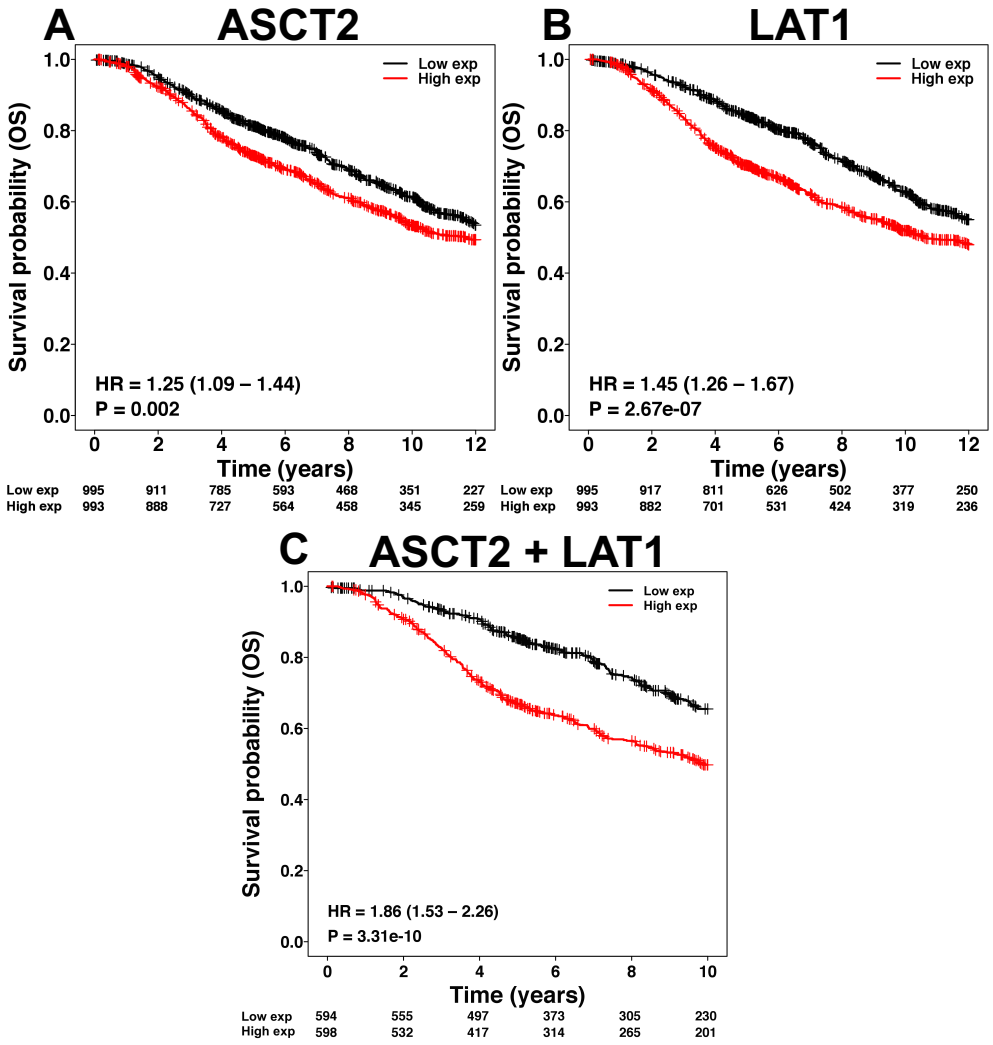

Figure 1.4: Association between ASCT2 and LAT1 with survival in breast cancer patients. Kaplan-Meier plots and Cox proportional hazards model statistics demonstrating the statistically significant association between increased breast cancer expression of (A) ASCT2, (B) LAT1, (C) combination of ASCT2 and LAT1 with overall survival (OS) in the METABRIC breast cancer microarray dataset. The high and low expression groups are stratified based on median mRNA dichotomisation of mRNA abundance levels. Courtesy of Dr. Syed Haider, Department of Oncology, Weatherall Institute of Molecular Medicine.

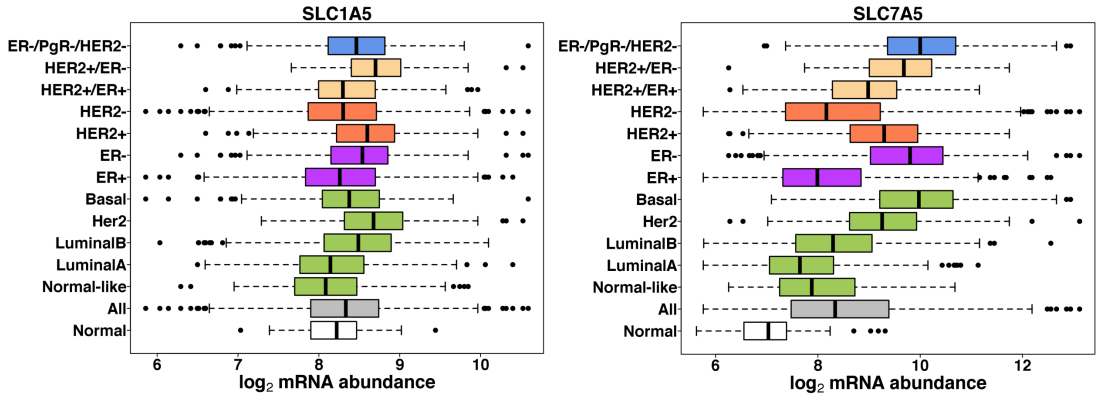

Figure 1.5: ASCT2 (SLC1A5) and LAT1 (SLC7A5) mRNA expression across different breast cancer subtypes in the METABRIC breast cancer microarray dataset. All: mRNA abundance across the entire cohort; Her2: status based on PAM50 subtype; HER2, ER: status based on immunohistochemistry; PgR: progresterone receptor status based on mRNA abundance. Courtesy of Dr. Syed Haider, Department of Oncology, Weatherall Institute of Molecular Medicine.

summarises publications describing LAT1 expression in breast cancer. Of note, studies have corroborated the observation in the METABRIC cohort, of higher LAT1 expression being associated with more aggressive phenotypes. Herein lies the potential for use of LAT1 targeted imaging alongside established diagnostic techniques to stratify tumour phenotypes for prognostication, tailoring treatment, and predicting and monitoring subsequent response.

Table 1.4: Publications reporting LAT1 in breast cancer.

Findings	Author
LAT1 and CD98 expression (IHC, membranous staining) is: • Higher in HER2+ and TN • Associated with poor prognosis in TNBC • Associated with increased risk of relapse in TNBC • Correlated with tumour size, nuclear grade and Ki67	Furuya et al. 2012 [68] N=129 (LAT1 +ve 56)
LAT1 expression (IHC) is: • Increased in higher stage tumours • Higher in more cases with node positive disease (92% v 60%) LAT1 knockdown reduces proliferation of MDA-MB-231 (proliferation assay and soft agar colony formation)	Liang et al. 2011 [69]
LAT1 expression (IHC, membranous staining) is: More frequent in intra-individual metastasis compared to primary tumour (breast cancer and other tumour sites) Correlated with Ki67, VEGF, CD31 and CD34 expression (all tumour sites)	Kaira et al. 2008 [70]
Inhibition of system L (BCH, D-leucine) inhibits the growth of breast cancer cell lines.	Shennan et al. 2004 [71]
Oestrogen (17β-estradiol) stimulates L-leucine uptake by MCF-7 (increase in Vmax of L-leucine uptake) but not by MDA-MB-231 cells	Shennan et al. 2008 [72]
Oestrogen (17β-estradiol) increases LAT1 RNA expression by 10-fold over 24 hours in ZR75-1 cells. Interestingly, treatment with tamoxifen increased LAT1 RNA expression by 2-fold.	Soulez et al. [73]
Based on transcriptomic data, high expression of LAT1 is associated with a shorter relapse free, and overall survival rate after tamoxifen treatment, and correlates with Ki67.	Mihaly et al. 2013 [74]
On large-scale IHC screening in breast cancer samples with known outcome, LAT1 expression is significantly associated with outcome and identified as a potentially important prognostic IHC marker for ER+ breast cancer. It is subsequently included as one of five markers in the Mammostrat expanded IHC test.	Ring et al. 2006, Ross et al. 2008 [75, 76]

While an analysis of ASCT2 expression in the METABRIC cohort also demonstrates strong associations between high mRNA expression and survival in ER+ tumours, the level of mRNA expression is less variable between the molecular subtypes (Figure 1.5).

1.5.3 Majority of cell mass is derived from amino acids

In a meticulous panel of work utilising stable and radioactive isotopes incorporated into various metabolites, the Vander Heiden group has demonstrated that amino acid-derived carbons, as opposed to glucose, contribute to the majority of cell mass in a variety of mammalian and cancer cell lines. The breast cancer cell line MDA-MB-468 formed part of this panel [77], indicating a central role of amino acids in maintaining proliferative capacity and metabolism. Based on this, one may also postulate that characterising a tumour by its uptake of amino acids would be of greater biological significance in terms of crude characterisation of the tumour metabolome, than by using glucose determined with ^{18}F-FDG (fluorodeoxyglucose).

1.5.4 Glutamine metabolism and its aberration in cancer

Of the amino acids, glutamine is a key metabolite of interest due to growing knowledge of its role in supporting cancer metabolism. Following transport into the cell by high-affinity transporters such as ASCT2, glutamine may be utilised for energy production and as a biosynthetic precursor, amongst other purposes. Glutamine is converted into glutamate by the enzyme glutaminase. Glutamate can then converted into α-ketoglutarate by either glutamate dehydrogenase or aminotransferases [78]. At this point, α-ketoglutarate may enter the tricarboxylic acid (TCA) cycle for energy production.

The biosynthetic fates of glutamine are diverse. Instead of being utilised downstream of the TCA cycle, α-ketoglutarate may instead undergo reductive carboxylation, which through the formation of citrate followed by acetyl-CoA, may proceed to feed into lipid biosynthesis [79]. The activity of aminotransferases leading to α-ketoglutarate formation also results in other amino acid formation, such as alanine and aspartate (by alanine and aspartate aminotransferase respectively) [78]. Glutamine acts as a nitrogen source, directly contributing to nucleotide biosynthesis, and via aspartate, acts as a contributor of carbon [80].

It is now well recognised that glutamine addiction is a hallmark of some cancers, driven by a myriad of oncogene activation and/or loss of tumour suppressor gene function [79]. One key example is the MYC oncogene, described as a master regulator of glutamine metabolism [81], which has been shown to be involved in transcriptional regulation of genes necessary for glutamine catabolism, including upregulation of glutamine transporters such as ASCT2, and enzymes involved in glutamine metabolism such as glutaminase [82, 83]. It has been shown that ASCT2 knockdown in HCC1806, a well-established MYC amplified breast cancer cell line, results in significant downregulation of MYC expression, alongside cell growth inhibition *in vitro* and *in vivo* [84].

1.5.5 Glutamine targeted therapies in cancer

Targeting of glutamine metabolism as a therapeutic strategy in cancer has therefore gained increasing interest, either as a monotherapy or in

combination with other treatments to achieve synthetic lethality [79], the latter forming the fundamental basis of targeting cancer metabolism [85]. Several compounds exist which allow targeting at various stages of glutamine metabolism and have been reported in the preclinical setting (): uptake by ASCT2 (specific inhibitor N-Glutaryl-L-phenylalanine p-nitroanilide (GPNA) [86], system ASC inhibitor benzylserine [87]), glutaminase (CB-839 [88], Bis-2-(5-phenylacetamido-1,3,4-thiadiazol-2-yl)ethyl sulphide (BPTES) [89]) and glutamate dehydrogenase (bithionol [90], R162 [91]).

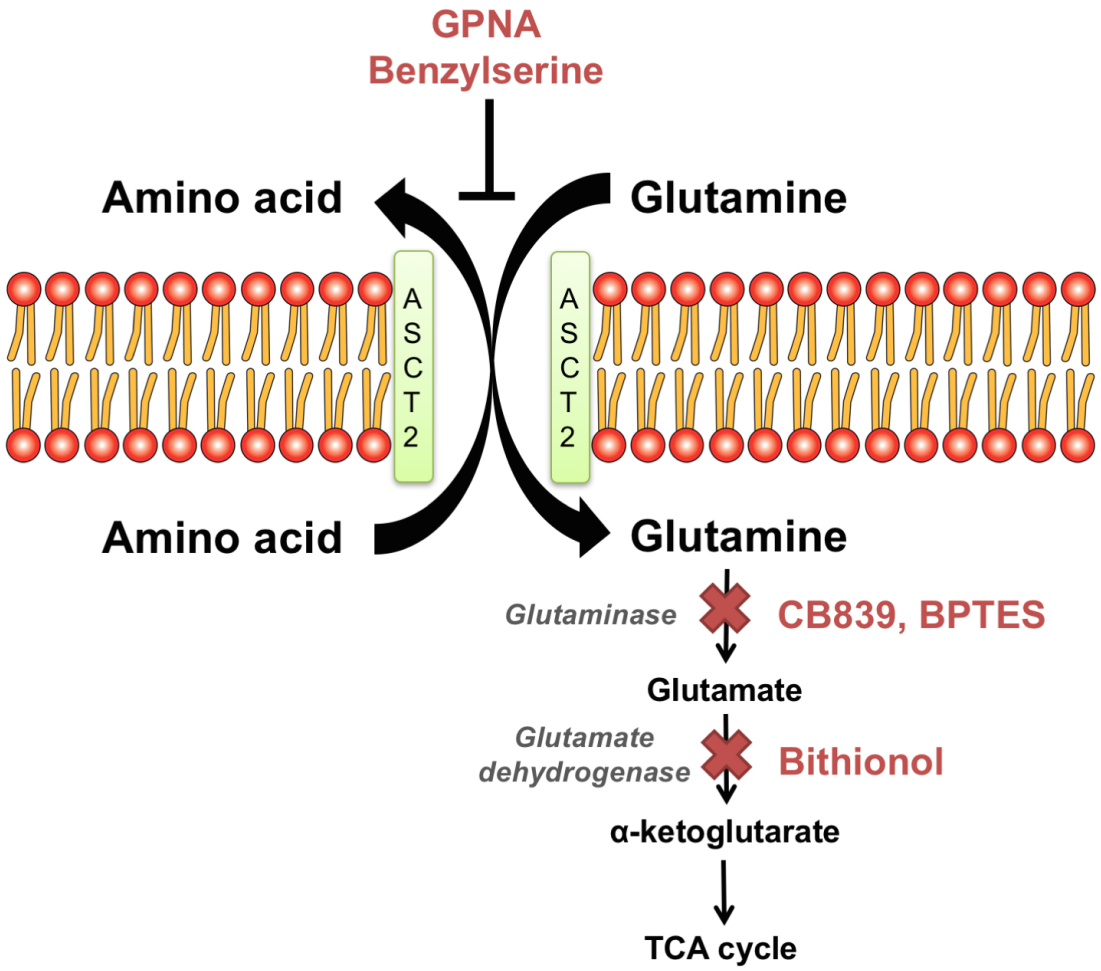

Figure 1.6 Targeting of glutamine metabolism in cancer. The use of different compounds in targeting various stages of glutamine metabolism has been described. This diagram also illustrates the antiporter mechanism of high-affinity glutamine transporter ASCT2, as described earlier in the chapter.

Targeting of ASCT2 by GPNA has been shown to inhibit growth, cell cycle progression and mTORC1 (mammalian target of rapamycin complex 1) activity of TN breast cancer cell lines, with the growth effect recapitulated in xenograft models exhibiting stable knockdown of ASCT2 [84]. CB-839 has been reported to have significant growth effect on several breast cancer cell lines *in vitro* and demonstrated significant antitumour effects in xenograft models both as a monotherapy and in combination with paclitaxel [88]. Published work with specific regards to bithionol in breast cancer is relatively sparse, with one report describing it to reduce breast cancer invasiveness *in vitro*, and inhibit xenograft growth in a mouse model [92].

Most of these compounds remain in preclinical use, with the exception of CB-839 which is now in early phase clinical trials, including one in TN breast cancer where its efficacy in combination with paclitaxel is being evaluated (NCT03057600).

1.5.6 Involvement of ASCT2 and LAT1 in mTOR signalling

Both ASCT2 and LAT1 have been implicated in signalling to the mammalian target of rapamycin (mTOR) pathway, via uptake of glutamine by ASCT2, followed by rapid efflux of glutamine by LAT1 in exchange for essential amino acids (such as leucine), which in turn activate mTORC1 [93]. mTOR is a serine/threonine kinase which functions as a key regulator of cellular growth and metabolism, being a downstream member of the PI3K, MAPK/ERK and AMPK pathways, and is a target for development of anti-cancer therapies.

A key example of an mTOR inhibitor in clinical use is everolimus, which targets mTORC1. Again, citing breast cancer as an example, everolimus has been licensed in the USA and Europe for the treatment of post-menopausal women with hormone receptor positive, HER2-negative breast cancer in combination with exemestane, after failure of an aromatase inhibitor (AI). There is extensive ongoing research in its use beyond this indication, including its use in isolation after failure of an AI, first-line with an AI for ER+ advanced breast cancer, combination with adjuvant endocrine therapy in high-risk disease introduced at different time points, combating trastuzumab resistance in HER2+ cancer and neoadjuvant treatment of TN cancer [94].

1.5.7 Hypoxia and amino acid metabolism

The hypoxic niche and its impact on cancer progression and treatment resistance is now well-recognised [95]. Integral to the tumour cell response to hypoxia, is the induction of hypoxia inducible factors (HIF) which mediate a panel of transcriptional responses to support survival under hypoxic stress [96]. These are wide ranging and include factors to support survival, stemness, dormancy, angiogenesis, redox homeostasis and metabolic re-programming [95]. The effects of HIF activation on the tumour metabolome are again far-reaching. With specific reference to amino acids, the uptake of glutamine, leucine and glutamate have been shown to increase under hypoxia [97]. LAT1 has been described to be a HIF-2α target, which induces its expression to potentiate mTORC1 signalling [98].

1.6 Imaging in personalised medicine and early treatment response assessment in cancer

1.6.1 Rationale

With an expanding repertoire of neoadjuvant, adjuvant and systemic therapies, there is an ongoing need for appropriate patient selection and accurate early assessment of treatment response, to inform optimisation of personalised treatment, while minimising the morbidity and cost of futile therapies.

A good example of the holy grail of imaging in personalised medicine to work towards, may be drawn directly from the aforementioned burgeoning development of therapeutics targeting glutamine metabolism. Here, the principle would be to guide patient selection for such therapies with amino acid PET imaging using knowledge-based interpretation of tracer uptake as a functional read-out of the relevant aspects of underlying tumour biology.

Another potential utility for amino acid imaging would be quantification of mTOR activity in such settings, using ASCT2 and LAT1 expression as a surrogate. This information could potentially be used to select appropriate candidates for mTOR targeted treatments, and monitoring response. This hypothesis could be extended to other therapies targeting other members of the mTOR axis, such as metformin in the context of mitochondrial complex 1 inhibition and consequent activation of the AMPK pathway.

While this remains some distance away, there are more immediate examples of personalising treatment and guiding decisions based on *early assessment* of response. One such example is in the setting of neoadjuvant chemotherapy (NAC) for breast cancer, where there has been evidence to suggest optimising the chemotherapy regimen during treatment may achieve higher rates of pathological complete response (pCR) [99-101].

1.6.2 Performance and limitations of ^{18}F-FDG as an early treatment response marker

Several studies have been performed to characterise the use of early treatment response using ^{18}F-FDG PET in predicting response to NAC, with a meta-analysis involving 745 patients reporting pooled sensitivities, specificities, positive predictive values and negative predictive values for predicting response to be 80.5% (95% CI, 75.9%-84.5%), 78.8% (95% CI, 74.1%-83.0%), 79.6% and 79.5% respectively [102]. Some groups have described the use of follow-up ^{18}F-FDG PET at as early as after one cycle of NAC [103-105]. Importantly, it has been observed that the degree of ^{18}F-FDG uptake at baseline and follow-up scans are highly dependent on the tumour subtype, with different patterns identified in each subtype [104, 106].

A prime example of this is in a study by Groheux et al. [107]. His team aimed to establish the best PET parameters for predicting complete pathological response to NAC for different receptor subtypes in a cohort of 169 patients, who had ^{18}F-FDG PET/CT scans at baseline and after two cycles of NAC. These were found to be changes in SUV_{max} and total lesion glycolysis (TLG)

in TN breast cancer (AUCs 0.86 and 0.88 respectively), absolute SUV_{max} after two cycles of NAC in HER2-positive breast cancer (AUC 0.93), and changes in TLG after two cycles of NAC in ER+/HER2-negative cancers (AUC 0.8 - this was associated with partial or complete response). Across the entire study cohort and individual receptor subtypes, there were significant differences in the percentage change in PET parameters between responders and non-responders. However, there was considerable overlap between the range of values. For example, the median percentage change of SUV_{max} in TN breast cancer was -73% in responders compared to -40% in responders ($p<0.001$). However, the ranges for these two groups were -95% to -49% and -89% to 17% respectively.

Trends for predicting response at the outset, based on SUV_{max} on baseline ^{18}F-FDG PET, were also reported by Groheux et al. [107]. Interestingly, a higher baseline SUV_{max} in TN breast cancer was found in responders, while the same observation in HER2-positive cancer was seen in non-responders. No significant trend was observed in ER+/HER2-negative cancers. The pathological complete response rate to NAC is low in ER+/HER-negative cancers because of low chemosensitivity, and the degree of ^{18}F-FDG uptake is relatively low compared to the other receptor subtypes, as demonstrated in Groheux's study and others [103, 107]. Therefore, PET imaging of a non-glucose metabolic pathway may be particularly useful in this tumour subset which may benefit from appropriate patient selection.

However more work is needed to characterise the use of ^{18}F-FDG PET in this area. Different thresholds for PET parameters have been proposed for the early response assessment to NAC, ranging from the use of absolute SUV_{max} values and thresholds of anywhere between 40% to 88% decrease in SUV_{max} on follow-up compared to baseline PET [102]. There may also be limitations to using glucose metabolism as a predictor, as, in regimens where anti-HER2 therapy is commenced at the outset for HER2-positive cancer, the accuracy of PET appears to be modest (accuracy 76% [103], AUC 0.35 [108]) compared to imaging during chemotherapy prior to anti-HER2 therapy (accuracy 90%, AUC 0.86 [109]). This has been postulated to be due to the impact of such agents on reducing GLUT1 and hexokinase II activity [110] and initial induction of inflammation [108], in addition to a cytotoxic effect [109, 110]. In the wider clinical setting, inflammation is a common non-malignant cause of increased ^{18}F-FDG uptake.

The pertinent caveat to consider with NAC guided by early response assessment, is that while it has been shown to achieve higher rates of pCR, its impact on overall survival is yet to be proven. The landmark German Breast Group GeparTrio phase III trial compared the outcomes of both early responders and early non-responders who received conventional NAC compared to an intensified / modified regimen of NAC, with early assessment of response evaluated by clinical examination and conventional imaging [99]. There was no difference in overall survival between the treatment regimens in either category of responders. An improvement in disease-free survival was observed with intensified / modified regimens in both early responders and

nonresponders, however, interestingly, this trend was restricted to patients with ER+ disease [99].

This leads on to another growing avenue of breast cancer therapy, namely the targeting of tumour metabolism, where interrogation of underlying metabolism by non-invasive PET imaging may have more translational avenues.

1.7 Experience of ^{18}F-fluciclovine in breast cancer

There has been limited experience of using fluciclovine in breast cancer to date, both in the preclinical and clinical research setting.

1.7.1 Preclinical experience

Prior to commencement of this doctorate, the only preclinical work of fluciclovine in breast cancer was described by Liang et al. [69]. They demonstrated increased ^{18}F-fluciclovine uptake in a panel of high grade breast cancer lines compared to low stage / non-malignant cell lines, and in an orthotopic breast cancer model [69]. Since then, Oka et al. have also performed comparisons of multiple tracers in visualising bone metastases in a rat breast cancer model [111]. Here, the authors showed that FDG and fluciclovine were both able to demonstrate early osteolytic bone metastases.

Despite the detailed work in characterising uptake mechanisms of fluciclovine in prostate cancer, this remains to be established in breast cancer.

1.7.2 Clinical experience

Only two groups have described their clinical experience of ^{18}F-fluciclovine imaging in breast cancer to date, published during the course of this doctorate.

Ulaner et al. characterised ^{18}F-fluciclovine uptake in a cohort of 27 women with newly diagnosed invasive carcinoma (19 ductal, 8 lobular) [112]. In addition to demonstrating positive ^{18}F-fluciclovine uptake in all primary tumours across the cohort, 95% (20/21) of patients with histopathologically proven axillary nodal disease had concordant ^{18}F-fluciclovine axillary nodal uptake on PET. The authors also anecdotally described 2 cases of unexpected ^{18}F-fluciclovine avid internal mammary lymphadenopathy which were histologically confirmed, one of which was ^{18}F-FDG negative.

In a subset (n=14) comparison with ^{18}F-FDG [112], increased ^{18}F-FDG uptake was reported across all the tumours as well [112]. Of interest, ^{18}F-fluciclovine uptake in the 4 lobular cancers in this cohort was higher than ^{18}F-FDG (median ^{18}F-fluciclovine SUV_{max} 6.1 (range 4.5-10.9) vs median ^{18}F-FDG SUV_{max} 3.7 (1.8-6.0)) raising potential diagnostic utility for this tumour type where ^{18}F-FDG has distinct limitations [113]. The trend was opposite in ductal carcinomas, bearing in mind positive uptake was demonstrated with both tracers across all the patients.

The same group published a follow-up report describing the changes in ^{18}F-fluciclovine uptake following *completion of* neoadjuvant chemotherapy (as

opposed to mid-treatment to assess early response) in the same cohort (n=24, after 3 withdrawals) [114]. They reported all tumours across the cohort demonstrated a decrease in ^{18}F-fluciclovine uptake, and the quantum of this decrease correlated strongly with the degree of tumour burden reduction on pathological assessment of the post-surgical resection specimen (Spearman's rho 0.79, $p<0.001$) [114]. Across both reports, apart from comparison of ^{18}F-fluciclovine uptake between ductal and lobular carcinomas, patterns of ^{18}F-fluciclovine uptake across molecular subtype or other histopathological / biological parameters were not described.

The only other group to report experience of using ^{18}F-fluciclovine in breast cancer provided some insight in this respect, in a small exploratory cohort of 12 women (17 lesions: 13 invasive carcinoma, 4 benign aetiology) who underwent ^{18}F-fluciclovine PET imaging prior to surgical resection of breast lesions [115]. When the 13 tumours were stratified according to molecular subtype, ^{18}F-fluciclovine uptake was highest in TN tumours, followed by ER+, then HER2+ disease. High Nottingham grade tumours (Grade 3) were reported to have higher ^{18}F-fluciclovine uptake compared to Grade 1-2 tumours, and there was a weakly positive correlation between ^{18}F-fluciclovine uptake and proliferation index (measured by Ki-67). They also reported that the 4 benign lesions all had ^{18}F-fluciclovine uptake close to background tissue.

1.8 Summary and aims

1.8.1 Summary

In the setting of the increasing evidence of the superior diagnostic performance of ^{18}F-fluciclovine PET/CT in BCR, investigations to establish its impact on clinical management, factors influencing scan positivity, and optimising the reconstruction techniques used are warranted. Limited clinical studies have reported preliminary results to suggest ^{18}F-fluciclovine as a potential alternative to ^{18}F-FDG for localised and systemic disease detection in breast cancer. The increased availability of biological therapies and metabolic targets in breast cancer suggests that the potential utility of ^{18}F-fluciclovine extends well beyond disease detection. Exploring these avenues warrant the robust characterisation of fluciclovine uptake mechanisms in breast cancer, to inform its use in the early assessment of treatment response *in vitro* and *in vivo*. Finally, investigation on using fluciclovine to characterise underlying breast cancer biology needs to be performed with a clinical focus, to allow the immediate translation of insights gained into future clinical research and practice.

1.8.2 Aims

Therefore, the overall aims of this DPhil project were to:

1. set up a multicentre clinical trial to investigate the impact of ^{18}F-fluciclovine imaging on clinical management of men with BCR of prostate cancer and factors influencing scan positivity, and optimise its application with modern PET image reconstruction technology as a substudy;
2. establish the transport mechanisms of fluciclovine in breast cancer;

3. explore the utility of fluciclovine in early assessment of response to treatments of related metabolic and biological targets;
4. set up a clinical study to investigate how ^{18}F-fluciclovine uptake can be used to characterise breast cancer biology.

Chapter 2 : Materials and methods

2.1 FALCON TRIAL

FALCON (Fluciclovine (^{18}F) PET/CT in biochemicAL reCurrence Of Prostate cancer) was a UK multi-centre study (NCT02578940).

2.1.1 Objectives and endpoints

The trial endpoints reported in this thesis are listed in and limited to the Oxford cohort.

Table 2.1: FALCON trial objectives and endpoints pertaining to this thesis.

	Objectives	**Endpoints**
Primary	To assess the clinical impact of ^{18}F-fluciclovine PET/CT in affecting management decisions in patients with BCR being considered for radical salvage treatment (with curative intent).	The record of the revised management plan post ^{18}F-fluciclovine PET/CT scan in comparison to the pre-scan intended management plan.
Secondary	To assess possible improvement in outcome of radical salvage treatment based on ^{18}F-fluciclovine PET/CT being included in the assessment.	The proportion of patients who have a sustained response to radical salvage therapy.
	To assess the PSA threshold for positive lesion detection by ^{18}F-fluciclovine PET/CT in BCR To assess the safety of ^{18}F-fluciclovine injection in patients undergoing PET/CT	PSA levels in relation to scan positivity will be analysed to determine the optimal PSA threshold for detecting recurrent PCa by ^{18}F-fluciclovine PET/CT.

The influence of other clinicopathological factors on scan positivity, namely PSA doubling time (PSA_{dt}), PSA velocity (PSA_{vel}), primary pathological variables and BCR-free survival were also explored.

2.1.2 Study design

The study population consisted of patients with first diagnosis of BCR of previous radically treated PCa who were being considered for radical salvage therapy. Patients had a ^{18}F-fluciclovine PET/CT scan in addition to standard work-up for radical salvage therapy. The clinical utility of ^{18}F-fluciclovine PET/CT was assessed by recording changes to the intended management plan influenced by the scan result.

In patients who went on to receive radical salvage therapy (irregardless of influence by ^{18}F-fluciclovine scan), PSA follow-up was performed between 7-8 months after completion of treatment. The study-wide design is illustrated in Figure 2.1. The methods and results reported in this thesis are limited to the Oxford cohort: Visits 1 to 4, and PSA follow-up of patients who underwent radical salvage therapy.

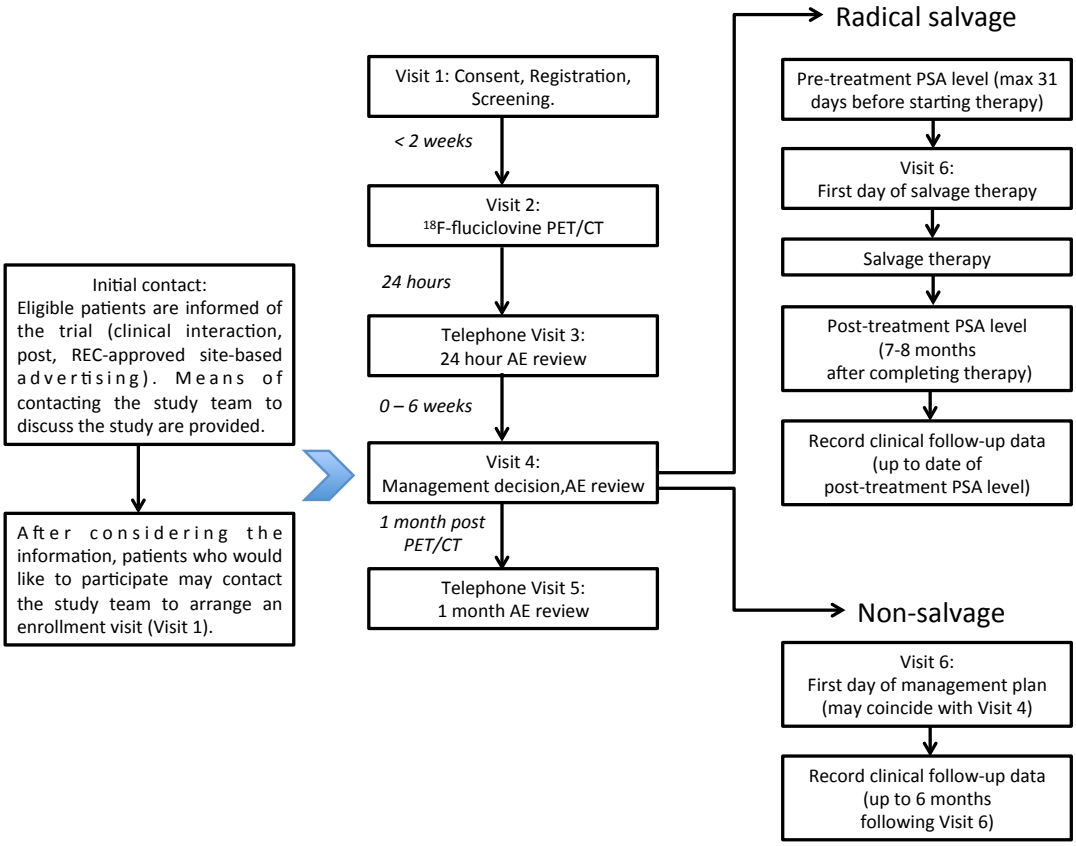

Figure 2.1: Summary flow chart of FALCON study design. REC: research ethics committee, AE: adverse event.

2.1.3 Regulatory approval

Research ethics committee (REC) approval (Berkshire REC 15/SC/0437), study-wide governance review (CSP 17789) and local R&D approval (PID 11458) were obtained. Written informed consent was obtained from all participants.

2.1.4 Inclusion criteria

(1) The subject is a male ≥18 years old.

(2) The subject has had an original diagnosis of PCa and underwent radical curative therapy at least 3 months before enrolment, and has been diagnosed with BCR on the basis of:

a. Post RRT / brachytherapy: Increase in PSA level ≥2.0 ng/mL above the nadir level after radiotherapy or brachytherapy (ASTRO-Phoenix criteria) [13], or

b. Post RP: EITHER two consecutive rises in PSA and final PSA >0.1 ng/mL OR three consecutive rises in PSA, This definition is also applicable to subjects with PSA persistence post RP (where the PSA fails to fall to undetectable levels).

    i. In addition, the subject post RP, should have a PSA doubling time of ≤15 months OR PSA level ≥1.0 ng/mL at time of recruitment. The PSA_{dt} will be calculated using the Memorial Sloan Kettering Cancer Centre nomogram (http://www.mskcc.org/nomograms/prostate/psa-doubling-time), based on a minimum of two PSA levels within 12 months of screening, taken after the last recorded nadir PSA available at time of screening.

(3) The subject has not had previous recurrences of PCa, i.e. this is the first diagnosis of BCR.

(4) The subject is being considered for radical salvage therapy.

(5) The subject is able and willing to comply with study procedures, and signed, dated and timed informed consent is obtained before any study-related procedure is performed.

(6) The subject's Eastern Cooperative Oncology Group [ECOG] performance status 0-2.

(7) The subject should not have received androgen-deprivation therapy within 3 months of screening.

(8) The subject has a normal or clinically acceptable medical history and vital signs findings at screening (up to 14 days before administration of study drug).

2.1.5 Exclusion Criteria

(1) The subject has been previously included in this study.

(2) The subject has received, or is scheduled to receive, another investigational medicinal product (IMP) from 1 month before to 1 week after administration of ^{18}F-fluciclovine injection.

(3) The subject has known hypersensitivity to ^{18}F-fluciclovine injection or any of its constituents.

(4) The subject has had a choline PET/CT scan within 3 months of the screening visit.

(5) The subject has bilateral hip prostheses.

2.1.6 Baseline measures

The intended management plan, age, prostate cancer treatment history (including primary treatment, primary histopathological variables), date of BCR and PSA values leading to BCR. The latter were used to calculate the PSA_{dt} and PSA_{vel} using the Memorial Sloan Kettering Cancer Centre PSA

doubling time online tool (https://www.mskcc.org/nomograms/prostate/psa-doubling-time).

2.1.7 ^{18}F-Fluciclovine PET/CT imaging protocol

PET/CT examinations were performed on a 3D mode time of flight (ToF) GE Discovery 710 PET/CT system (GE Healthcare, Milwaukee, USA). The patients were required to fast for at least 4 hours prior to their scan. Imaging commenced 3-5 minutes post-injection of ^{18}F-fluciclovine (320 to 430 MBq) and covered the skull base to proximal thighs. The PET images were acquired under normal tidal respiration, commencing caudally, for five minutes per bed position for the first two bed positions (over the pelvis), and three minutes per bed position for the remainder of the acquisition. The CT was performed using a pitch of 0.984, 120 kV, automA with a noise index of 25. Scans were performed within a median of 7 days (range 1-15 days) from the screening PSA measurement.

2.1.8 ^{18}F-Fluciclovine PET/CT image interpretation

All scans were interpreted by Dr. Eugene Teoh, and two other consultant radiologists, all of whom have completed formal image interpretation training and assessment.

2.1.9 Revised management plan

Scan reports were prospectively reviewed by the clinician in charge of the participant's care, and a revised management plan (or lack thereof) would be documented on the basis of the scan report.

2.1.10 PSA follow-up

Patients who went on to receive radical salvage therapy (irregardless of scan outcome) had a repeat PSA performed 7-8 months post-treatment. Patients who had a reduction of PSA ≥50% were classed as responders, while non-responders were defined as having had a reduction of PSA <50%, or increase in PSA [15].

2.1.11 Statistical analysis

Differences in PSA, PSA kinetics and BCR-free survival between patients with positive and negative scans were evaluated using the Mann-Whitney U test. Differences in primary pathological variables between patients with positive and negative scans were evaluated using the Chi-square test. Uni-variate and multi-variate analyses were performed using binary logistic regression. Differences in proportion of responders to ^{18}F-fluciclovine guided versus standard radiotherapy was evaluated using Fisher's exact test. Statistical analyses and graphical output were performed on IBM SPSS Statistics 24.0 (IBM Corporation, New York, USA) and GraphPad Prism version 7.0a for Mac OS X (GraphPad Software, La Jolla California, USA) respectively. P values <0.05 were considered statistically significant.

2.1.12 BPL substudy: Aim

The aim of this study was to compare BPL to standard PET reconstruction of ^{18}F-fluciclovine images and determine the optimum penalisation factor (β) for clinical use of BPL in ^{18}F-fluciclovine whole body imaging.

2.1.13 BPL substudy: Image reconstruction

Fifteen ^{18}F-fluciclovine whole body scans performed in the FALCON trial (Oxford site) between October 2015 and August 2016 for biochemical recurrence of prostate cancer were retrospectively selected. Sinograms of the 15 whole body scans were reconstructed using three different algorithms, each of which used the CT scan for attenuation correction and the same normalisation correction factors with scatter and randoms corrected as has been previously described [8-10]. The first algorithm was OSEM (ToF OSEM, VPFX, GE Healthcare), used with 2i, 24ss and 6.4mm filter. The second was using OSEM+PSF, henceforth referred to as PSF (ToF OSEM PSF, 3i, 24ss, 2mm filter [11]), and the third was BPL using a range of penalisation factors (β): 100, 200, 300, 400, 500 and 600.

2.1.14 BPL substudy: Semi-quantitative analysis

The following parameters were measured on each of the reconstructions: lesion SUV_{max}, SUV_{mean} and standard deviation (SUV_{dev}, noise) of reference organs (marrow, spleen, blood pool, liver). Lesions were defined as small foci of presumed local or distant recurrence. The SUV_{max} of each lesion was recorded using a standard volume of interest (VOI) tool. Organ SUVs were measured as follows: marrow - L3 vertebra using a 1.5cm edge cube VOI, spleen – interpolar region using a 2.0cm diameter spherical VOI, blood pool – mid-thoracic aorta using a 1.0cm diameter, 2.0cm long cylindrical VOI, liver - right lobe of liver using a 3.0cm diameter spherical VOI. Signal-to-noise (SNR) and signal-to-background (SBR) were calculated. Lesion SNR was defined as lesion SUV_{max} divided by marrow SUV_{dev}. Lesion SBR was defined as lesion SUV_{max} divided by marrow SUV_{mean}. Marrow uptake was used for

normalisation. Organ SNR was calculated as organ SUV_{mean} divided by organ SUV_{dev}.

2.1.15 BPL substudy: Statistical analysis

Statistical comparisons were made with reference to OSEM as the most widely used PET reconstruction to date, and performed using the one-way ANOVA with Dunnett's multiple comparisons post-hoc test. Statistical analyses were performed using GraphPad Prism version 7.0a for Mac OS X (GraphPad Software, La Jolla California, USA). P values ≤0.05 were considered to be statistically significant.

2.1.16 BPL substudy: Clinical evaluation – reconstruction and visual analyses

Ten of the 15 scans were used for this component of the study. Visual analyses of the OSEM, PSF, BPL β 200, 300, 400, 500 and 600 reconstructions, were performed by two consultants (designated Reader 1 and 2 respectively) with dual accreditation in clinical radiology and nuclear medicine, both with more than 10 years of subspecialty experience. The reconstructions were labelled A to G in a randomised order, with the CT component available for image fusion and non-attenuation corrected images for reference. Cases were reviewed sequentially, and the reconstructions were scored (from 1 to 5) according to four image quality parameters (Table 2.2).

Table 2.2: Scoring system applied to the four image quality parameters in the visual analysis.

Score	Overall image quality / Lesion conspicuity	Overall noise level (excluding marrow) / Background marrow image quality
1	Not reportable	Non-diagnostic
2	Poor	Numerous heterogeneities throughout entire study, reduced diagnostic quality
3	Satisfactory	Numerous small heterogeneities
4	Good	Minimal heterogeneities
5	Excellent	No significant noise

Readers also indicated their most and least preferred reconstruction for each case. The proportions of the highest and lowest ranked reconstructions were calculated for each parameter.

2.2 PRE-CLINICAL WORK

2.2.1 Cell culture

All cell lines were obtained from authenticated laboratory stock (Molecular Oncology Laboratories, WIMM) and maintained up to 25 passages. Cells were maintained in 25 mM glucose DMEM (Life Technologies) supplemented with 10% FCS. Cells were passaged when they reached approximately 80% confluence. In experiments involving CB-839 and bithionol, cells were maintained in RPMI 1640 (Life Technologies) medium supplemented with 10% FCS.

2.2.2 Drugs

The following drugs were used in this project: CB-839 (Selleckchem), bithionol (Sigma), metformin (Calbiochem) and everolimus (Cell Signalling).

2.2.3 Baseline expression of AATs in cell line panel

Cells were seeded and grown in 10 cm culture dishes for 3 days in 5 mM glucose DMEM supplemented with 10% FCS, and harvested for protein and RNA at approximately 80% confluence.

2.2.4 RNA extraction and quantitative PCR

RNA extraction was performed using TRIzol® reagent (Life Technologies) according to manufacturer's instructions. cDNA was synthesized from 900 ng of RNA per sample using the High-Capacity cDNA Reverse Transcription Kit (Applied Biosystems) according to manufacturer's instructions. RNA quantification was performed with NanoDrop (Thermo Fisher Scientific).

Primers for qPCR were designed using either the Universal ProbeLibrary Assay Design Centre (Roche Applied Science) or PrimerBank (Massachusetts General Hospital) and were synthesised by Life Technologies Ltd. The sequences are detailed in .

qPCR was performed with the SensiMix SYBR No-Rox kit (Bioline) according to manufacturer's instructions using the Applied Biosystems 7900HT Fast Real-Time PCR System (Thermo Fisher Scientific) with the following steps: enzyme activation at 95 ^{o}C for 10 minutes, 40 cycles of denaturing at 95 ^{o}C for 15 seconds and extension at 60 ^{o}C for 1 minute. Beta-actin was used as the housekeeping gene.

Table 2.3: Primer sequences used for qPCR.

AAT/protein	Gene	Forward sequence (5'-3')	Reverse sequence (5'-3')
ASCT2	SLC1A5	cggtcgaccatatctccttg	ctacattgaggacggtacagga
Beta actin	ACTB	ctggaacggtgaaggtgaca	aagggacttcctgtaacaacgca
LAT1	SLC7A5	ccgtgaactgctacagcgt	cttcccgatctggacgaagc

2.2.5 Protein extraction and Western blotting

Cells were washed twice in cold PBS, scraped in lysis buffer (RIPA buffer (Sigma) supplemented with protease inhibitor cocktail (cOmplete, Roche Diagnostics) and phosphatase inhibitor cocktail (PhosSTOP, Roche Diagnostics)) and incubated on ice for 5 minutes. The lysates were collected into tubes and centrifuged at 13,000 rpm for 10 minutes at 4 ^{o}C. The supernatants were transferred into new tubes and protein levels measured using a modified Lowry assay (DC Protein Assay, Bio-Rad). Samples were mixed with loading buffer, loaded on 4-12% Bis-Tris gels (Life Technologies) and ran with MPS SDS running buffer (Life Technologies) for 50 minutes at 200 V.

Semi-dry transfer of the gels was performed at 20 V for 60 minutes using 2X transfer buffer (Life Technologies). Blocking was performed for 1 hour at room temperature in 5% BSA in TBS-Tween. The primary antibodies () were diluted to the appropriate concentration in 5% BSA in TBS-Tween. The membranes were incubated with primary antibody overnight at 4 ^{o}C. After washing, the membranes were incubated with the appropriate HRP-linked secondary antibody, diluted to the appropriate concentration in 5% BSA in TBS-Tween, for 1 hour at room temperature. After washing, chemiluminescent detection

reagent was applied to the membranes, and visualisation was performed using the ImageQuant LAS 4000 (GE Healthcare).

Densitometry was performed using ImageJ (imagej.nih.gov), and normalised to beta-actin.

Table 2.4: Antibodies used for Western blotting.

Antibody	Dilution	Catalogue no	Source
4EBP1	1:1000	9644S	Cell Signaling
Actin-HRP	1:25000	A3854	Sigma
ASCT2	1:1000	5345	Cell Signaling
LAT1	1:1000	5347	Cell Signaling
P70S6K	1:1000	9202	Cell Signaling
phospho-4EBP1	1:1000	2855P	Cell Signaling
phospho-P70S6K Thr389	1:1000	9234P	Cell Signaling
phospho-S6	1:1000	2211S	Cell Signaling
Rabbit-HRP	1:1000	P0448	Dako
SNAT2	1:1000	BMP081	MBL International
S6	1:1000	2217	Cell Signaling

2.2.6 ASCT2 and LAT1 knockdown using siRNA transfection

Knockdown of ASCT2 and LAT1 expression was achieved using the respective siRNA pools (SMARTpool ON-TARGETplus, Dharmacon, GE Healthcare) and reverse transfection with Lipofectamine® RNAiMAX (Thermo Fisher Scientific) according to manufacturer's instructions, in 5 mM glucose DMEM (Life Technologies). Fresh culture medium was introduced 24 hours post-transfection. Cells were utilised for respective assays (protein extraction, ^{14}C-FACBC uptake assay, fixation) 72 hours post-transfection.

2.2.7 Proliferation assays

Depending on cell line, 1,000-5,000 cells per well were seeded in 96-well plates and allowed to settle overnight. Cells were then treated using a range of concentrations of drug in 5 mM glucose DMEM (RPMI 1640 medium for CB-839 and bithionol). Cells were treated for 5 days, with supplementation of fresh culture medium every 2 days. Proliferation assays were performed using the CyQUANT® Cell Proliferation Assay Kit (Life Technologies) according to manufacturer's instructions.

2.2.8 Measurement of fluciclovine uptake in vitro

Anti 1-amino-3-fluorocyclobutane[^{14}C]carboxylic acid (^{14}C-FACBC, 2.15 GBq/mmol) was synthesised by Quotient Bioresearch (Cardiff, UK) and supplied by Blue Earth Diagnostics Ltd (Oxford, UK).

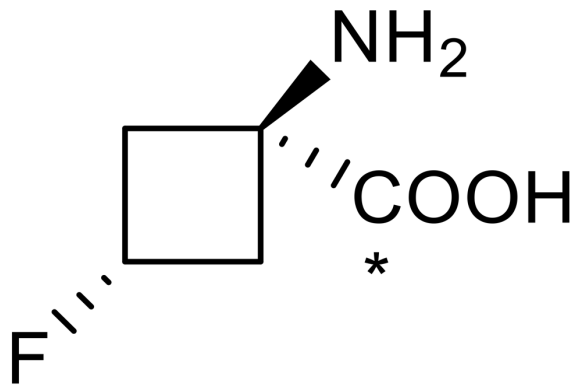

Figure 2.2: Chemical structure of ^{14}C-FACBC used in this project, demonstrating the ^{14}C (denoted by *) within the carboxyl group, and stable fluorine (^{19}F) within the cyclobutane ring in lieu of radioactive ^{18}F.

Cells were seeded on 24-well flat bottom tissue culture plates with 1 mL of culture medium. The number of cells seeded was dependent on the cell line and duration of experiment, optimised for the uptake assay to be performed

when cells were approximately 80% confluent in the control wells. ^{14}C-FACBC uptake assays were performed using ^{14}C-FACBC suspended in a buffer of 140 mM sodium chloride, 5 mM potassium chloride, 0.9 mM calcium chloride, 1.0 mM magnesium chloride and 10 mM HEPES, pH corrected to 7.3 with sodium hydroxide.

Following removal of culture medium, cells were washed twice with buffer, and incubated with 300 µL of buffer containing ^{14}C-FACBC. Following optimisation, the concentration of ^{14}C-FACBC used was 2.5 µM and incubation time was 5 minutes. After the requisite incubation time, the buffer was removed and the cells were washed twice with ice-cold buffer prior to lysis with 0.1 M sodium hydroxide. Radioactivity in the cell lysate was measured with the LS 6500 Multi-Purpose Scintillation Counter (Beckman Coulter, Brea, CA, USA) using Optiphase Hisafe 3 scintillation cocktail (Perkin Elmer, Waltham, MA, USA). For every assay, a separate duplicate plate was prepared for protein quantification using a modified Lowry assay (as described in the technique for Western blotting). Tracer uptake was then expressed as pmol/mg protein. Technical duplicates were performed in each assay and a minimum of three biological replicates were performed for each experiment.

2.2.9 Competitive inhibition of ^{14}C-FACBC uptake

The respective amino acid or synthetic inhibitor was reconstituted in the buffer to be used in the uptake assay, pH corrected to 7.3. A final concentration of 1 mM of amino acid / inhibitor was applied uniformly across the panel, and the

^{14}C-FACBC uptake assay was performed as described in the respective part of this section. To define basal transport levels, ^{14}C-FACBC uptake was also performed on ice.

Table 2.5: Amino acid / inhibitor used for competitive inhibition experiments.

Amino acid / inhibitor	Catalogue	Source
L-Alanine	A7627	Sigma
L-Asparagine	100794	MP Biomedicals
L-Cysteine	C1276	Sigma
L-Glutamine	17-605E	Lonza
Glycine	G7126	Sigma
GPNA (L-Glutamic acid γ-(p-nitroanilide) hydrochloride)	G6133	Sigma
L-Histidine	101954	MP Biomedicals
L-Isoleucine	I2752	Sigma
L-Leucine	L8000	Sigma
MeAIB (α-(Methylamino)isobutyric acid)	M2383	Sigma
L-Methionine	M3508	Sigma
L-Phenylalanine	78019	Sigma
L-Serine	S4500	Sigma
L-Threonine	T8625	Sigma
L-Tryptophan	T0254	Sigma
L-Valine	V0500	Sigma

2.2.10 Hypoxia work

Incubation under hypoxic conditions was performed at either 1% or 0.1% oxygen (5% CO_2) using an INVIVO2 400 hypoxic chamber (Pro-Lab Diagnostics, Toronto, Canada).

2.2.11 In vivo experiments

All protocols were performed under Home Office regulations. Five to 6 week old female Balb/c nu/nu mice underwent subcutaneous injection of tumour cells into the mammary fat pad. Tumour cells were suspended in a mixture of 50 µL of serum free medium and 50 µL Matrigel (BD Biosciences). For each cell line, the number of cells injected per mouse were as follows: HCC1806 $2x10^6$ cells, MDA-MB-231 $2x10^6$ cells and MDA-MB-468 10^7 cells. All treatments were commenced two weeks after tumour injection, when >75% of xenografts had a GMD ≥ 4 mm.

2.2.12 ^{18}F-fluciclovine synthesis for in vivo imaging

^{18}F-Fluciclovine was synthesised by Thomas Wilson and Dr. Stefan Verhoog from the Gouverneur Group, University of Oxford using previously described methods [116]. ^{18}F was produced by Alliance Medical (UK) and radiosynthesis was performed on a NanoTek® automated microfluidic device (Advion). Synthesis was completed within 97 ± 5 minutes (n=7) after the start of synthesis. The overall radiochemical yield was 22.1 ± 2.1% of start of synthesis (n=7). The radiochemical purity of ^{18}F-fluciclovine was >99% on all occasions, assessed by radio-thin layer chromatography (MeCN: MeOH: H_2O : AcOH, 20:5:5:1) R_f: 0.40 – 0.50 (visualisation with ninhydrin).

2.2.13 ^{18}F-Fluciclovine PET/CT in vivo imaging protocol

Imaging was performed by Dr. Veerle Kersemans, supported by the Imaging Core, CRUK/MRC Oxford Institute for Radiation Oncology. Mice were fasted of solid food for ≥4 hours prior to tracer injection of ^{18}F-fluciclovine (10 MBq ±

20%) into the lateral tail vein at a rate of approximately 30 µL / 10 seconds. A static 10-minute acquisition was performed using the VECTor4 micro PET/CT imaging platform (MILabs, Utrecht, Netherlands) after a 20-minute uptake time, with the mouse lay prone on a heating pad and anaesthetised by 2-4% isofluorane on room air/oxygen (80/20). Core body temperature of the mice was maintained at 37 ˚C and respiration rate was maintained at 40-60/min for the duration of the scan acquisition.

PET data was acquired in list mode using MILabs acquisition software v7.39 at 15 min p.i. using 2 frames of 5 minutes (10 bed positions per frame). CT images were acquired at 50 kV and 0.24 mA using continuous rotation (40 degrees/s). All images were reconstructed with MILabs reconstruction software v3.24 on 0.8 mm isotropic 3D voxel grids using pixel-based ordered-subset expectation maximization (POSEM; 16 subsets, 6 iterations). Triple-energy-window based scatter correction (18F: 460-562 keV with background windows set to 439.6-460 keV and 562-582.4 keV) and CT-based non-uniform attenuation correction was applied. The CT scans were reconstructed using cone-beam filtered backprojection (Feldkamp algorithm) on a 0.2 mm voxel grid. The PET images were registered to the CT images and a quantification factor was applied to allow absolute quantitation of the PET data.

2.2.14 ^{18}F-Fluciclovine PET/CT in vivo image analysis

The images were analysed using Hermes Hybrid Viewer (HERMES Medical Solutions AB, Stockholm, Sweden). Radioactivity was quantified using the standardised uptake value (SUV) as performed in clinical practice. Measurement of tumour ^{18}F-fluciclovine uptake was performed using a 2 mm diameter spherical volume of interest (VOI) centred over the area of maximal uptake, adopted from the principles of SUV_{peak} measurement in clinical PET imaging. Tumour uptake is hereafter referred to as SUV_{peak}. For organ activity, SUV_{mean} was measured using spherical VOIs in the quadriceps muscle contralateral to the xenograft, liver and heart, measuring 3 mm, 4 mm and 4 mm in diameter respectively.

2.2.15 Bithionol experiment

HCC1806 xenografts were used for this experiment. Prior to commencing treatment, a ^{18}F-fluciclovine PET/CT was performed on all the mice to establish baseline levels of xenograft ^{18}F-fluciclovine uptake. The mice were then treated with daily oral gavage for 7 days. The control group received 2% DMSO in corn oil. The treatment group received 100 mg/kg bithionol suspended in 2% DMSO and corn oil. After 7 days of treatment, the mice underwent a repeat ^{18}F-fluciclovine scan. Thereafter, the mice received treatments for 5 days of the week with interleaving 2 day breaks until endpoint, defined as the first xenograft reaching GMD 12 mm.

2.2.16 Metformin experiment

MDA-MB-468 and HCC1806 xenografts were used for this experiment. Prior to commencing treatment, a ^{18}F-fluciclovine PET/CT was performed on all the mice to establish baseline levels of xenograft ^{18}F-fluciclovine uptake. The mice were then treated with daily intraperitoneal injections for 7 days. The treatment group received 250 mg/kg of metformin, dissolved to 50 mg/ml in PBS (i.e. 5 ml/kg). The control group received the equivalent 5 ml/kg of PBS. After 7 days of treatment, the mice underwent a repeat ^{18}F-fluciclovine scan. Thereafter, the mice received treatments for 5 days of the week with interleaving 2 day breaks until endpoint, defined as the first xenograft (cell line specific) reaching GMD 12 mm.

2.3 FRONTIER: An open-labelled study to characterise Fluciclovine (^{18}F) uptake measured by positron emission tomography in breast cancer

2.3.1 Objectives and endpoints

The trial endpoints are listed in Table 2.6. A preliminary analysis was planned on the first few participants accrued to ensure samples and images can be analysed and there were no changes required to processing or collection. This was not designed to be a formal interim analysis of results.

Table 2.6: FRONTIER study objectives and endpoints.

Primary Objective	**Endpoint**
To characterise the uptake of ^{18}F-fluciclovine on PET imaging in different breast cancer subtypes	Tumour standardised uptake values (SUV) in invasive breast cancer, classified by molecular type, on ^{18}F-fluciclovine PET imaging.
Secondary Objectives	**Endpoints**
To correlate the uptake of ^{18}F-fluciclovine on PET imaging in breast cancer with amino acid transporter (AAT) and related growth pathway expression	AAT and related growth pathway expression (including mTOR) quantified by immunohistochemical analysis, correlated with tumour SUVs.
To correlate the uptake of ^{18}F-fluciclovine on PET imaging in breast cancer with metabolomic analysis.	Tumour metabolite levels from metabolomics analysis, correlated with tumour SUVs.
Tertiary/Exploratory Objectives	**Endpoints**
To study metabolites and biomarkers in peripheral blood for relationship to ^{18}F-fluciclovine uptake, dependent upon initial results.	Correlation of tumour SUVs with: • Blood amino acid concentration including leucine and glutamine • Biomarkers including microRNA, circulating tumour DNA and exosome profiling.
To explore the use of dynamic PET parameters in characterising ^{18}F-fluciclovine uptake	Correlation of different dynamic PET parameters with the described pathological and biological entities.
To explore the use of ^{18}F-fluciclovine in the characterisation of AAT and related growth pathway gene expression profiles.	Correlation of tumour SUVs with AAT and related growth pathway network related gene expression.
To characterise the uptake of ^{18}F-fluciclovine in axillary lymph nodes involved with different breast cancer subtypes.	Nodal SUV of different breast cancer subtypes on ^{18}F-fluciclovine PET imaging.

2.3.2 Study design

This was an open labelled study designed to include up to 45 participants recruited from 1 site in the UK. Participants were to be women with

histologically proven ductal breast cancer measuring ≥ 2 cm scheduled to be treated by primary surgical resection. All participants would undergo ^{18}F-fluciclovine PET/CT of the breast tumour before surgery, and breast tumour sample collection during surgery. ^{18}F-Fluciclovine uptake by the tumour will then be compared to the tumour molecular type and results of the tumour sample analyses.

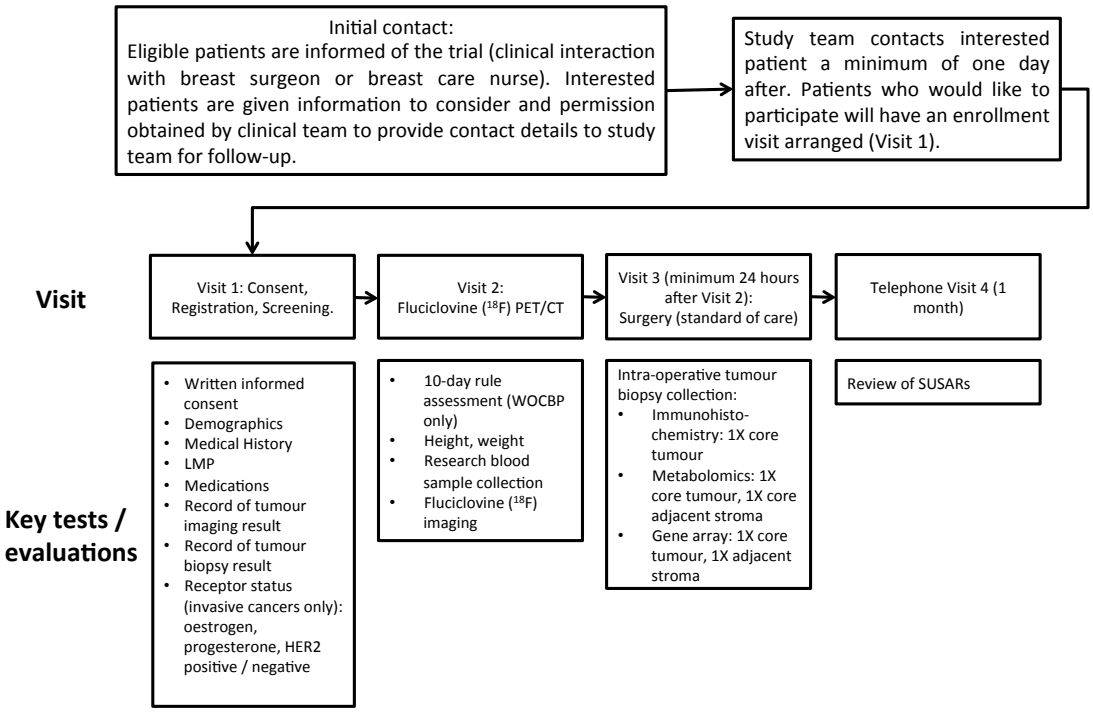

Figure 2.3: Summary flow chart of FRONTIER study design. WOCBP: women of childbearing potential, SUSAR: suspected unexpected serious adverse reaction.

2.3.3 Regulatory approval

Research ethics committee (South Central – Oxford A REC) approval (16/SC/0645) and Health Research Authority approval (IRAS 207769) were obtained. Written informed consent was obtained from all participants.

2.3.4 Inclusion criteria (version 3.0)

1. Biopsy proven breast cancer (invasive ductal or ductal carcinoma in situ (DCIS)) measuring ≥ 2 cm scheduled to be treated by primary surgical resection
    a. Tumour size should be based on the longest diameter measured on ultrasound, mammogram or MRI performed within 2 months prior to enrolment.
2. No prior treatment for breast cancer.
3. Female, Age ≥ 40 years.
4. The patient is willing and able to comply with the protocol scheduled visits and examinations for the duration of the study. Women of childbearing potential must follow contraception guidance given as standard of care at breast cancer diagnosis.
5. Written (signed and dated) informed consent.

2.3.5 Exclusion Criteria (version 3.0)

1. Pregnant or breast- feeding women.
2. Major surgery or significant traumatic injury within four weeks prior to enrolment.
3. Treatment with any other investigational agent, or participation in another interventional clinical study within 4 weeks prior to enrolment.
4. Multifocal breast cancer (defined as more than two tumours, either unilateral or bilateral).
5. Known hypersensitivity to ^{18}F-fluciclovine or any of its constituents.

6. Other psychological, social or medical condition, physical examination finding or a laboratory abnormality that the Investigator considers would make the patient a poor study candidate or could interfere with protocol compliance or the interpretation of study results.
7. Any other active malignancy or any previous diagnosis of melanoma.

2.3.6 Baseline measures

The following baseline measures were recorded during the first visit.

- Demographic details: age, sex
- Medical History: clinically significant disease history, concomitant diseases, prior surgery.
- Medications: drug allergies, concomitant medications.
- Date of onset of last menstrual period
- Measured length of tumour on standard of care imaging (longest diameter in millimetres)
- Record of tumour biopsy result:
- Type: standard breast histology description including subtype and grade
- Molecular type (invasive cancers only)

2.3.7 Blood samples

On the day of the ^{18}F-fluciclovine scan, blood samples for exploratory objectives were drawn on intravenous cannulation. This consisted of 30 mL in EDTA tubes and 4.5 mL in a sodium citrate tube. All samples were kept on ice

on collection and processed within 30 minutes. Sample processing steps are described in .

Table 2.7: Blood sample processing protocol for FRONTIER.

Application	Processing steps	Blood tube	Storage
Metabolomics	Centrifuge blood samples at 1,600 G at room temperature for 10 minutes. Re-centrifuge supernatant plasma at 16,000 G at room temperature for 5 minutes.	EDTA	-80^{o}C
Circulatory tumour DNA and microRNA profiling	Centrifuge blood samples at 1,600 G at room temperature for 10 minutes. Re-centrifuge supernatant plasma at 4,500 G at room temperature for 10 minutes. Transfer and pool buffy coat.	EDTA	-80^{o}C
Exosome profiling	Centrifuge blood samples at 3,000 G at room temperature for 10 minutes.	EDTA	-80^{o}C
Proteomics	Centrifuge blood samples at 500 G at room temperature for 15 minutes.	Sodium citrate	-80^{o}C

2.3.8 ^{18}F-Fluciclovine PET/CT imaging protocol

This comprised of two phases: a 20-minute dynamic acquisition centred over the breast tumour, followed by a 5-minute static acquisition centred over the axilla. PET/CT examinations were performed on a 3D mode ToF GE Discovery 710 PET/CT system (GE Healthcare, Milwaukee, USA).

The patients were required to fast for at least 4 hours prior to their scan. All doses of ^{18}F-fluciclovine were diluted to 7.5 mL with 0.9% saline. Following intravenous cannulation of the arm (contralateral to the tumour where practicable), dynamic acquisition in list mode commenced 30 seconds before steady intravenous injection of ^{18}F-fluciclovine (average 344 MBq, range 299-

372 MBq), with the breast tumour centred within the field of view. Tracer administration was followed by an intravenous flush of 0.9% saline to ensure full delivery of the dose. Following the 20-minute dynamic acquisition, a single bed position 5-minute static acquisition over the axilla was performed. The PET images were acquired under normal tidal respiration. The CT was performed using a pitch of 0.984, 120 kV, automA with a noise index of 25.

2.3.9 Image analysis

The dynamic PET acquisition was split into four 5-minute frames, following an initial 30-second delay, and reconstructed using a Bayesian penalised likelihood algorithm (ß300) (Q.Clear, GE Healthcare). Tumours were delineated using a threshold of 40% SUV_{max}, and SUV_{max} and SUV_{peak} measured. To determine the most appropriate time frame for primary characterisation of tumour ^{18}F-fluciclovine uptake, SUV_{max} and SUV_{peak} was measured on all four 5-minute frames for the first 5 scans. The frame which consistently demonstrated the highest uptake was then used for primary characterisation of tumour ^{18}F-fluciclovine uptake for all scans.

Images were also reviewed for ^{18}F-fluciclovine positive axillary lymph nodes or other ^{18}F-fluciclovine positive sites (lung/ bone/ non-axillary lymph nodes/ other sites). Determination of ^{18}F-fluciclovine positivity in lymph nodes and lung was based on uptake visually greater than blood pool, and for the bones, focal increased uptake visually greater than surrounding marrow. The CT appearances were also taken into account. SUV_{max} and SUV_{peak} for ^{18}F-fluciclovine positive nodes/ other sites were derived using an ROI tool, on the

the same frame as pre-determined for the primary tumour. All analyses were performed using HERMES Hybrid Viewer (HERMES Medical Solutions AB, Stockholm, Sweden).

2.3.10 Tissue sample collection

Intra-operative 14-gauge 2 cm core biopsies of the tumour and surrounding "normal" stroma (as distant as surgically practicable), were obtained prior to surgical resection. Immediate sample handling steps are summarised in .

Table 2.8: Tumour sample handling protocol in FRONTIER.

Application	Handling steps	Storage
Metabolomics (1 core tumour, 1 core "normal")	Immediately place into cryovial and snap freeze in liquid nitrogen.	-80^{o}C
Immuno-histochemistry (1 core tumour)	Place into 10% formalin. Transfer to 70% ethanol after 24-72 hours.	Room temperature
Gene array (1 core tumour, 1 core "normal")	Place into RNAlater solution (Thermofisher) and initially store at 4^{o}C. After 24-72 hours, remove from solution using RNAase-free forceps and store at -80^{o}C.	-80^{o}C

2.3.11 Metabolomic analysis of tumour samples

Tumour samples were weighed and placed in homogeniser tubes pre-filled with ceramic beads (Stretton Scientific, Derbyshire, UK). Metabolite extraction buffer (50% methanol, 30% acetonitrile, 20% Milli-q water, 100ng/ml HEPES) was added to the samples to obtain 25 µL/mg tissue. Tissue samples were lysed using a Precellys 24 homogeniser (Stretton Scientific Ltd., Derbyshire, UK), mixed for 15 minutes at 4 °C and centrifuged at 16,000 G for 15 min at 4 °C. The supernatant was then transferred into autosampler glass vials, stored at -80 °C until liquid chromatography–mass spectrometry (LC-MS) analysis.

LC-MS analysis was performed by Dr. Sofia Costa, from Dr. Christian Frezza's group (MRC Cancer Unit, Cambridge University). Samples were randomised in order to avoid bias due to machine drift and processed blindly. Analysis was performed using a Q Exactive mass spectrometer coupled to a Dionex U3000 UHPLC system (Thermo Fisher). The liquid chromatography system was fitted with a ZIC-HILIC column (150 mm × 4.6 mm) fitted with a guard column (20 mm × 2.1 mm) (both Merck Millipore). The aqueous mobile phase solvent used was 0.1% formic acid in water and the organic mobile phase was 0.1% formic acid in acetonitrile. The flow rate was set at 300 µL/min and the column oven set to 30°C. The mobile phase gradient was described previously [117]. The mass spectrometer was operated in full MS and polarity switching mode. The acquired spectra were analysed using XCalibur Qual Browser and XCalibur Quan Browser software (Thermo Fisher).

2.3.12 Immunohistochemistry techniques for FRONTIER

2.3.12.1 Generation and sectioning of cell pellets

Cells grown in two-dimensional culture were trypsinised and centrifuged at 1,200 rpm for 5 minutes. The supernatant was removed and the cell pellets were washed once with PBS. The cell pellets were then resuspended in 10% formalin (approximately 4% formaldehyde, Sigma) and fixed overnight at 4 ^{o}C.

After overnight fixation, the supernatant was removed, and the cells were gently and partially re-suspended in 2% agarose. After allowing to set, the agarose blocks were processed. The samples were then embedded in paraffin, and 4 µm sections were cut and mounted on glass slides. The slides were left to dry at room temperature overnight.

2.3.12.2 Immunohistochemistry protocol

The samples were deparaffinised and rehydrated by heating at 60^{o}C for 10 minutes and then washed sequentially, for 5 minutes per wash:

Histolene X2

100% industrial methylated spirit (IMS) X2

70% IMS X1

50% IMS X1

Tap water X1

Heat-induced antigen retrieval was performed using a sodium citrate buffer at pH 6 or 9 (depending on target), in a pressure cooker for 3 minutes. After washing the samples with wash buffer (K8007, Dako), blocking was performed with a peroxidase-blocking reagent (SM801, Dako) for 5 minutes. The samples were washed once and then incubated with the primary antibody for 30 to 60 minutes (antibody dependent) at room temperature. Dilutions of the primary antibody were prepared with antibody diluent (DM830, Dako).

After primary incubation, the samples were washed and incubated with the appropriate HRP-linked secondary antibody (SM802, Dako) for 20 minutes at room temperature. The samples were washed and incubated with DAB (SM803 and DM827, Dako) for 5 minutes, counterstained with Gill's haemotoxylin, and mounted using DPX Mountant (Sigma).

2.3.12.3 Antibody validation overview

Validation of antibodies for three amino acid transporters (ASCT2, LAT1 and SNAT2) were performed. Appropriate positive and negative control cell pellets were generated for each antibody and sectioned. Staining was perform using a variety of different antigen retrieval pH settings, primary incubation times and primary antibody concentrations. The slides were reviewed with Prof. Francesco Pezzella (Professor of Tumour Pathology, Nuffield Division of Clinical Laboratory Sciences) to select the optimum conditions.

2.3.12.4 Validation of ASCT2 antibody

Anti-ASCT2 (HPA035420, Sigma) was used. HCC1806 cells were transfected with either 1nM si-ASCT2 or si-Control for 72 hours prior to cell pellet generation. The conditions chosen were antigen retrieval pH 6, 30 minute primary incubation, 1:10,000 dilution (Figure 2.4).

2.3.12.5 Validation of LAT1 antibody

Anti-LAT1 (Cell signalling 5347) was used. HCC1806 cells were transfected with either 1 nM si-LAT1 or si-Control for 72 hours prior to cell pellet

generation. The conditions chosen were antigen retrieval pH 6, 60 minute primary incubation, 1:300 dilution (Figure 2.5).

2.3.12.6 Validation of SNAT2 antibody

Anti-SNAT2 (HPA035180, Sigma) was used. HCC1806 and MCF7 cells, cultured in 5 mM glucose DMEM at normoxia for 72 hours, demonstrate considerably different levels of SNAT2. Pellets of both cell lines grown under these conditions were generated. The conditions chosen were antigen retrieval pH 6, 60 minute primary incubation, 1:50 dilution (Figure 2.6).

2.3.12.7 pS6 staining

In terms of related pathways, mTORC1 was chosen for initial analysis given the aforementioned relationship between amino acids and its activation. pS6 was chosen as a marker for this, and had been previously validated by the group [118]. HCC1806 and MCF7 cells, cultured in 5 mM glucose DMEM at normoxia for 72 hours, demonstrate considerably different levels of pS6. Appropriate cell pellets were generated and stained with pS6 ribosomal protein (Ser 235/236) antibody (Cell Signalling 2211) using the previously validated conditions (antigen retrieval pH 9, 1:600, 1 hour primary incubation) to affirm these (Figure 2.7).

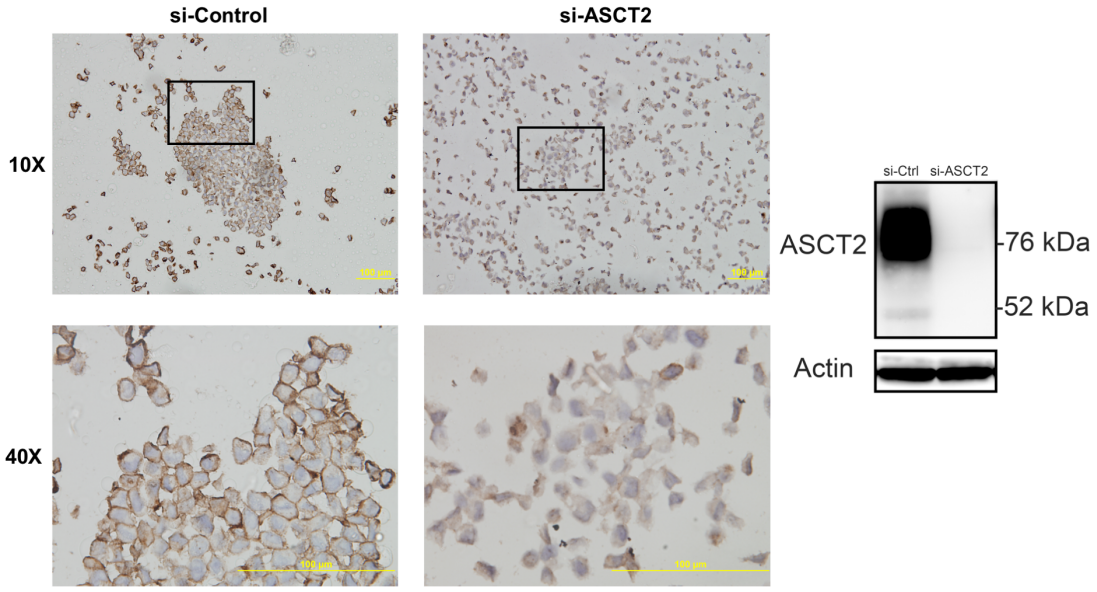

Figure 2.4: ASCT2 staining of HCC1806 cell pellets, with siRNA knockdown of ASCT2. Corresponding differences in ASCT2 expression are demonstrated on Western blotting.

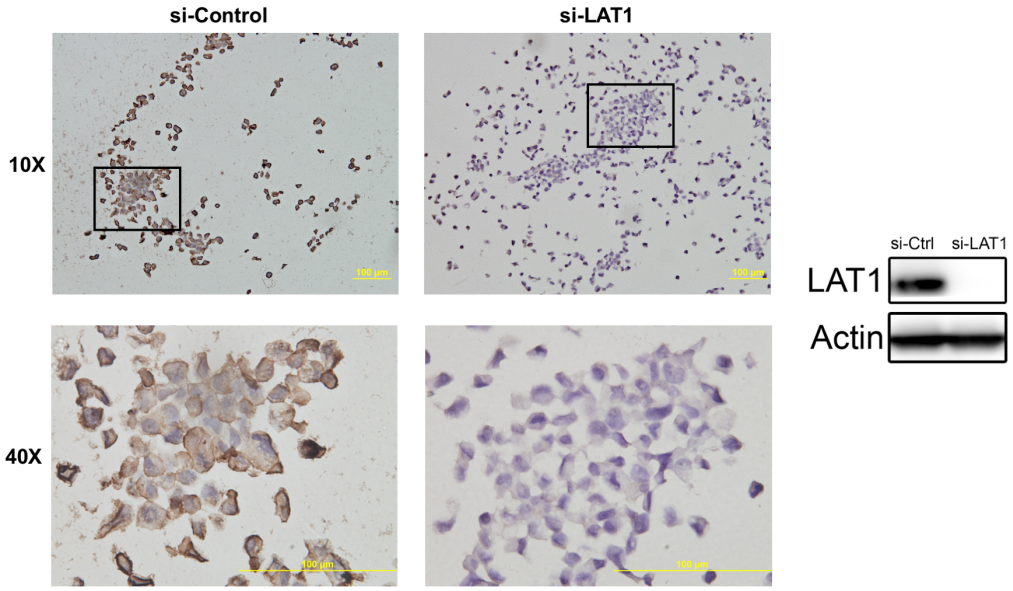

Figure 2.5: LAT1 staining of HCC1806 cell pellets, with siRNA knockdown of LAT1. Corresponding differences in LAT1 expression are demonstrated on Western blotting.

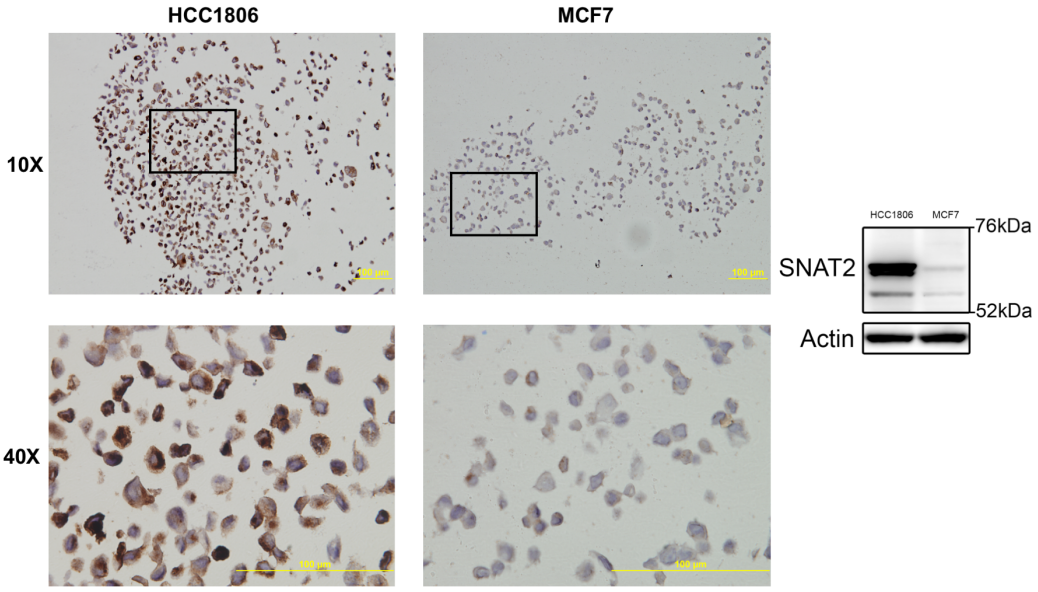

Figure 2.6: SNAT2 staining of HCC1806 and MCF7 cell pellets. Corresponding differences in SNAT2 expression are demonstrated on Western blotting.

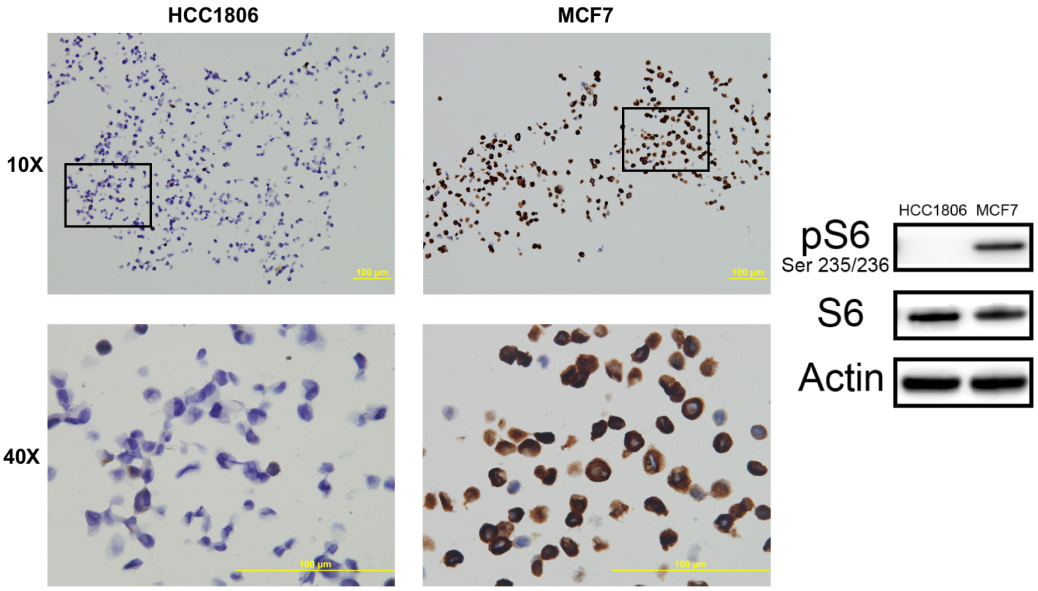

Figure 2.7: pS6 staining of HCC1806 and MCF7 cell pellets. Corresponding differences in pS6 expression are demonstrated on Western blotting.

2.3.13 Statistical analysis

For analysis of the metabolomics data, the tumour level of each metabolite was correlated with tumour ^{18}F-fluciclovine uptake using Spearman's rank

correlation coefficient. Statistical analyses and graphical output were performed on GraphPad Prism version 7.0a for Mac OS X (GraphPad Software, La Jolla California, USA). P values <0.05 were considered statistically significant.

Chapter 3 : ^{18}F-Fluciclovine PET/CT has an impact on the clinical management of recurrent prostate cancer

Content from this chapter has been published:

Teoh EJ, McGowan DR, Schuster DM, Tsakok MT, Gleeson FV, Bradley KM. Bayesian penalised likelihood reconstruction (Q.Clear) of ^{18}F-fluciclovine PET for imaging of recurrent prostate cancer: semi-quantitative and clinical evaluation. Br J Radiol. Published online 22 Jan 2018. doi:10.1259/bjr.20170727

Declaration of work

E.J. Teoh was primary author of the FALCON multicentre trial protocol, and the application for regulatory approval, with input from Prof. Fergus Gleeson, the Prinicipal Investigators and Blue Earth Diagnostics Ltd.

E.J. Teoh recruited the participants, collected and analysed the FALCON trial data presented. All ^{18}F-fluciclovine scans were reported by E.J. Teoh, in conjunction with two other radiologists including Dr. Kevin Bradley, Prof. Fergus Gleeson, Dr. Ruth Macpherson, Dr. Neel Patel and Dr. Manil Subesinghe. Identification of suitable participants in Oxford was supported by Dr. Gerard Andrade, Dr. Philip Camilieri, Dr. Katherine Hyde, Dr. Robert Stuart and Dr. Ami Sabharwal.

E.J. Teoh designed the BPL reconstruction sub-study with input from Dr. Kevin Bradley and Dr. Daniel McGowan. The semi-quantitative analyses, preparation of cases for image scoring, and analysis of image scoring results, were performed by E.J. Teoh. Image scoring was performed by Dr. Kevin Bradley (Oxford University Hospitals NHS Foundation Trust) and Prof. David Schuster (Emory University, Atlanta).

3.1 Introduction

In the setting of growing evidence of superior diagnostic performance of ^{18}F-fluciclovine PET/CT in BCR, its impact on clinical management of patients with BCR remained to be defined at the outset of this project. This chapter describes results from the Oxford site of a multi-centre study designed to assess this. In addition, the PSA level, kinetics and other clinicopathological factors associated with probability of a positive scan, pertinent to forming appropriate use criteria for this scanning agent, are reported.

With expectant clinical demand of ^{18}F-fluciclovine, research need also was identified to compare an advanced PET reconstruction method, BPL, to standard PET reconstruction of ^{18}F-fluciclovine images. This was to determine the optimum penalisation factor (β) for clinical use of BPL in ^{18}F-fluciclovine whole body imaging. This was performed as an Oxford site sub-study.

3.2 Results

3.2.1 Patients

Thirty-two patients were recruited between November 2015 to March 2017. Key patient demographics are summarised in . In Oxford, salvage therapy in BCR is limited to post-prostatectomy patients, which explains the low median PSA of 0.37 ng/mL.

3.2.2 ^{18}F-fluciclovine PET/CT findings

Across the cohort, 12 scans (38%) were positive for prostate cancer.

Remarkably, when stratified according to PSA level (), 32% of scans at PSA ≤0.5 ng/mL were positive, including the finding of extra-prostatic disease in one case (Figure 3.1). An additional 3 scans were positive for incidental findings (Figure 3.2).

Table 3.1: Patient demographics of Oxford FALCON trial participants.

Demographic	Median (range)
Age	66 (48-80) years
PSA at screening	0.37 (0.1-2.53) ng/mL
PSA_{dt} at screening	4.8 (0.6-32.5) months
PSA_{vel} at screening	0.4 (0.1-7.7) ng/mL/yr
Gleason score	7 (7-9)

Table 3.2: Positive detection rate of ^{18}F-fluciclovine PET/CT stratified by PSA.

PSA (ng/mL)	Number of scans (positive/total, %)	Localised (prostatectomy bed) disease	Extra-prostatic disease
≤ 0.5	7/22 (32%)	6/7	1/7
> 0.5 - ≤ 1.0	2/4 (50%)	2/2	0/2
> 1.0	3/6 (50%)	1/3	2/3

3.2.3 Clinical impact

Congruent with local trends in management of recurrent prostate cancer, all participants had an intended management plan of salvage radiotherapy to the prostate bed.

Following ^{18}F-fluciclovine PET/CT, the management plan was revised in 14 out of 32 cases (44%). This was due to prostate cancer-related findings in 12 cases, and incidental findings in the remaining two. The nature of management changes are described in .

Table 3.3: Nature of revised management classified by scan outcome.

Scan outcome	Number	Revised management
Localised disease	9	Salvage radiotherapy to the prostate bed with boost to ^{18}F-fluciclovine-avid areas (example Figure 3.3)
Extra-prostatic disease	2	Androgen deprivation therapy
	1	Watch and wait
Incidental finding	1	Androgen deprivation therapy
	1	Watch and wait

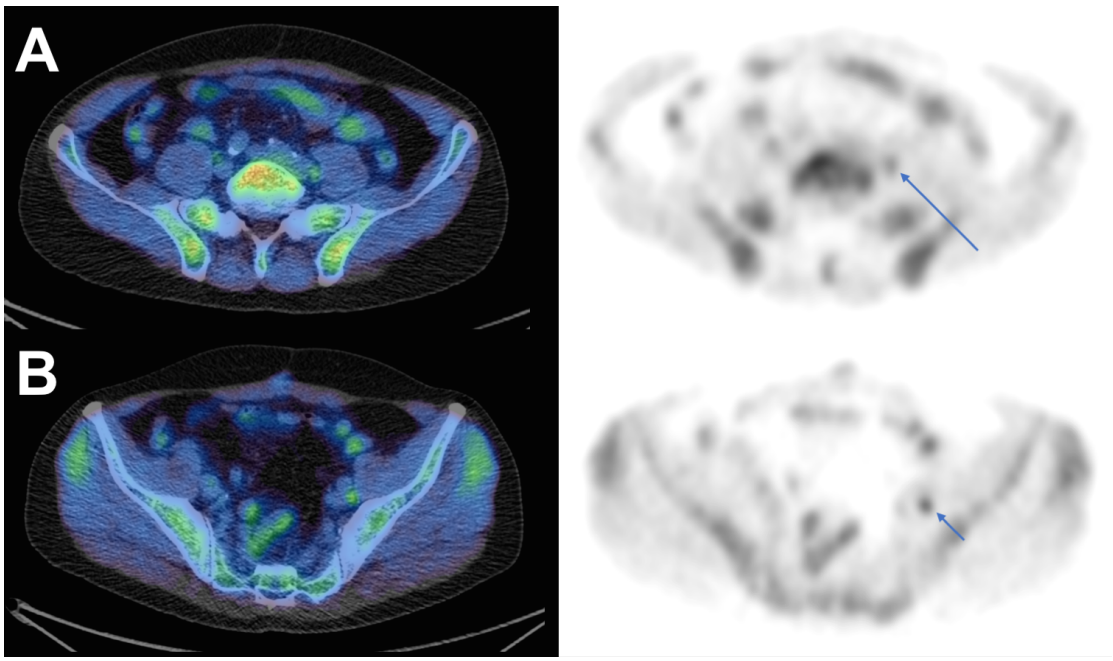

Figure 3.1: FALCON case example: Fused PET/CT and PET axial images of the pelvis of a 72-year-old man who presented with a PSA of 0.21 ng/mL 9 months post-radical prostatectomy, intended for salvage radiotherapy to the prostate bed. He had a history of high risk disease with pT3b, Gleason score 9 cancer, and multiple left-sided positive margins on histology. ^{18}F-Fluciclovine PET/CT demonstrated mildly avid sub-centimetre (A) left common iliac (long arrow) and (B) left external iliac (short arrow) lymph nodes. He was subsequently switched to watch and wait management.

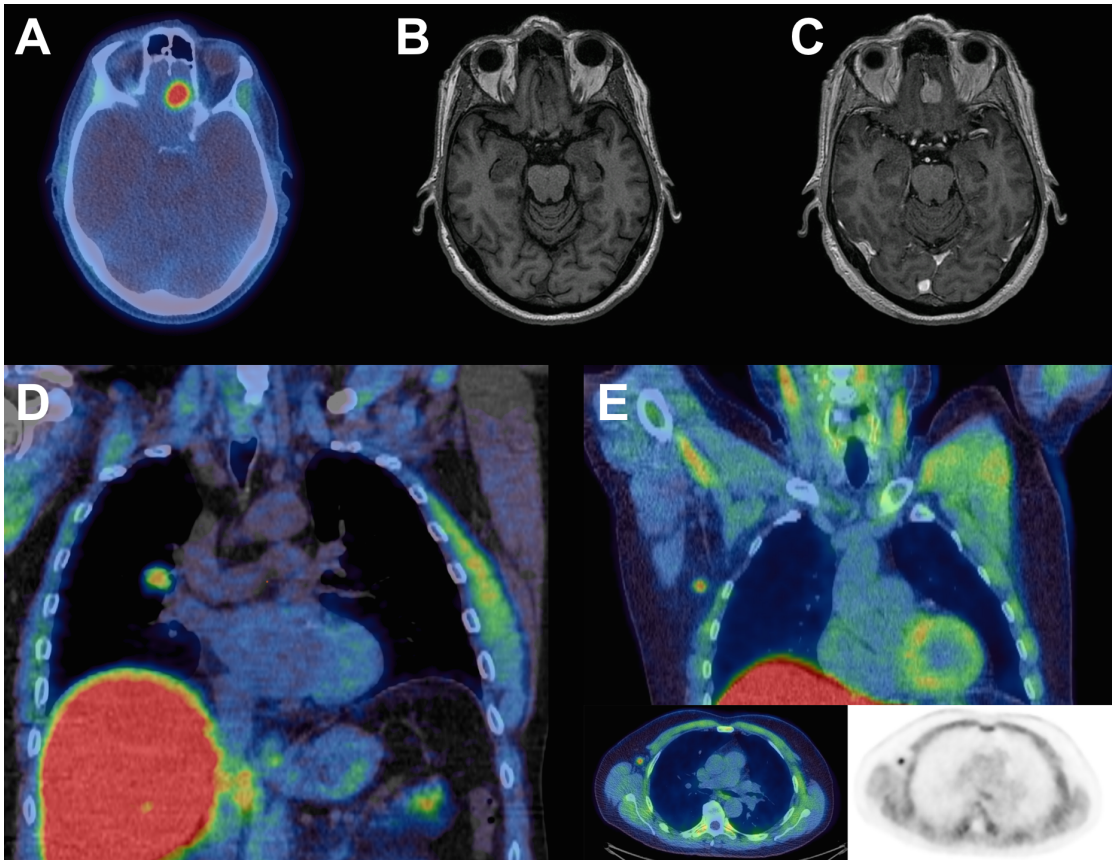

Figure 3.2: Incidental findings on ^{18}F-fluciclovine PET/CT. (A) A ^{18}F-fluciclovine avid focus in the anterior cranial fossa of this patient was visualised on the last bed position. Pre- and post-contrast enhanced MRI of the brain (B and C respectively) demonstrated a uniformingly enhancing midline extra-axial mass, with a characteristic "dural tail", in keeping with a meningioma. The patient went on to have salvage treatment for prostate cancer and is under active monitoring for the meningioma. (D) A ^{18}F-fluciclovine avid nodule was demonstrated in the right lung of this patient. He was switched to androgen deprivation therapy for prostate cancer to undergo treatment for this incidental finding. It was subsequently resected and confirmed to be neuroendocrine in origin. (E) This patient had a history of resected truncal stage IIIC malignant melanoma, with bilateral axillary node involvement on sentinel node biopsy, in complete remission for 3 years. ^{18}F-fluciclovine PET/CT demonstrated a ^{18}F-fluciclovine-avid right axillary node, confirmed on diagnostic sampling to be recurrent malignant melanoma. He was commenced on androgen deprivation therapy for prostate cancer to allow for melanoma treatment.

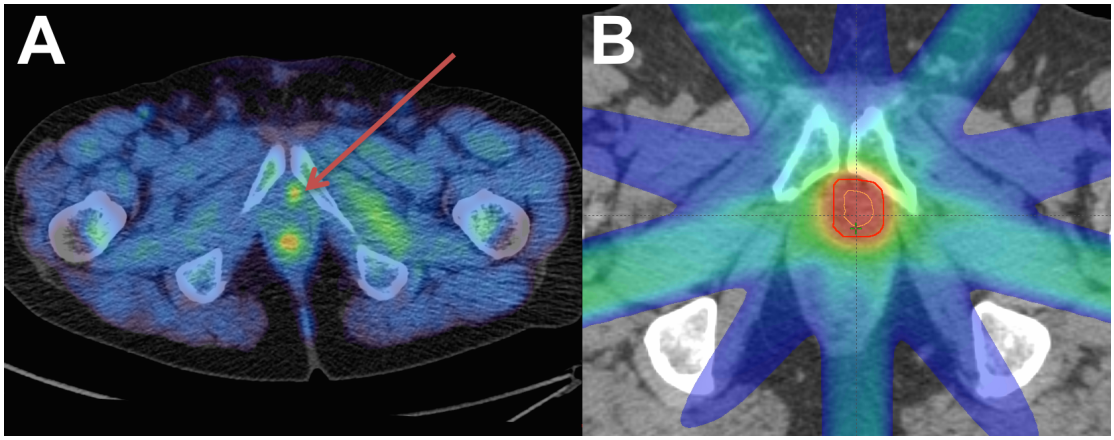

Figure 3.3: FALCON case example: (A) Fused PET/CT image showing a single ^{18}F-fluciclovine avid focus of disease (red arrow) in the prostatectomy bed of a patient who had a PSA of 0.6 ng/mL. In addition to the standard radiotherapy of 66Gy/30 fractions to the prostate bed, he also received 8Gy/5 fractions boost to this area, delineated on this dose colour map (B). The gross tumour volume and planning target volume are delineated by the red and orange contours respective. His PSA was undetectable on follow-up.

Of the 9 patients who had revised salvage radiotherapy plans, two subsequently decided against active treatment and agreed with their clinician for a watch and wait approach.

At the time of writing, 7-8 month PSA follow-up was available for 22 patients who had completed salvage radiotherapy (both standard and ^{18}F-fluciclovine guided) (Figure 3.4). Ten of the 22 patients received standard salvage radiotherapy to the prostate bed, of whom 8 had responded (53%), and 7 were non-responders. Of the 7 patients who received salvage radiotherapy to the prostate bed with boost to ^{18}F-fluciclovine-avid areas, 5 had responded (71%) and 2 had not. The difference in proportion of responders between the two groups was not statistically significant (p=0.648).

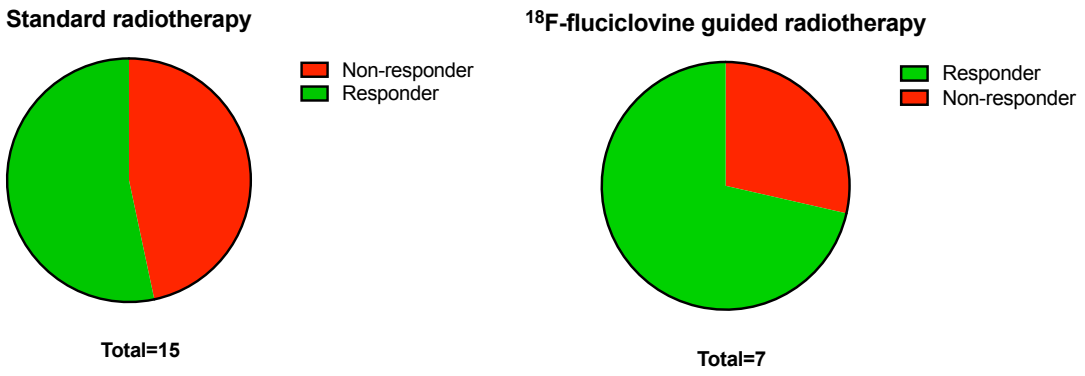

Figure 3.4: Pie charts demonstrating the distribution of response type in patients who underwent salvage radiotherapy. There was a higher proportion of responders in patients who received salvage radiotherapy to the prostate bed with boost to ^{18}F-fluciclovine-avid areas (71%, 5/7), compared to patients who received standard radiotherapy (53%, 8/15). This was not statistically significant.

3.2.4 Clinicopathological factors influencing scan positivity

It is well-established that PSA, PSA kinetics and primary histopathological factors have a bearing on choline PET scan positivity. The influence of these parameters, and BCR-free survival on ^{18}F-fluciclovine scan positivity was investigated.

In participants with positive scans, there was a higher mean PSA level, PSA velocity, and lower PSA doubling time (), consistent with published literature on these metrics in predicting scan positivity on choline PET. There were also higher proportions of scan positivity in patients with a higher Gleason score, T stage and positive surgical margin on primary histopathology (). Of these, only the difference observed based on Gleason score was statistically significant.

Both uni- and multivariate analysis also demonstrated that a higher Gleason score had greater odds (univariate OR 5.667 (95% C.I. 1.067-30.085)

p=0.042, multivariate OR 6.535 (95%C.I. 0.961-44.418) p=0.055) of resulting in a positive scan outcome. PSA, T stage and positive surgical margin had marginally greater odds (, Figure 3.5, Figure 3.6), however, these were statistically insignificant.

Table 3.4: PSA, PSA kinetics and BCR-free survival of patients with positive and negative scans.

Variable	Positive scan Mean (SEM)	Negative scan Mean (SEM)	p value
PSA (ng/mL)	0.825 (0.280)	0.588 (0.123)	0.360
PSA_{dt} (months)	4.145 (0.970)	6.700 (1.522)	0.403
PSA_{vel} (ng/mL/year)	1.391 (0.658)	0.670 (0.239)	0.387
BCR-free survival (days)	574 (148)	784 (176)	0.954

Table 3.5: Primary pathological variables in patients with positive and negative scans.

Variable	Positive detection rate (Category)		p value
Gleason score	67% (Score 9)	26% (Scores 7-8)	0.033
T stage	41% (T3)	22% (T2)	0.324
Surgical margin	38% (Positive)	30% (Negative)	0.660

Table 3.6: Multi- and uni-variate binary logistic regression analysis of factors predicting ^{18}F-fluciclovine scan positivity.

Variable	Multivariate analysis		Univariate analysis	
	Odds ratio (95% C.I.)	p value	Odds ratio (95% C.I.)	p value
PSA	1.546 (0.380-6.285)	0.543	1.482 (0.529-4.147)	0.454
PSA_{dt}	0.833 (0.556-1.248)	0.375	0.922 (0.769-1.105)	0.379
PSA_{vel}	0.903 (0.426-1.913)	0.789	1.311 (0.775-2.217)	0.313
T stage	1.517 (0.175-13.137)	0.705	2.423 (0.406-14.463)	0.332
Surgical margin	1.282 (0.167-9.823)	0.811	1.436 (0.286-7.212)	0.660
Gleason score	6.535 (0.961-44.418)	0.055	5.667 (1.067-30.085)	0.042
BCR-free survival	1.001 (0.999-1.002)	0.576	1.000 (0.999-1.001)	0.555

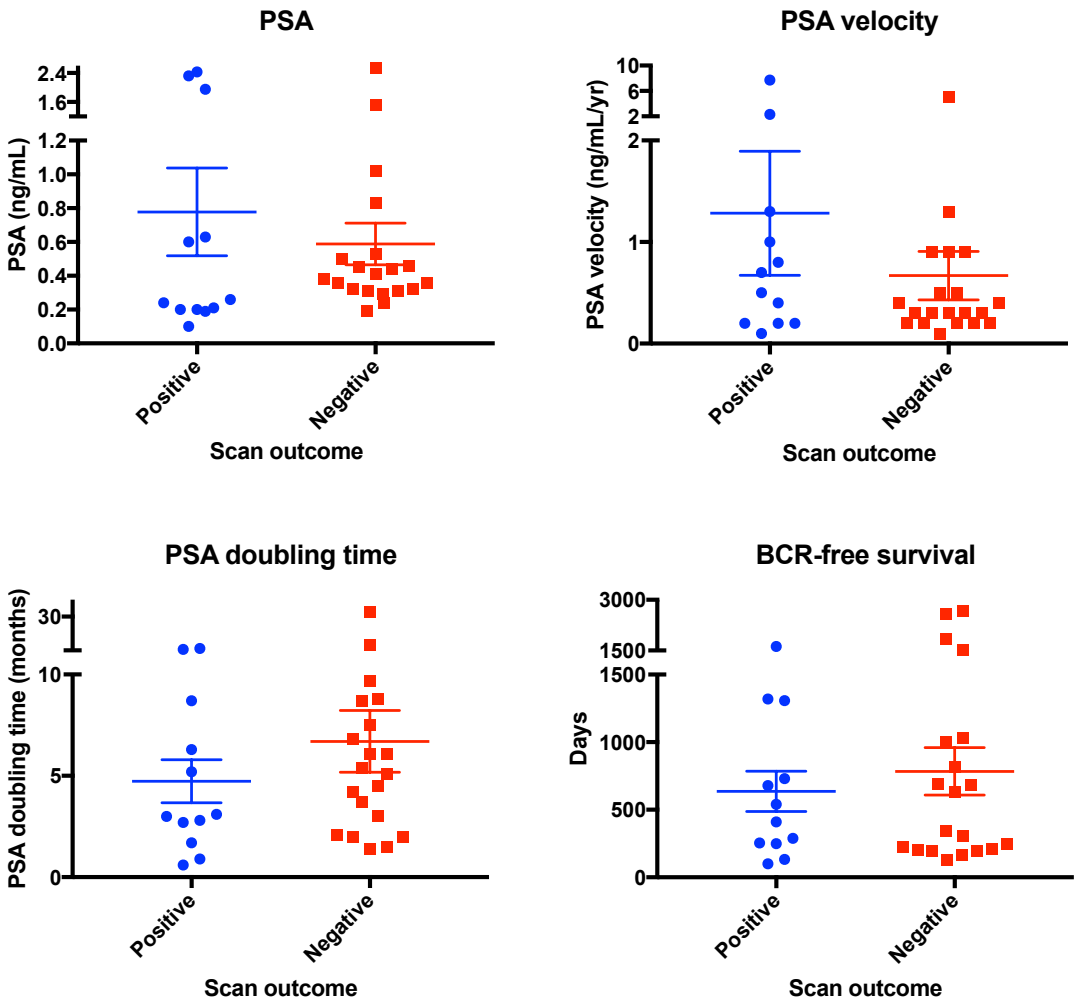

Figure 3.5: Graphs of PSA, PSA kinetics and BCR-free survival are dichotomised by scan positivity. These demonstrate a trend of elevated PSA and rapid PSA kinetics in positive scans, albeit statistically insignificant on the logistic regression analyses. All data points shown with error bars depicting mean ± SEM.

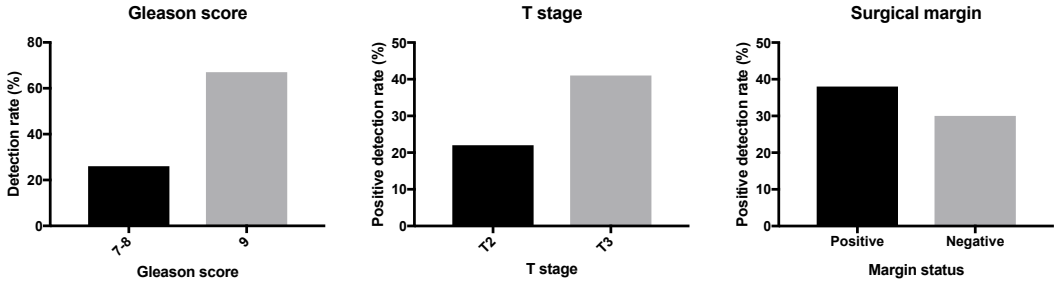

Figure 3.6: Graphs of ^{18}F-fluciclovine scan positive detection rate stratified by Gleason score, T stage and surgical margin status. The trend of increased positive detection in patients with higher Gleason score, T-stage and positive surgical margin is affirmed by matching ORs for these variables in the logistic regression analyses.

3.2.5 BPL substudy – Semi-quantitative analysis

An example image for each reconstruction is depicted in Figure 3.7. Lesion SUV_{max} and SBR increased in β100-400 and PSF (comparison to OSEM), with highest gain in β100 images (mean ΔSUV_{max} 3.9, $p<0.0001$) (Figure 3.8). Comparing BPL reconstructions to OSEM, lesion SNR increased where β≥300 (Figure 3.8), with no statistically significant inter-group difference between β300-600 ($p=0.562$). When compared to PSF, lesion SNR was increased in all BPL reconstructions ($p=0.0001$-0.021), with the exception of β100.

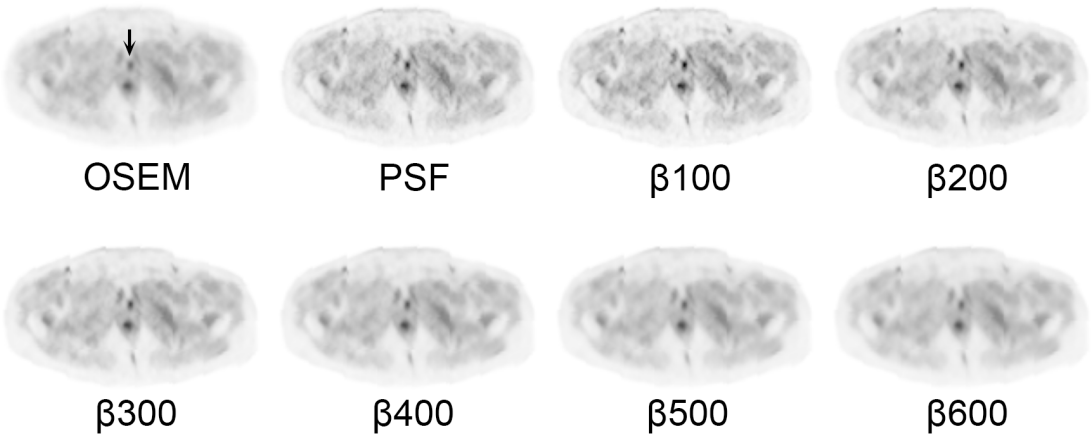

Figure 3.7: Axial images of different PET reconstructions at the level of the pubic symphysis. These demonstrate a sub-centimetre ^{18}F-fluciclovine-avid focus of disease (arrow) in the anterior prostatectomy bed. Consistent with the semi-quantitative results, the lesion is rendered more conspicuous on BPL reconstructions with relatively less background noise. All images are displayed on SUV scale 0-6.

There was no change in SUV_{mean} of spleen and blood pool across all reconstructions (Figure 3.9). While such changes in the liver and marrow were statistically significant (Figure 3.9), these were deemed to be clinically insignificant (highest ΔSUV_{mean}: 0.05 in liver, 0.015 in marrow).

Across the BPL reconstructions, there was an incremental reduction in organ noise with increasing β, which compared to OSEM, were significant beyond β300-500 (organ-dependent) (Figure 3.10). Compared to OSEM, organ noise levels increased on PSF, β100 and β200 reconstructions (Figure 3.10). This trend was also demonstrated in organ SNR, with statistically significant gains (over OSEM) in marrow, liver and blood pool when β≥400, and the spleen when β≥300 (Figure 3.11).

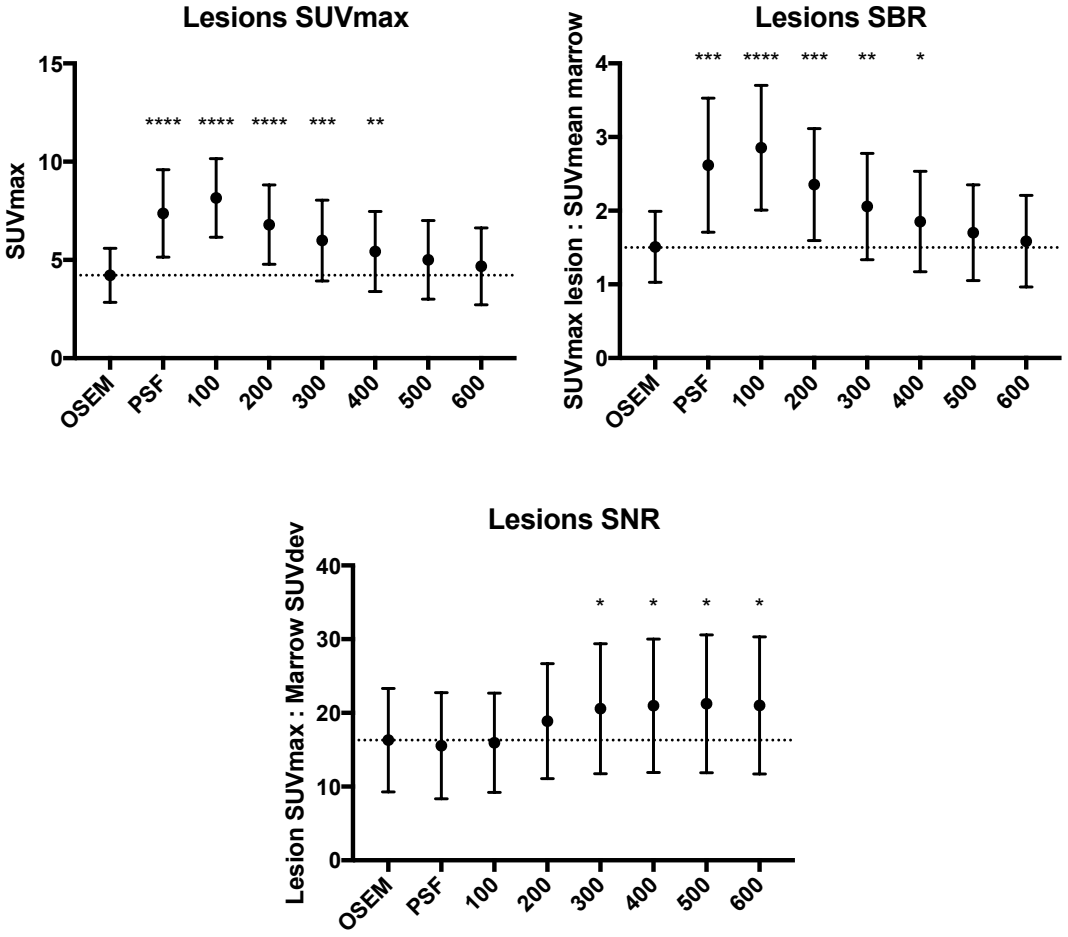

Figure 3.8: Graphs of lesion SUVmax, SBR and SNR across different PET reconstructions (mean±SD, dotted line represents mean value on OSEM reconstruction). Statistical comparisons to OSEM are represented (*=p ≤0.05, **=p≤0.01, ***=p≤0.001, ****=p≤0.0001).

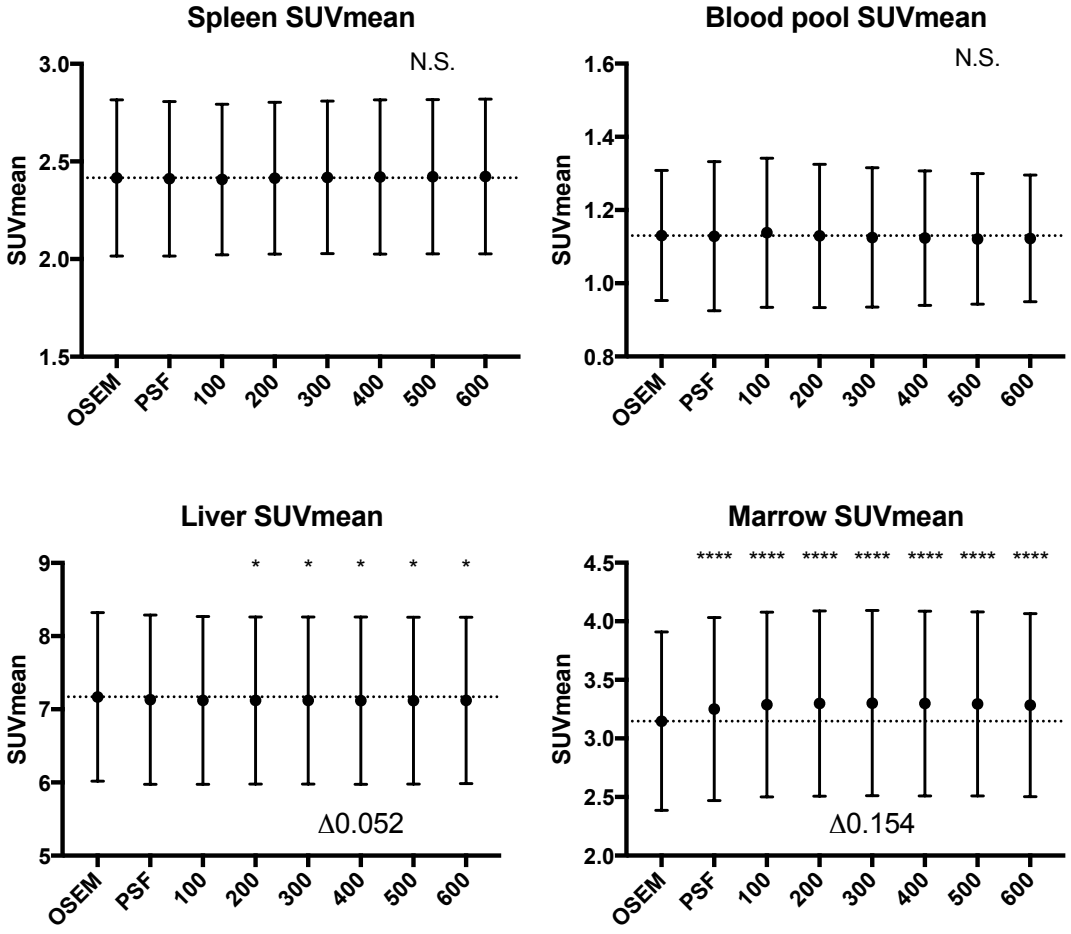

Figure 3.9: Graphs of organ SUVmean across different PET reconstructions (mean±SD, dotted line represents mean value on OSEM reconstruction). Statistical comparisons to OSEM are represented (*=p ≤0.05, ****=p≤0.0001).

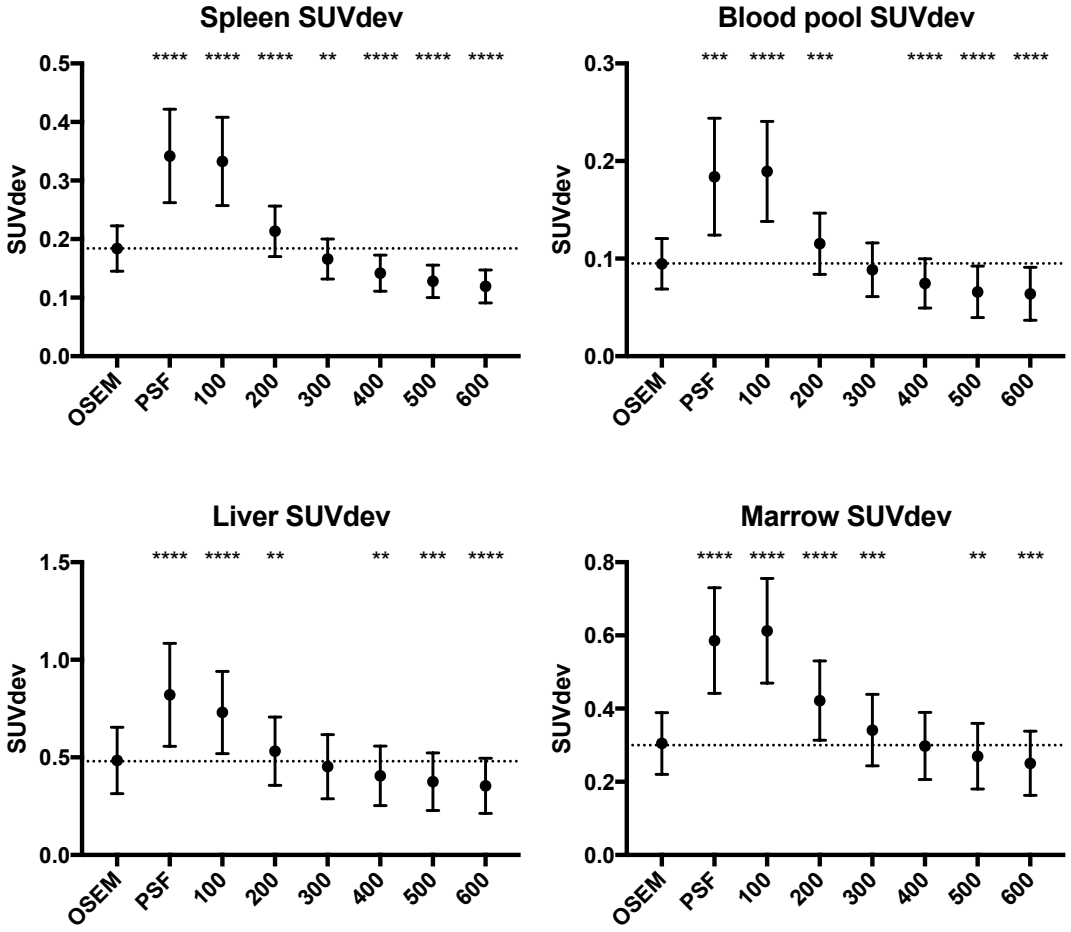

Figure 3.10: Graphs of organ SUV_{dev} across different PET reconstructions (mean±SD, dotted line represents mean value on OSEM reconstruction). Statistical comparisons to OSEM are represented (=p≤0.01, ***=p≤0.001, ****=p≤0.0001).**

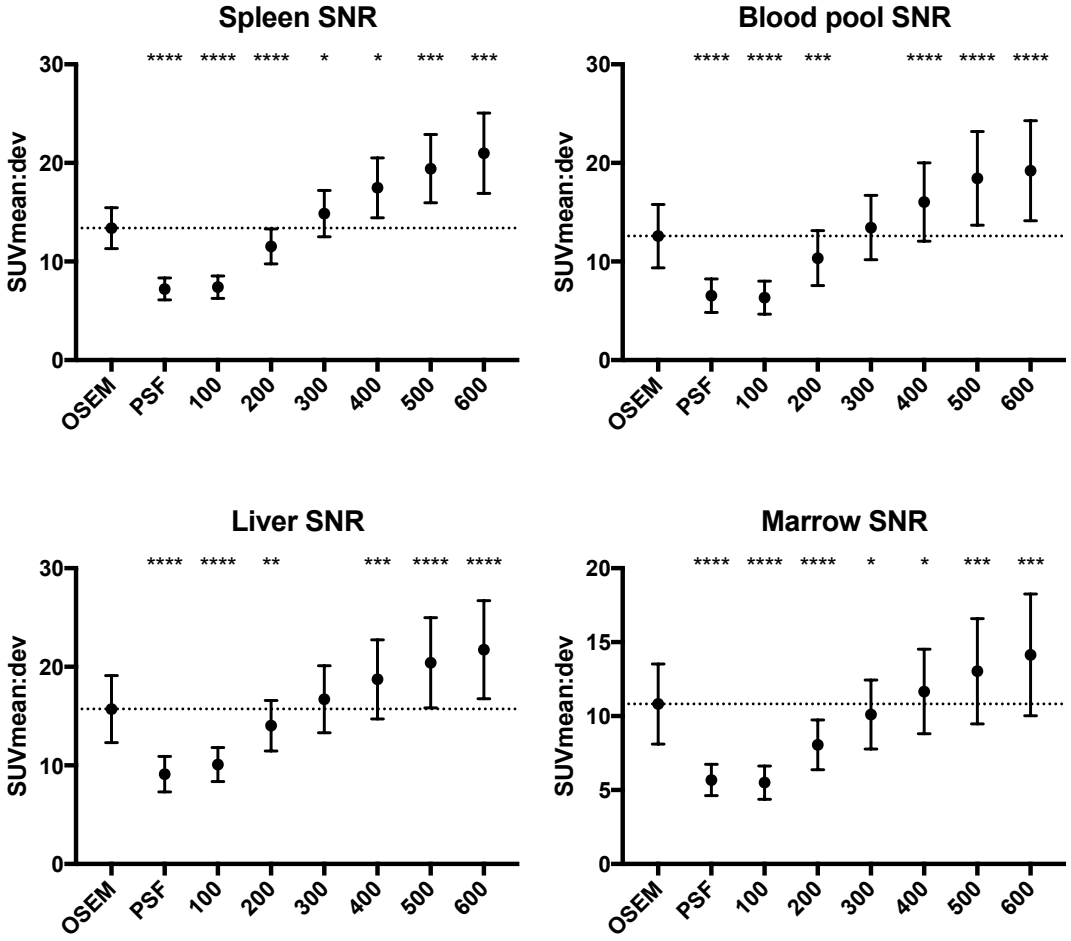

Figure 3.11: Graphs of organ SNR across different PET reconstructions (mean±SD, dotted line represents mean value on OSEM reconstruction). Statistical comparisons to OSEM are represented (*=p ≤0.05, **=p≤0.01, ***=p≤0.001, ****=p≤0.0001).

3.2.6 BPL substudy – Clinical evaluation

In the clinical evaluation, β300 had the first and second highest scores (between both readers) for image quality, PSF and β200 had first and second highest scores for lesion conspicuity, β500 and β600 had the joint highest scores for marrow image quality and overall noise level (i.e. least noise) (). These findings complemented those of the semi-quantitative analyses.

In terms of overall preferences, Reader 1 preferred β300 in 90% of cases and Reader 2 preferred β200 in all cases. There was a greater polarisation of opinion with regards to least preferred reconstructions, with Reader 1 indicating PSF in 80% and Reader 2 chose β600 in 90% of cases.

Table 3.7: Scores of image quality parameters in the visual analysis.

Recon-struction	Overall image quality		Lesion conspicuity		Overall noise level		Background marrow image quality	
	Reader 1	Reader 2	Reader 1	Reader 2	Reader 1	Reader 2	Reader 1	Reader 2
OSEM	34	37	19	20	43	36	44	39
PSF	27	39	30	29	22	21	21	20
β200	36	50	30	28	33	33	31	29
β300	50	47	27	22	44	39	44	33
β400	45	40	22	22	49	45	49	41
β500	39	30	21	16	50	50	50	50
β600	36	30	19	15	50	50	50	50

3.3 Discussion

In this study, we set out to establish the clinical impact of ^{18}F-fluciclovine PET/CT in patients with BCR being considered for radical salvage treatment (with curative intent), characterised by change of management. Clinico-pathological variables affecting scan positivity were explored, and a substudy was performed to inform the best use of an advanced PET reconstruction method, BPL, in ^{18}F-fluciclovine whole body imaging.

In the Oxford cohort, 44% of patients had their intended management plan revised following ^{18}F-fluciclovine PET/CT. This result is considerably significant for two key reasons. Firstly, the median PSA in this post-prostatectomy cohort was remarkably low at 0.37 ng/mL (range 0.1-2.53 ng/mL). Secondly, based on local practice, most of these patients would have undergone salvage radiotherapy to the prostatectomy bed without any prior

imaging. The impact is further underscored by a higher proportion of short-term responders to ^{18}F-fluciclovine guided radiotherapy (71%, 5/7) compared to standard radiotherapy (53%, 8/15). The dominant factor contributing to the lack of statistical significance in this difference is the small sample size, and it will be interesting to see the result of this from across the trial. Towards the end of this project, a trial-wide interim analysis on the primary endpoint was presented, reporting a change in management in 61% (52/85) of a pre-dominantly low PSA (median 0.63 ng/ml) cohort [119]. This exceeded the threshold for stopping the trial early due to overwhelming effectiveness (set at 53% (>45 subjects with change in management)).

Despite the small sample size, a statistically significant association with scan positivity was observed with Gleason score in the univariate analysis, and approaching significance (p=0.055) in the multivariate analysis (). Furthermore, an encouraging trend of elevated PSA and rapid PSA kinetics in positive scans was observed (Figure 3.5), which will be robustly characterised in the trial-wide analysis, and most useful for informing appropriate use criteria. While these collective findings are in keeping with the known variables influencing performance of imaging in prostate cancer (described in the main Introduction), it comes with a remarkable frameshift in sensitivity, with almost 1 in 3 scans (32%,) at a PSA ≤0.5 ng/mL affording disease localisation.

During the course of this project, there has been exponential growth in the use of prostate specific membrane antigen (PSMA) targeted imaging,

particularly in Europe and Australia. Also known as glutamate carboxypeptidase II, PSMA is a transmembrane protein that is expressed mainly in the prostate, with relatively lower levels in proximal tubules of the kidney and gastrointestinal tract, and highly expressed in primary and recurrent prostate cancer [120]. The latter characteristic coupled with internalisation of PSMA upon ligand binding, affording means to accumulate imaging ligands, has made it an incredibly attractive target for prostate cancer imaging [121]. Numerous PET tracers targeting PSMA have been described, with ^{68}Ga-labelled compounds predominating clinical use [122] although ^{18}F-labelled agents are in active development [123, 124].

While none of these agents have received regulatory approval, the expansive adoption of PSMA imaging warrants discussion in the context of ^{18}F-fluciclovine. Bearing in mind that approximately 5% of prostate cancers do not significantly over-express PSMA [122], it appears to yield reasonable positive detection at low PSA levels as well, with a meta-analysis reporting ^{68}Ga-PSMA to have a positive detection rate of 58% in patients with a PSA of 0.2-1.0 ng/ml (pooled from 6 studies, 1 prospective) [125]. Furthermore, the same meta-analysis reported similar subject-level sensitivity of 86% but higher specificity of 86% (pooled from 4 retrospective studies) [125], compared to ^{18}F-fluciclovine [126]. The latter study was a patient-by-patient retrospective multicentre analysis which described subject-level (n=143) sensitivity and specificity of ^{18}F-fluciclovine to be 91% and 40% respectively.

Considering the more pertinent theme of clinical utility, a recent prospective multicentre study in Australia reported change in management intent in 62% of patients with BCR after ^{68}Ga-PSMA imaging [127]. This is remarkably similar to that reported in the FALCON trial-wide interim analysis (61%), and probably underscores the frameshift in practice that could be introduced by more sensitive imaging. What remains to be defined between PSMA imaging and ^{18}F-fluciclovine, and for any other emerging highly sensitive imaging technique of prostate cancer, is the impact of image-guided management on long term outcomes, which may well be the defining factor of its clinical use.

To some extent, long-term outcomes will be biased by the efficacy of the treatment modality employed, some of which remain to be robustly characterised. This is paradoxically due to prior lack of sensitive imaging techniques to delineate disease to allow rigorous use and trials of developing therapies, particularly targeted ones. Good examples are disease detection at low PSA levels, and in the prostatectomy bed which is prone to interference from radioactivity in the urinary bladder, an area of relative susceptibility in PSMA-targeted imaging [122]. This work now raises the potential for introducing advanced imaging to inform much-needed research into targeted therapies. The advantage in this respect with ^{18}F-fluciclovine is that it is an approved agent, subject to regulated manufacturing and interpretation guidelines, which may afford better translatability / repeatability of results.

There are limitations to the design of FALCON which have to be considered. Firstly, unlike standard late phase therapeutic trials, there was no comparative

arm. This was significantly perpetuated by the heterogeneity of both imaging and therapeutic management of recurrent prostate cancer across the UK sites involved with FALCON, which we encountered as we designed the study. This also ties in with a limitation specific to the Oxford cohort, which being all salvage prostate bed radiotherapy candidates, would have benefitted from a control arm of standard radiotherapy regardless of positive detection of disease in the prostatectomy bed, followed by long term follow-up. This would have afforded a step-up in elucidating the value of visualising and targeting disease in this setting compared to the current analysis, but was not possible to introduce in the context of a multicentre study involving previously naïve readers of a novel PET imaging agent. Finally, while short-term follow-up has demonstrated a possible trend of better response in patients receiving ^{18}F-fluciclovine guided salvage radiotherapy, longer term follow-up remains pivotal and would ideally have been prospectively planned. However this may be performed in the form of a separate retrospective study at appropriate timepoints.

The latter component of this chapter aimed to compare BPL to standard PET reconstruction of ^{18}F-fluciclovine images and determine the optimum penalisation factor (β) for clinical use of BPL in ^{18}F-fluciclovine whole body imaging. This was addressed using a combination of semi-quantitative and visual analyses performed on a range of reconstructions of clinical scans.

Consistent with prior observations [55, 59-61], the majority of BPL reconstructions demonstrated an increase in lesion signal and reduction in

noise. The increase in lesion signal compared to OSEM reached statistical significance in the BPL reconstructions up to β400 (Figure 3.8), while that of noise level showed a decrease in 3 out of 4 organs (one statistically significant) at β300 (Figure 3.10). At β400 and higher, noise was decreased in all organs compared to OSEM (3 statistically significant at β400, Figure 3.10). Accordingly, an increase in lesion SNR was demonstrated in all reconstructions at β300 and higher, with no statistical advantage on semi-quantitative parameters, of one reconstruction over the other beyond this point (Figure 3.8). These collective findings tentatively placed either β300 or β400 as the optimal BPL reconstruction setting.

The visual analysis proved useful in stratifying this outcome. Between the readers, β300 had the first and second highest scores for overall image quality for image quality of clinical scans, while β400 scored second and third highest respectively. This trend was also mirrored in scoring of lesion conspicuity where, after PSF and β200 (which demonstrate a detrimental increase in noise despite signal gain), β300 was scored higher than β400 by both readers.

β300 was indicated as the most preferred reconstruction in 90% of cases by one reader. On balance, the relatively minor difference in overall reader preference is deemed relatively immaterial to the strength of the other overarching findings. Optimised BPL reconstruction is shown to improve lesion conspicuity by increased SNR and SBR compared to standard OSEM reconstruction [55, 60, 61]. Therefore, β300 should be considered as the

optimal penalisation factor for BPL reconstruction of ^{18}F-fluciclovine PET images. A case example is presented in Figure 3.12.

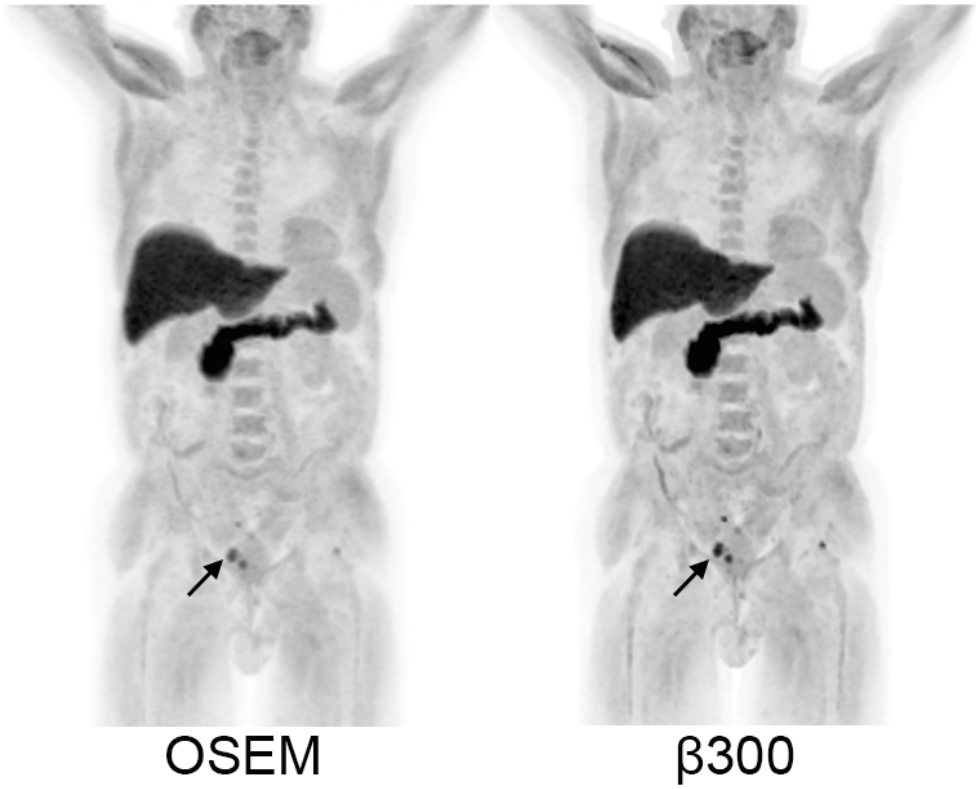

Figure 3.12: Maximum intensity projection images (SUV scale 0-7) of a patient demonstrating small foci of disease recurrence in the pelvis and left femoral head, rendered more conspicuous on the BPL β300 reconstruction compared to OSEM. For example, the largest focus of uptake (arrow), corresponding to right seminal vesicle disease, had an SUV_{max} of 6.9 on OSEM, increased to 9.1 on BPL β300.

These findings are important because the use of newer PET reconstruction algorithms incorporating PSF modelling such as BPL may have implications for the interpretation of oncological PET/CT, particularly as it has been shown to increase sensitivity at a cost of reduced specificity for a given SUV threshold [55]. Adoption of new reconstruction algorithms into well-established clinical practice, notably with interpreting ^{18}F-FDG PET, demands dedication on the part of the reader to re-calibrate their approach to reading studies.

Widespread adoption of advanced reconstruction algorithms is challenging due to the variant experience with ^{18}F-FDG PET reconstruction across the globe, which has been in constant iteration since the use of filtered back projection and 2D-mode scanning [128].

The landscape is encouragingly different with ^{18}F-fluciclovine, which has recently been approved for a focused clinical indication (recurrent prostate cancer), with interpretation guidelines built on cumulative experience of a small consortia of readers using relatively modern scanner and reconstruction technology [126, 128, 129]. Furthermore, being an amino acid, it may be less fallible to non-specific uptake by inflammatory/benign entities compared to ^{18}F-FDG as described *in vitro* [130], and anecdotally in published literature [115, 131].

The difference in optimal β compared to ^{18}F-FDG whole body PET, previously described to be β400 [59], can be explained by the differences in physiological distribution and pathological uptake compared to ^{18}F-fluciclovine. In prostate cancer, nodal recurrence tends to occur within the pelvis and retroperitoneum, where adjacent background uptake is relatively low. Improved demonstration of pathological uptake, particularly in small nodes, would then be afforded by a relatively low β, which generates increased signal at minimal penalty to surrounding background noise [128].

Being in the early stages of clinical rollout, there is an opportunity for naïve readers to gain their formative clinical experience with ^{18}F-fluciclovine

interpretation based on advanced image reconstruction from the start. Apart from affording a step-up in patient care, through improved image quality and confidence in interpretation, this should avoid the unnecessary complexities of re-learning should current mainstream reconstruction technology get eclipsed [128].

Our experience with this process supports an ongoing collaborative effort amongst academic leaders and industry involved in this and other novel radiotracers, to maintain clear interpretation guidelines based on collective experience with different reconstruction technologies. This has to be supported by prospective study of diagnostic performance based on advanced reconstruction technology, and retrospective evaluation of the like where possible, using the same approach as this study, exploiting saved sinogram data. We also propose these actions for forthcoming imaging agents as they attain regulatory approval [128].

There are limitations to consider in this sub-study. It was not possible to completely blind the scorers to the different reconstruction algorithms, as BPL has a different visual appearance compared to PSF at all beta values, and to OSEM to a limited extent. This may have introduced bias as readers progressed through the scoring process, mitigated to some extent by the wide range of BPL reconstructions used. Finally, caution should be adopted in the event of expanded clinical use for ^{18}F-fluciclovine, and re-visiting optimisation of image reconstruction based on disease type and/or organ of interest, particularly the brain, may be warranted [128].

3.4 Conclusion

^{18}F-Fluciclovine PET/CT has a substantial impact on the clinical management of post-prostatectomy patients presenting with BCR. In addition to upstaging and preventing otherwise futile radiotherapy in some patients, there is a trend suggestive of improved short-term treatment response with ^{18}F-fluciclovine guided salvage radiotherapy compared to standard radiotherapy. Reconstruction of ^{18}F-fluciclovine PET images with advanced algorithm BPL improves SNR compared to OSEM, affirmed by overall reader preferences for BPL reconstructions. Based on this work, β300 is recommended for ^{18}F-fluciclovine whole body PET image reconstruction using BPL.

Chapter 4 : Fluciclovine uptake is mediated by high-affinity glutamine transporter ASCT2

Declaration of work
All of the *in vitro* work was performed by E.J. Teoh, with material support, ^{14}C-FACBC, from Blue Earth Diagnostics Ltd.

4.1 Introduction

As described in the first chapter, a firm understanding of the uptake mechanisms of fluciclovine in breast cancer are required in order to establish its potential utility as an imaging biomarker. Majority of the previous *in vitro* work in characterising uptake mechanisms have been performed in prostate cancer cell lines, and all the work has been performed by a single group with fluciclovine labelled with ^{14}C (^{14}C-FACBC) [4]. In view of this, and the lack of published data using this compound in breast cancer cell lines, optimisation of this technique is essential. In this chapter, the uptake mechanisms of fluciclovine was ascertained in breast cancer cell lines representative of the main molecular subtypes. This was achieved by competitive inhibition experiments using a variety of natural and synthetic amino acids, and knockdown of expression of specific transporters.

4.2 Heterogeneity of amino acid transporter expression in breast cancer

Expression of the key transporters described as major contributors of fluciclovine uptake, ASCT2 and LAT1, were evaluated in a panel of breast cancer cell lines grown for 3 days under baseline conditions (5mM glucose DMEM, normoxia). Cell lines representative of each main molecular subtype were selected. These were triple receptor (TN) negative (MDA-MB-231, HCC1806), oestrogen receptor positive (MCF7, T47D) and HER2 positive (BT474, SKBR3).

At the mRNA level assessed by qPCR, expression of both AATs was found to be heterogeneous, with relatively high expression of both AATs in HCC1806. In this cell line, ASCT2 expression was highest and LAT1 expression was second-highest across the panel. LAT1 expression was highest in MCF7. Overall, LAT1 expression was found to be between 5.4-fold (HCC1806) to 10-fold (T47D) higher across the cell line panel compared to ASCT2 (Figure 4.1).

At the protein level assessed by immunoblotting, similar patterns of heterogeneity of expression were observed (Figure 4.2) and statistically significant correlations were demonstrated between mRNA and protein expression (Figure 4.3). Corroborating the qPCR data, the protein levels of ASCT2 and LAT1 were highest in HCC1806 and MCF7 respectively. Both HER2 positive cell lines (BT474 and SKBR3), and TN cell line MDA-MB-231, had relatively low expression of these transporters.

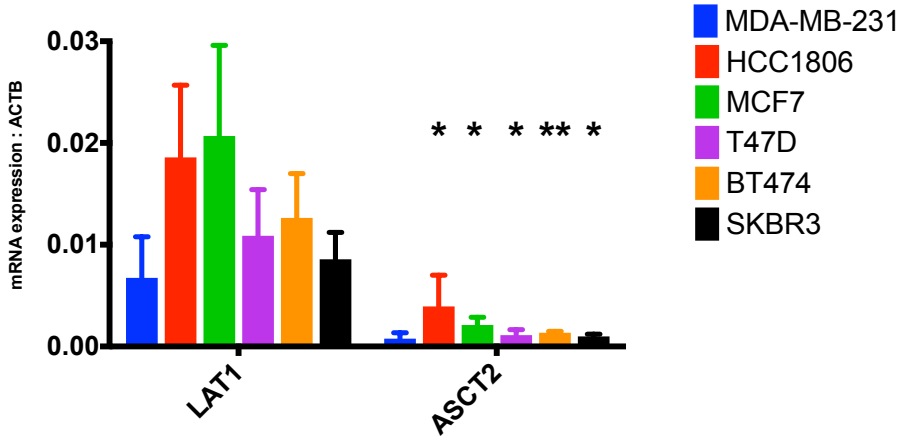

Figure 4.1: LAT1 mRNA expression is higher than ASCT2 across several breast cancer cell lines (N=3). Data represented as mean ± SD relative to mRNA expression of ß-actin (ACTB) (*=p<0.05, **=p≤0.01, ***=p≤0.001, ****=p≤0.0001).

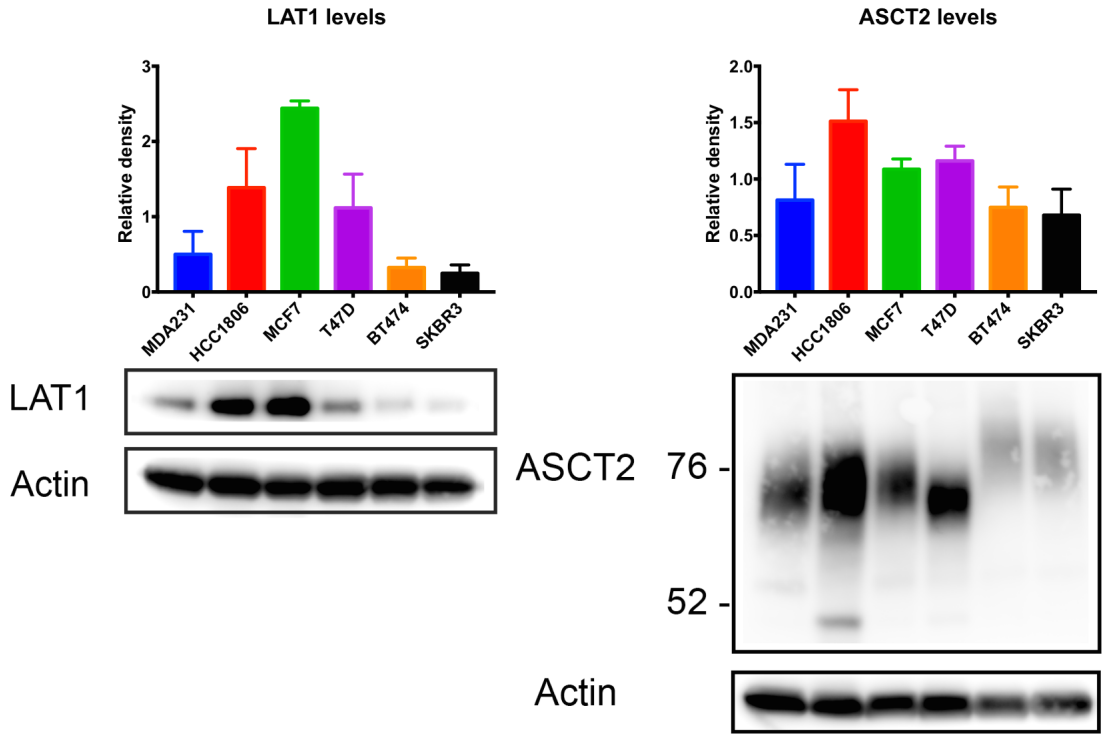

Figure 4.2: Protein expression of LAT1 and ASCT2 across the breast cancer cell line panel. Protein levels of ASCT2 and LAT1 were highest in HCC1806 and MCF7 respectively.

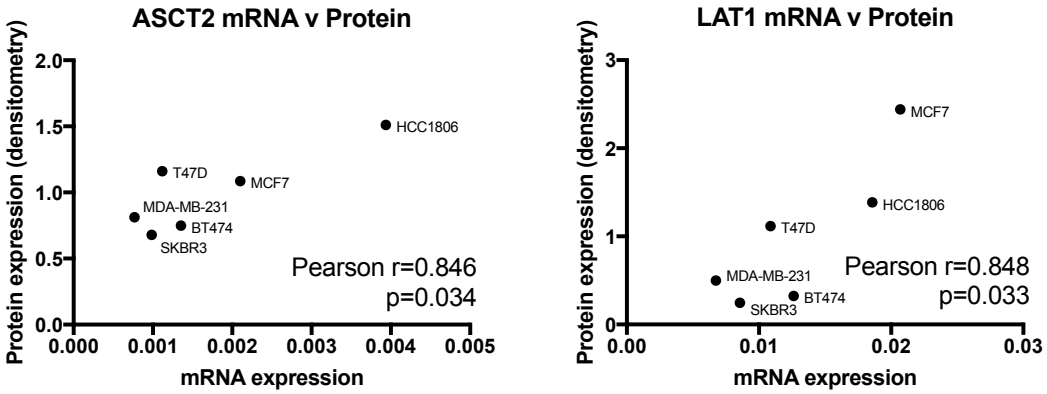

Figure 4.3: Correlation between mRNA and protein expression of ASCT2 and LAT1 across the breast cancer cell line panel. Statistically significant correlations were demonstrated between mRNA and protein expression.

4.3 Optimisation of an *in vitro* fluciclovine uptake assay

For this work, it was important to use cell lines exhibiting distinctly different levels of ^{14}C-FACBC uptake. To guide this choice, reference was made to the inter-cell line differences in relevant AAT expression, and HCC1806 and BT474 were chosen. This was based on the expectation that HCC1806 would have be representative of a 'high uptake' cell line and BT474 of a 'low uptake' cell line, aligned with the differences in AAT expression between the two. Optimisation experiments were repeated once.

4.3.1 Concentration

The first step was to optimise the concentration of ^{14}C-FACBC used in the assay. The concentration used in prior publications was 10 μM. The uptake assay was performed using a range of concentrations (1, 2.5, 5 and 10 μM) of ^{14}C-FACBC and a fixed incubation time of 5 minutes. The choice of incubation time at this first step of optimisation was guided by existing literature [4]. As a negative control, the same assays were performed on ice.

There was a linear increase in ^{14}C-FACBC uptake with increasing concentration in both cell lines (Figure 4.4A and B). ^{14}C-FACBC uptake was significantly higher in HCC1806 across all concentrations (Figure 4.4C), broadly consistent with the differences in AAT expression. While ^{14}C-FACBC uptake was consistently higher than compared to uptake on ice, there was still an apparent increase in ^{14}C-FACBC uptake with increasing concentration observed with the assay performed on ice (Figure 4.4A and B). This suggests

either low but persistent levels of amino acid transport or a degree of adherent ^{14}C-FACBC on the cell surface or extra-cellular matrix, incremental with concentration. To take this observation into account in the decision of optimal concentration, the degree of ^{14}C-FACBC uptake at room temperature was compared to ice for each concentration (Figure 4.4D).

In the 'low uptake' cell line BT474, the largest difference between uptake at room temperature compared to ice was 4.1-fold at a concentration of 2.5 μM. In 'high uptake' HCC1806, this difference was 3.4-fold at 2.5 μM, while the largest difference of 4.0-fold was observed at a concentration of 10 μM. Balancing these observations with the need to minimise type I error in "low uptake" scenarios (more prone with higher concentrations), optimise resources and adhere to best practice of handling radioactive substances, a working concentration of 2.5 μM was chosen.

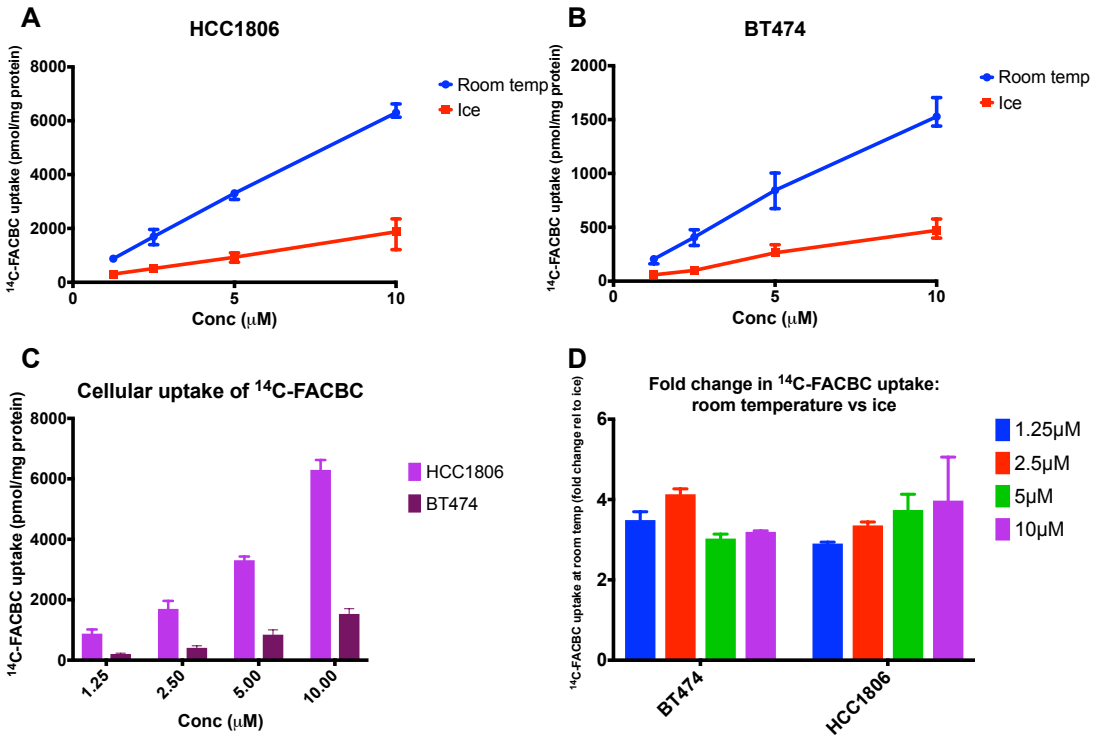

Figure 4.4: Linear increase in ^{14}C-FACBC uptake with increasing ^{14}C-FACBC concentration. This was observed in both cell lines HCC1806 (A) and BT474 (B). ^{14}C-FACBC uptake was significantly higher in HCC1806 across all concentrations (C). The largest difference between uptake at room temperature compared to ice in the 'low uptake' cell line BT474, was 4.1-fold at a concentration of 2.5 μM, lending weight to the choice of this as a working concentration (D). Data represented as mean ± range (N=2).

4.3.2 Time course

The next step was to optimise the incubation time for the fluciclovine uptake assay. Using the working concentration of 2.5 μM, the uptake assay was performed using a range of incubation times (1, 2.5, 5, 7.5, 10, 15 minutes), in HCC1806 and BT474.

There was a linear increase in ^{14}C-FACBC uptake with time in both cell lines (Figure 4.5), providing reassurance that transport was not saturated in both

'high uptake' and 'low uptake' scenarios across this time course, which would otherwise increase the risk of type II error.

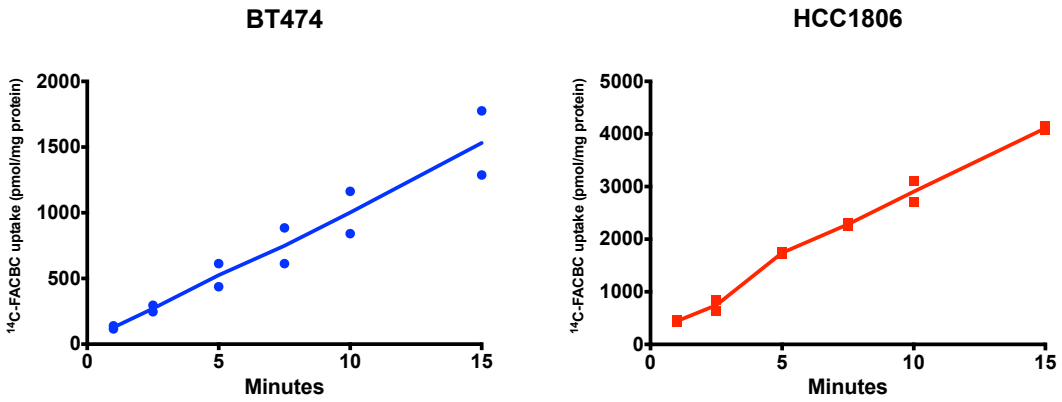

Figure 4.5: Linear increase in ^{14}C-FACBC uptake up to 15 minutes in the 'low' (BT474) and 'high' (HCC1806) uptake cell lines. Individual data points presented with line graphs depicting the mean values (N=2).

With this result, it was decided to adhere to a working incubation time of 5 minutes, aligned with pre-existing literature and working knowledge provided in the first optimisation step. Furthermore, this would provide a balance between maintaining an optimal readout of ^{14}C-FACBC uptake and delicate experimental conditions such as hypoxia, where a protracted period of re-oxygenation may erroneously influence the results.

4.4 Mechanisms of fluciclovine uptake in breast cancer

4.4.1 Heterogeneity of fluciclovine uptake across a panel of breast cancer cell lines

To gain an understanding of the inter cell line differences in fluciclovine uptake to guide experimental choice, this was assessed in the same panel of

6 breast cancer cell lines described in the prior section, after 3 days under baseline conditions (5 mM glucose DMEM, normoxia).

Heterogeneity of ^{14}C-FACBC uptake was observed between different molecular subtypes, as well as within each molecular subtype (Figure 4.6). Of note, TN cell line HCC1806 had the highest uptake, while HER2 positive cell line BT474 had the lowest uptake. There was an approximately 3-fold difference in uptake between TN cell lines HCC1806 and MDA-MB-231, illustrative of the intra-molecular subtype differences in ^{14}C-FACBC uptake.

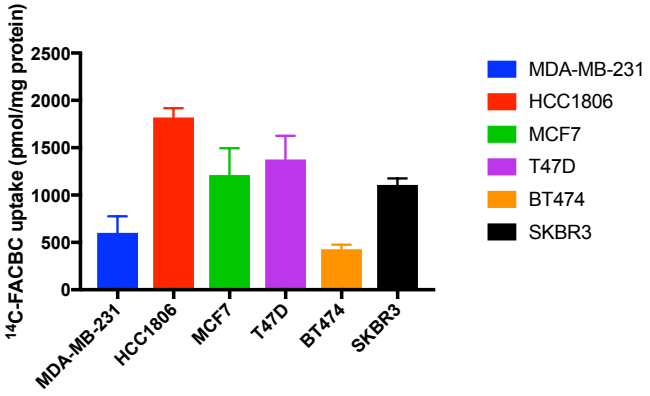

Figure 4.6: ^{14}C-FACBC uptake across a panel of breast cancer cell lines under baseline conditions. Data represented as mean ± SD (N=3).

4.4.2 Fluciclovine uptake correlates with ASCT2 but not LAT1 expression in breast cancer

Based on observations that LAT1 mRNA expression was significantly higher than ASCT2 in this panel, and having met the crude expectation that a cell line expressing high levels of these AATs would exhibit high fluciclovine uptake and vice versa, the anticipation was that fluciclovine uptake would be highly representative of LAT1 expression. This was also fuelled by anecdotal description of fluciclovine as a leucine analogue [1].

To explore this, the baseline protein expressions of LAT1 and ASCT2 were correlated with ^{14}C-FACBC uptake. Intriguingly, there was a statistically significant correlation between uptake and ASCT2 expression (r=0.847, p=0.033), but not with LAT1 (r=0.545, p=0.263) (Figure 4.7), raising possibility of ASCT2 as the dominant transporter, despite the aforementioned.

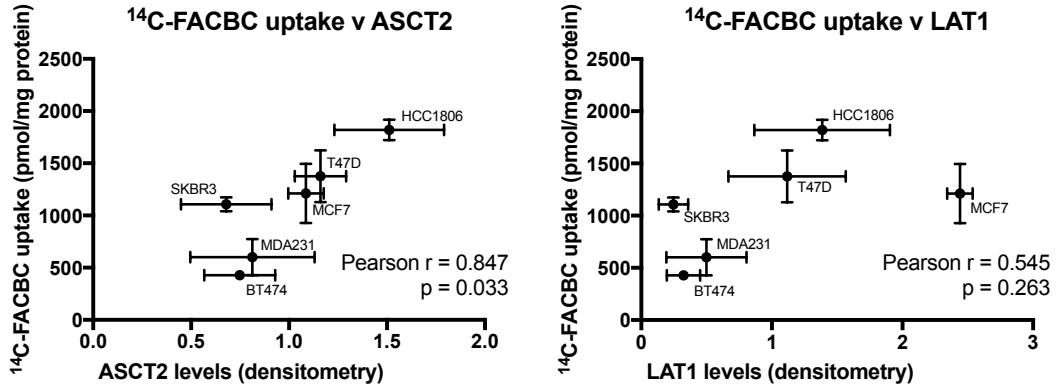

Figure 4.7: ^{14}C-FACBC uptake correlates with ASCT2 protein expression but not LAT1. Data represented as mean ± SD (N=3).

A series of experiments were then undertaken to further explore this unexpected observation.

4.4.3 High affinity natural amino acids for ASCT2 but not LAT1 inhibit fluciclovine uptake in breast cancer

Competitive inhibition of ^{14}C-FACBC uptake by a wide panel of natural amino acids was performed in the HCC1806 cell line. The amino acids were selected based on moderate-high affinity to the respective transporters of interest. As there has been a brief description of SNAT2 being a minor contributor (up to 17%) of fluciclovine transport in prostate cancer [2], high affinity substrates for

SNAT2 were also included. Inhibition by GPNA, the only transporter-specific inhibitor (of ASCT2) amongst those of interest, was also evaluated.

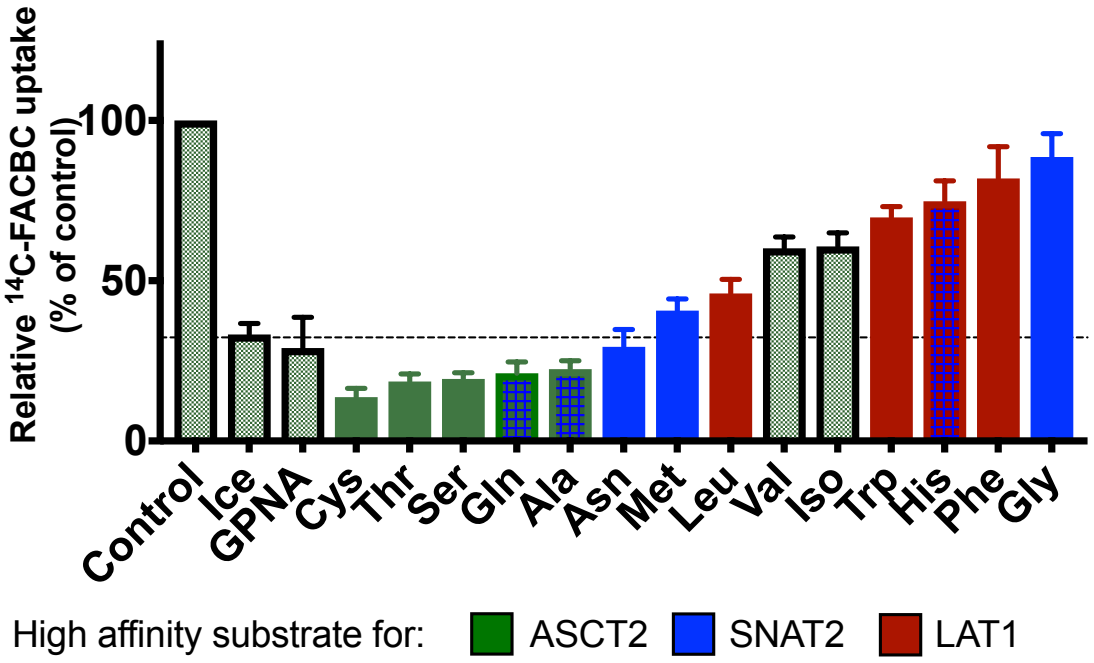

Figure 4.8: Competitive inhibition of ^{14}C-FACBC uptake by natural amino acids in HCC1806. Bars containing a cross hatched pattern of two colours indicate high affinity for two corresponding transporters. Dashed line represents the degree of uptake on ice. Data represented as mean ± SD (N=3).

High-affinity substrates of ASCT2 (glutamine, alanine, serine, cysteine and threonine) caused marked inhibition of ^{14}C-FACBC uptake (14-21% of control) (Figure 4.8) to below that on ice, which was considered to be the basal level of uptake. With the ASCT2 inhibitor GPNA, the level of ^{14}C-FACBC uptake was inhibited to 29% of control, just below basal activity on ice. This finding strongly supported the correlative data presented in the prior section.

The reduction of ^{14}C-FACBC uptake was less with high-affinity substrates of LAT1 (41-82% of control). Specifically, L-leucine inhibited uptake to 46% of control. The degree of uptake inhibition was widely varied with the high-affinity

substrates of SNAT2. Here, asparagine and methionine inhibited ^{14}C-FACBC uptake to 29% and 41% of control respectively, while histidine and glycine inhibited uptake to only 75% and 89% of control respectively.

As asparagine and methionine are also known substrates of ASCT2, the data as it stood supported only a potential limited role of SNAT2 in fluciclovine transport in this breast cancer cell line. To evaluate this further, competitive inhibition of uptake using MeAIB, an inhibitor of SNAT1, 2 and 4, was evaluated in HCC1806, MCF7 and BT474. MeAIB was used as no specific inhibitors of SNAT 2 were commercially available at the time of the project. The 3 cell lines were chosen to represent the 3 molecular subtypes, as well as varying degrees of baseline ^{14}C-FACBC uptake.

There was no significant inhibition of ^{14}C-FACBC uptake by MeAIB, while GPNA inhibited ^{14}C-FACBC uptake to 21%-27% of control across the 3 cell lines (Figure 4.9). This supports a dominant role of ASCT2 in fluciclovine transport across the representative molecular subtypes of breast cancer, with a nominal contribution by SNAT2, supported only in part by a minor degree of competitive inhibition by its substrates.

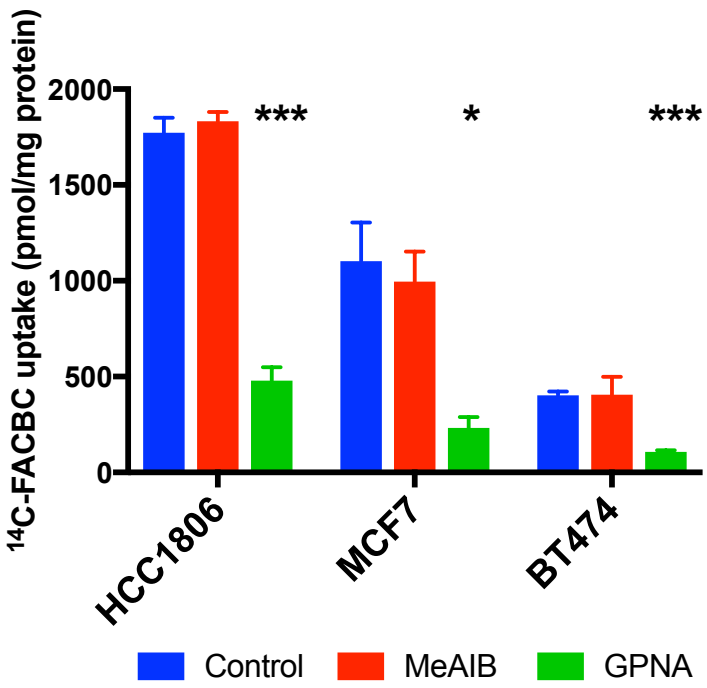

Figure 4.9: Competitive inhibition of ^{14}C-FACBC uptake by MeAIB compared to GPNA. There was no significant inhibition of ^{14}C-FACBC uptake by MeAIB, while GPNA inhibited ^{14}C-FACBC uptake to 21%-27% of control across the 3 cell lines. Statistical comparisons made to control. Data represented as mean ± SD (*=p<0.05, **=p≤0.01, ***=p≤0.001, ****=p≤0.0001) (N=3).

4.4.4 siASCT2 confirms ASCT2 as the dominant transporter of fluciclovine in breast cancer

To delineate specific transporter contribution to fluciclovine transport, siRNA knockdown of ASCT2 and LAT1 was performed in the 3 representative cell lines (HCC1806, MCF7 and BT474).

^{14}C-FACBC uptake was markedly decreased to 22-28% in the presence of GPNA, and 16-28% with ASCT2 knockdown (Figure 4.10). This was consistently lower than the basal levels of transport on ice (consistently approximately 30% across all cell lines). There was no significant difference in uptake in the presence of control siRNA and LAT1 knockdown across the cell

lines (Figure 4.11). Interestingly, there was a small additive effect of LAT1 knockdown in the presence of GPNA on inhibition of uptake (18-30% in control siRNA with GPNA, dropping to 11-23% in LAT1 knockdown with GPNA, p<0.05).

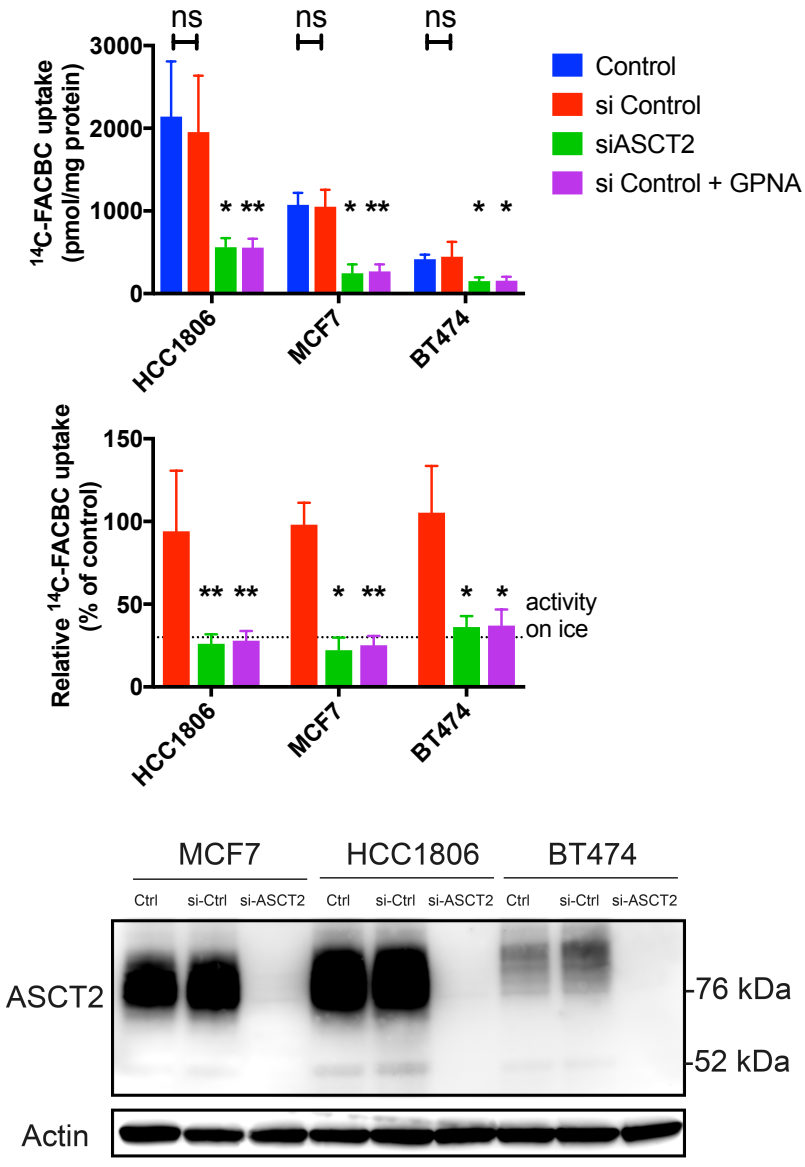

Figure 4.10: Effects of si-ASCT2 (1 nM) and competitive inhibition by 1 mM GPNA on ^{14}C-FACBC uptake in 3 representative breast cancer cell lines. Across the cell lines, ^{14}C-FACBC uptake was significantly decreased in the presence of GPNA, and with ASCT2 knockdown. Statistical comparisons made to si-Control unless otherwise indicated. Data represented as mean ± SD (*=p<0.05, **=p≤0.01) (N=3).

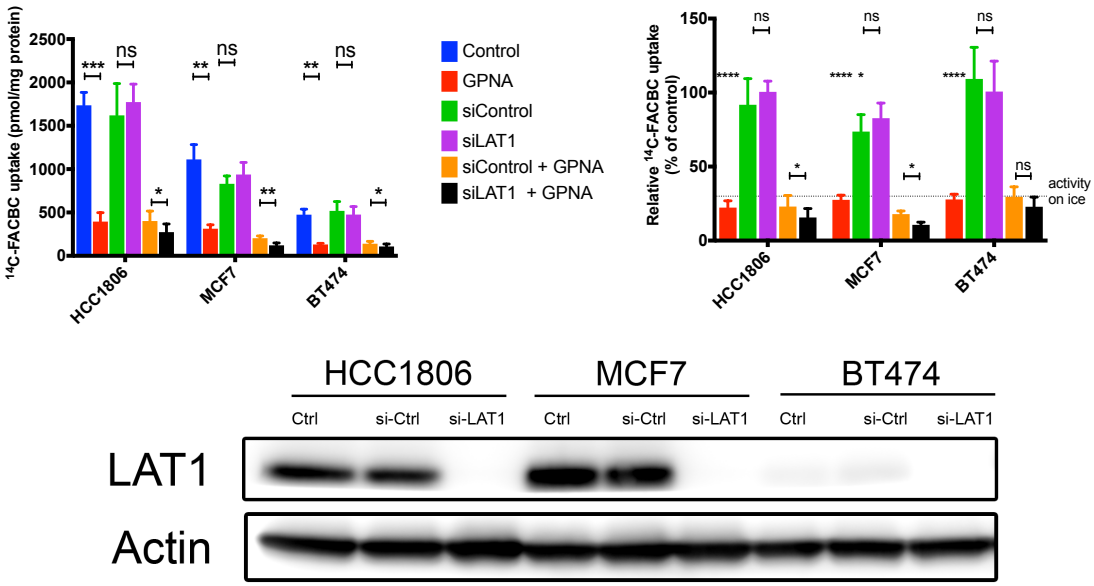

Figure 4.11: Effect of si-LAT1 (1 nM) ± competitive inhibition by 1 mM GPNA on ^{14}C-FACBC uptake in 3 representative breast cancer cell lines (N=3). There was no significant difference in uptake in the presence of control siRNA and LAT1 knockdown. This was with exception of a small additive effect of LAT1 knockdown in the presence of GPNA, observed in all 3 cell lines. Statistical comparisons made to control, unless otherwise indicated. Data represented as mean ± SD (*=p<0.05, **=p≤0.01, ***=p≤0.001, ****=p≤0.0001) (N=3).

4.5 Discussion

This aspect of the project focused on characterising the transport mechanisms of fluciclovine in breast cancer. The main finding is that fluciclovine transport in breast cancer is predominantly mediated by the high-affinity glutamine transporter ASCT2, contrary to initial expectations based on its prior attribution as a leucine analogue and greater LAT1 expression compared to ASCT2.

Interestingly, a small additive effect of LAT1 knockdown was observed with competitive inhibition of ^{14}C-FACBC uptake by GPNA. One explanation for this observation would be a minor role of LAT1 in overall fluciclovine uptake, masked by the dominant influx of fluciclovine mediated by ASCT2, where the latter is uninhibited. As an adjunct to this, ASCT2 may be driving significant fluciclovine uptake indirectly, by influx of glutamine which is then exchanged by LAT1 for intake of fluciclovine. Given both transporters have substrates in common (e.g. threonine, tryptophan, phenylalanine) but with differing affinities, it may well be that other substrates are involved in this roulette. In either mechanism, ASCT2 remains central. This underscored the next hypothesis that fluciclovine uptake could be used to interrogate early response to therapies targeting / augmenting glutamine metabolism.

Chapter 5 : Fluciclovine is a biomarker of early response to modulation of glutamine metabolism

Declaration of work

All of the *in vitro* work was performed by E.J. Teoh, with material support, ^{14}C-FACBC, from Blue Earth Diagnostics Ltd.

Animal work: E.J. Teoh undertook overarching project management, image processing and analysis, and data analysis. Dr. Esther Bridges executed the day-to-day experimental procedures described herein, assisted by Dr. Christos Zois. Dr. Veerle Kersemans, and other members of the Radiobiology Research Institute Imaging Core led by Dr. Sean Smart, performed the *in vivo* imaging with assistance from Dr. Esther Bridges and Dr. Christos Zois. Synthesis of ^{18}F-fluciclovine was performed by Thomas Wilson and Dr. Stefan Verhoog from the Gouverneur Group.

5.1 Introduction

In addition to testing hypotheses described in the first chapter, that fluciclovine imaging could be useful in the context of mTORC1 inhibition and hypoxia, the utility of fluciclovine in assessing early response to treatment was assessed in selected drugs, guided by the underlying uptake mechanisms.

Alongside *in vitro* experiments to test the generated hypotheses, *in vivo* imaging is essential as a first step towards clinical translation. In this respect, there is also a paucity of experience in the published literature, warranting careful optimisation of experiments. The results of these will be presented in this chapter.

At the time of planning this work, the only publication describing ^{18}F-fluciclovine imaging in breast cancer xenograft models was by Liang et al. [69], where proof of concept imaging was performed in MDA-MB-231 xenografts. Here, the scan acquisition was performed 1 hour after tracer administration, which is vastly different from the clinical scanning protocol for prostate cancer where acquisition is commenced 3-5 minutes after injection. In order to optimise image signal while supporting high throughput scanning of animal models, it was pertinent to investigate the optimum scan acquisition timings. Along the same vein of optimising image signal, a time course of ^{18}F-fluciclovine imaging characteristics of breast cancer xenografts is vital to inform data interpretation and selection of ideal scanning timepoints.

The need for fasting in clinical PET imaging with ^{18}F-FDG is well-established. While the use of ^{18}F-fluciclovine for recurrent prostate cancer imaging in patients is recommended with a period of fasting, the collective evidence to support or refute the need for fasting in amino acid PET imaging, let alone ^{18}F-fluciclovine, is sparse and require investigation in this work.

On short term fasting (for at least 4 hours), it has been reported that levels of 9 non-essential amino acids (with affinity for system L, excluding glutamine) are normal [132]. Another study has reported that concentrations of all amino acids rise and peak at up to 4 hours following ingestion of a meal [133]. In a study of 11 patients who underwent ^{11}C-methionine PET imaging after a 4-hour fast, there was no significant correlation between system L amino acid levels and organ uptake of ^{11}C-methionine, including the brain [132]. In contrast, an inverse correlation between system L amino acid levels and transport of ^{18}F-phenylalanine into the brain has been described in 14 non-fasted patients [134]. Both radiotracers are transported by system L amino acid transporters, as opposed to ASCT2, limiting translatability to ^{18}F-fluclovine imaging. Furthermore and of greater pertinence, the effect on pathological uptake of radiotracer was not ascertained.

Based on the limited aforementioned evidence, it would be reasonable to postulate that pre-scan fasting would optimise tumour signal, due to relatively reduced / normalised circulating amino acid levels in direct competition with ^{18}F-fluciclovine for tumour cell internalisation. However, it is important to consider if the effect of circulating amino acid pool size on intra-cellular amino

acid levels, if any. As ASCT2 is an antiporter, requiring exchange of an intra-cellular substrate amino acid for transport of another substrate into the cell, raised intra-cellular amino acid levels may in fact increase fluciclovine uptake in the short term, and vice versa. It has been shown *in vitro* that injection of cells with the pre-requisite substrate increases amino acid tracer influx (phenylalanine as a substrate for LAT1, using the tracer ^{123}I-2-iodotyrosine [135]).

Given the compounded complexity of the myriad of amino acid transporters which recognise multiple substrates with different affinities, it is difficult to assimilate this quantum of information to inform the true need for a short fast pre-imaging. In view of this, establishing the differences in fluciclovine uptake in the fasted and non-fasted state is indicated, to determine the best form of preparation to optimise tracer uptake.

5.2 Optimisation of ^{18}F-fluciclovine imaging in vivo

5.2.1 Scan acquisition timing

To optimise workflow and image signal, a 60-minute dynamic scan acquisition of a HCC1806 xenograft was performed. The imaging data were binned into 2-minute segments and tracer activity in the tumour, heart, liver and muscle was measured to generate time activity curves (TACs).

This demonstrated tumour uptake of ^{18}F-fluciclovine to peak at 10 minutes, remain at this plateau up to 22 minutes, and undergo a very gradual washout thereafter (Figure 5.1). At the 60-minute timepoint, tumour activity was still

approximately 66% of the 10-minute peak. This pattern was similar to prostate cancer TACs derived from humans [3]. TACs for the organs were similar. With regards to the liver which had the highest uptake, there was a more visually distinct washout after 20 minutes, although 68% of peak activity remained at 60 minutes.

Based on this, and workflow considerations, an optimal timepoint of 15 minutes post-injection was chosen for ^{18}F-fluciclovine imaging.

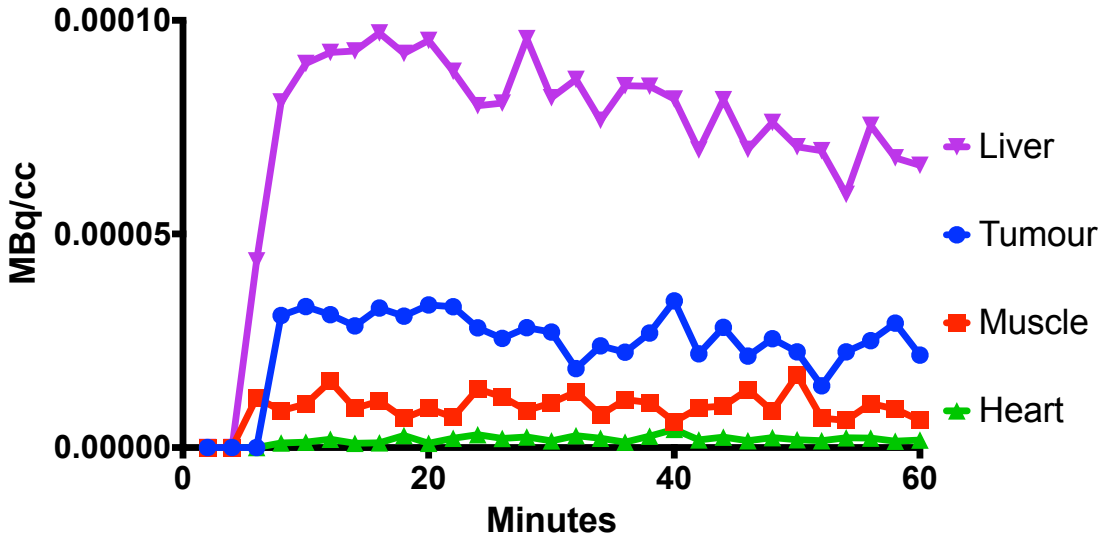

Figure 5.1: Time activity curves from analysis of tumour and organs in a HCC1806 xenograft model. Tumour tracer uptake peaked at 10 minutes, and underwent a very gradual washout after 22 minutes, with a similar pattern demonstrated in the organs.

5.2.2 Fasting improves tumour uptake of ^{18}F-fluciclovine

To evaluate this, ^{18}F-fluciclovine imaging was performed in 6 mice, previously injected with HCC1806 xenografts at the same time. Half of the group were fasted at the same time, at least 4 hours before tracer administration, and the other half were allowed to eat freely. At the time of imaging, there was no

significant difference in tumour size (GMD) between the groups (fasted 6.1 ± 0.2 mm vs non-fasted 5.3 ± 0.6 mm, p=0.092) (Figure 5.2). In the fasted group, xenograft ^{18}F-fluciclovine uptake was close to 50% higher (SUV_{peak} 2.9 ± 0.4) compared to the non-fasted group (SUV_{peak} 2.0 ± 0.4, p=0.030) (Figure 5.2 and Figure 5.3).

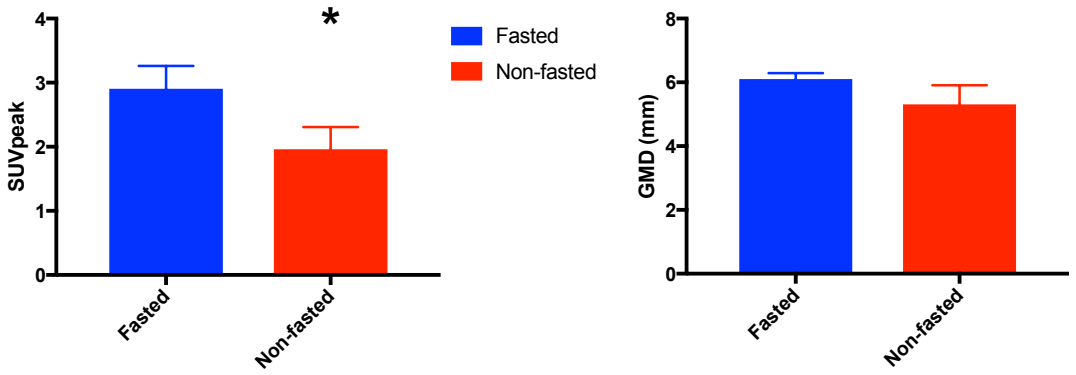

Figure 5.2: ^{18}F-Fluciclovine uptake in HCC1806 xenografts is higher in fasted mice. There was no significant difference in xenograft size. Data represented as mean ± SD (*=p<0.05) (N=3).

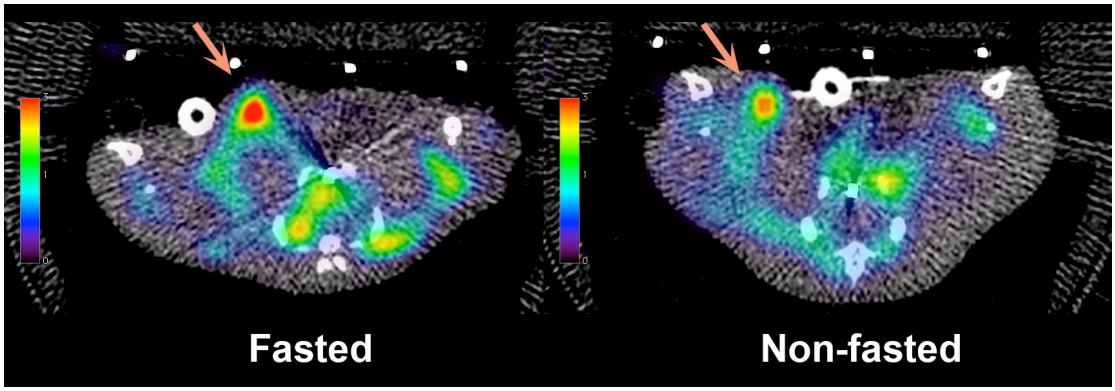

Figure 5.3: Representative ^{18}F-Fluciclovine PET/CT axial images of CD1-nude mice bearing HCC1806 xenografts, fasted and non-fasted pre-tracer administration. SUV_{peak} of the xenograft in the fasted mouse was 2.9, compared to 2.0 in the non-fasted mouse.

5.2.3 Tumour uptake of ^{18}F-fluciclovine is highly dependent on size

In order to determine the optimum timepoints for imaging where maximum signal could be obtained, and gain familiarity with ^{18}F-fluciclovine uptake

characteristics over time, an imaging time course was performed. Mice bearing HCC1806 xenografts were imaged at 2, 5 and 7 weeks post tumour injection, analogous to the commencement, midpoint and end of a treatment course.

^{18}F-Fluciclovine uptake was highest at the first timepoint, with a consistent decrease in uptake at subsequent time points (mean uptake across all timepoints: SUV_{peak} 2.9, 2.4, 1.7). There was a statistically significant negative correlation with xenograft size (r=-0.743, p=0.042), and also noted that ^{18}F-fluciclovine uptake became limited to the periphery and more rim-like with increasing xenograft size, and central necrosis. This provided useful information to plan imaging timepoints early in order to maximise tumour signal. More importantly, in the context of planning experiments with drug treatments, it underpinned the need to establish baseline ^{18}F-fluciclovine uptake for comparison with uptake during/after treatment, analogous to clinical imaging practice. For this purpose, results involving drug treatments were expressed as uptake ratios.

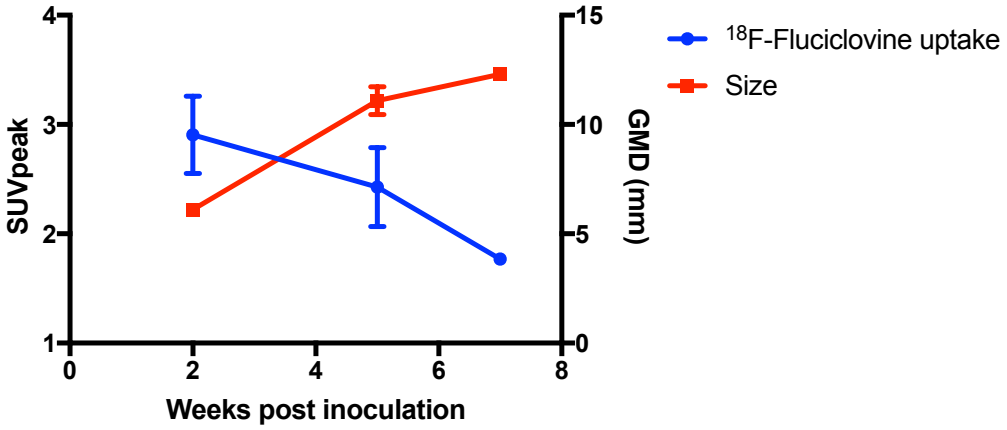

Figure 5.4: Time course of ^{18}F-Fluciclovine uptake in HCC1806 xenografts. Data represented as mean ± SD (N=3 in weeks 2 and 5, N=2 in week 7).

5.2.4 Test re-test variability of ^{18}F-fluciclovine uptake

To evaluate the reproducibility of ^{18}F-fluciclovine measurements *in vivo*, uptake in the liver, muscle and heart was quantified on two separate scans 7 days apart in 10 CD1-nude mice. Overall, the test re-test values were reproducible in the heart and liver, with a bias (mean percentage change between test and re-test values) of -2.0 to -3.4%, low variability (standard deviation of the bias) of 8.2-8.8%, and with intra-class coefficients (ICC) exceeding 0.9 (). While there was relatively higher variability (15.4%) in the muscle, the other metrics were well within the ranges reported for other PET radiotracers ().

Table 5.1: Test re-test reproducibility metrics of ^{18}F-fluciclovine uptake in various organs measured 1 week apart. SUV_{mean} values represented as mean ± SD (n=10).

	Test SUV_{mean}	Re-test SUV_{mean}	Bias	Variability	Reliability (ICC)
Liver	1.9 ± 0.4	1.9 ± 0.3	-2.0%	8.2%	0.936
Heart	1.7 ± 0.4	1.8 ± 0.4	-3.4%	8.8%	0.960
Muscle	1.0 ± 0.3	0.9 ± 0.3	5.6%	15.4%	0.883

5.3 Fluciclovine as a biomarker of early response to treatment

Having established that the high-affinity glutamine transporter ASCT2 is the dominant transporter of fluciclovine in breast cancer cell lines, it raised the potential for using fluciclovine in early imaging response to inhibitors of glutamine metabolism and pathways which augment glutamine utilisation.

5.3.1 Increase in fluciclovine uptake predicts response to glutaminase inhibition in sensitive breast cancer cell lines

An appropriate candidate drug to evaluate this theme was identified. CB-839 is a glutaminase inhibitor that has been demonstrated to have an anti-proliferative effect on TN breast cancers *in vitro* [88] and is currently being evaluated in early phase clinical trials for the treatment of various malignancies. In the former work by Gross et al, cellular glutamine metabolism (characterised by quantification of cell medium glutamine and glutamate concentrations) was found to decrease with increasing doses of CB-839 in the sensitive HCC1806 cell line, with consequent increase in intracellular glutamine pool in under 24 hours. This formed the basis for a working hypothesis that change in fluciclovine uptake, as a surrogate for this biochemical change, could be a biomarker of subsequent response to treatment. In this case, fluciclovine uptake was hypothesised to increase, based on the build-up of intracellular glutamine pool to exchange for fluciclovine via the antiporter mechanism of ASCT2.

To establish a suitable working concentration of CB-839 for this experiment, dose response curves across the three representative breast cancer cell lines were generated. Cells were treated with increasing doses of CB-839 up to 10 μM for 5 days and a proliferation assay (Cyquant) was performed. This demonstrated MCF7 and HCC1806 to be sensitive to CB-839 (IC_{50} 8 nM and 24 nM respectively), while BT474 was resistant (Figure 5.5). Despite a relatively higher modelled IC_{50} than MCF7, HCC1806 appeared to be the

most sensitive cell line as there was an incremental effect of CB-839 dose on growth to 1 μM, where growth was 29% of control. In MCF7, the growth effect seemed to reach a nadir at approximately 100 nM where growth was 58% of control. The growth of MCF7 only fell just under 50% at a concentration of 10μM. Based on these observations, a working concentration of 250 nM was chosen to ensure a clear effect of CB-839 treatment on fluciclovine uptake could be elucidated, if any.

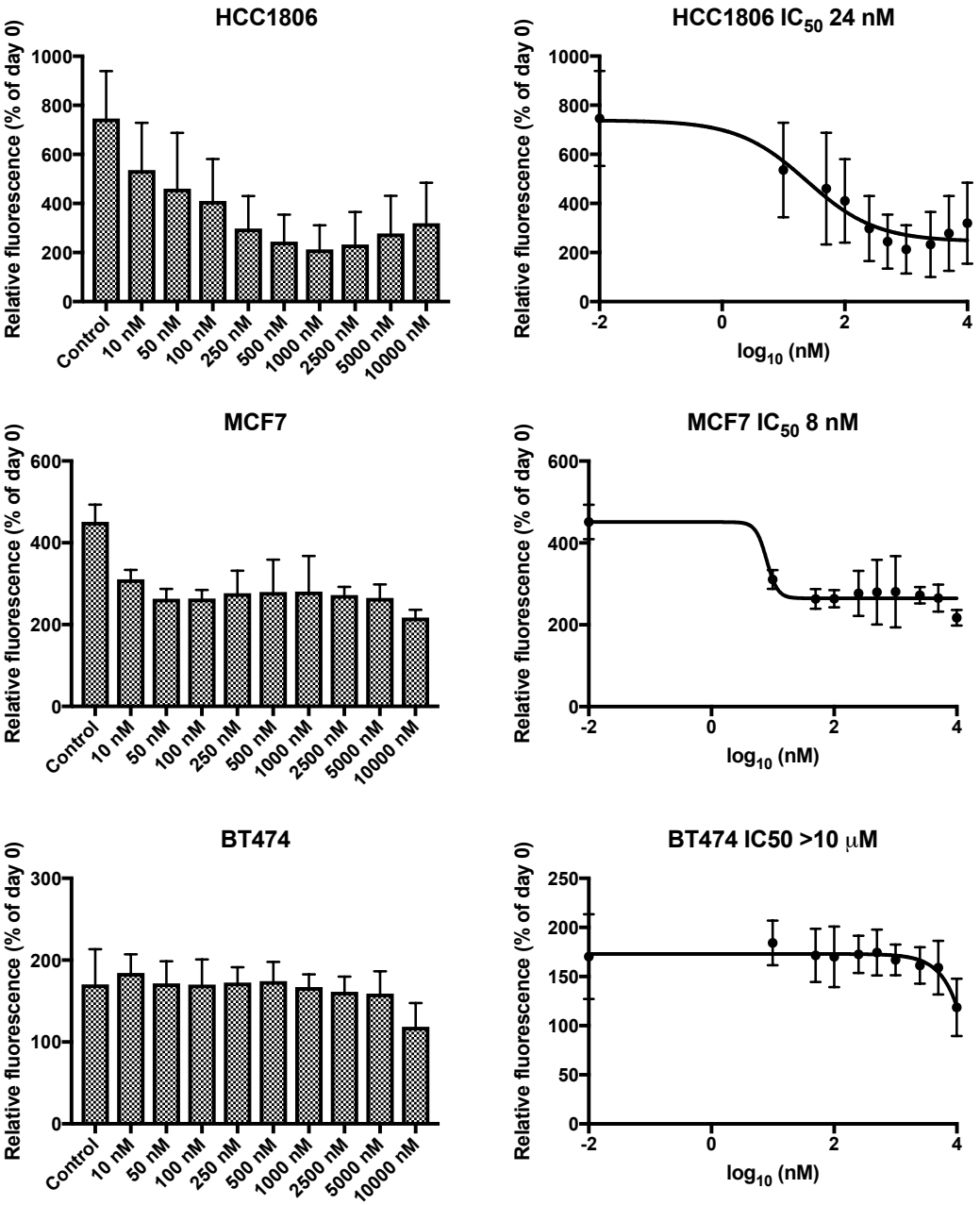

Figure 5.5: Dose response graphs for HCC1806, MCF7 and BT474 treated with CB-839 for 5 days. Data represented as mean ± SD (N=3).

^{14}C-FACBC uptake was assessed in these cell lines after 48 hours of CB-839 treatment. At this time, there was no significant difference in growth between control and CB-839 treated groups (Figure 5.6). In the most sensitive cell line HCC1806, ^{14}C-FACBC uptake almost doubled with CB-839 treatment (170 ±

5% of control (mean ± SD), p<0.01) (Figure 5.7). ^{14}C-FACBC uptake increased in MCF7 as well (153 ± 22% of control (mean ± SD)), albeit not statistically significant (Figure 5.7). There was only a minor, non-statistically significant, increase in fluciclovine uptake in the resistant BT474 cell line (121 ± 9% of control (mean ± SD)).

These findings support the working hypothesis that fluciclovine could act as a biomarker of response to glutaminase inhibition, purportedly by acting as a surrogate of intracellular glutamine levels.

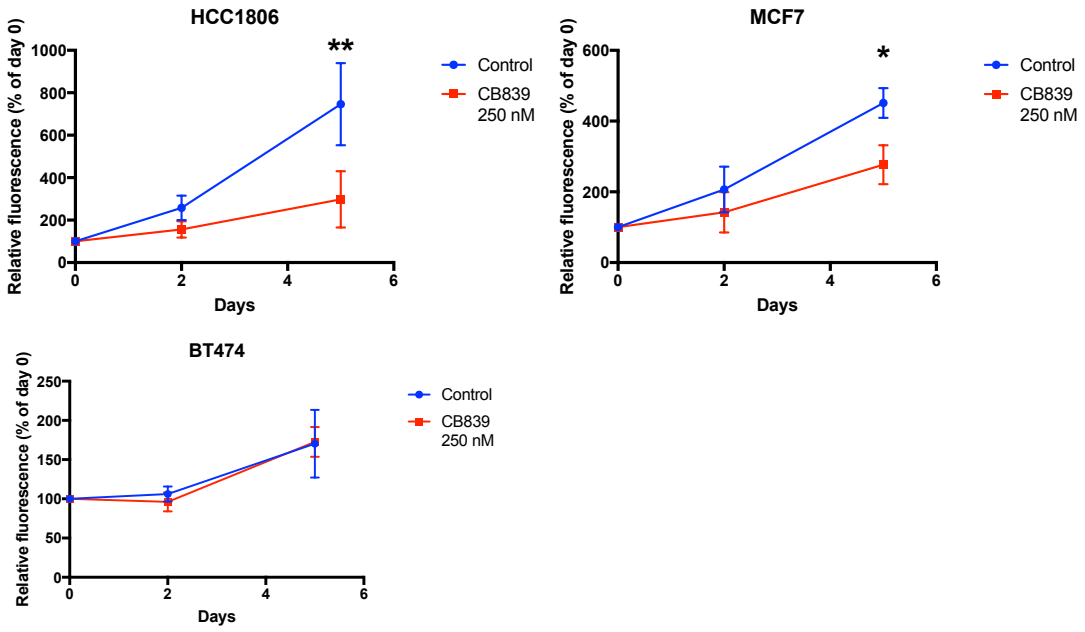

Figure 5.6: Growth of HCC1806, MCF7 and BT474 treated with CB-839 at 2 and 5 days. ^{14}C-FACBC uptake was evaluated at 2 days, before a growth effect was observed in the sensitive cell lines. Data represented as mean ± SD (*=p<0.05, **=p≤0.01) (N=3).

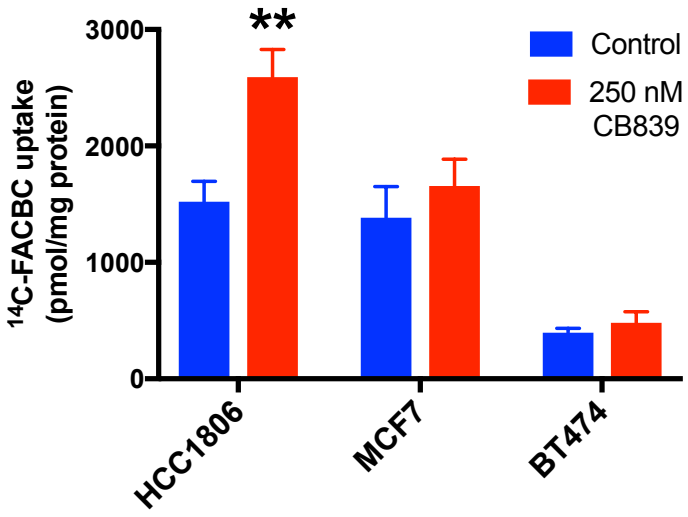

Figure 5.7: ^{14}C-FACBC uptake after 2 days of CB-839 treatment. There was an increase in uptake in the sensitive cell lines, highest in HCC1806. Data represented as mean ± SD (*=p<0.05, **=p≤0.01) (N=3).

5.3.2 Decrease in fluciclovine uptake predicts response to metformin in sensitive breast cancer cell lines in vitro

With this result, it was necessary to evaluate if the opposite phenomenon of increased glutamine metabolism, could be interrogated by fluciclovine uptake. The mitochondrial complex I inhibitor metformin was identified as a suitable drug for this purpose. Previous work in our group has shown increased glutamine metabolism to be a hallmark of breast cancer cell lines sensitive to metformin [118]. In the sensitive MCF7 cell line, metformin treatment induced a shift of substrate use for *de novo* lipogenesis from glucose to glutamine. Furthermore, when starved of glutamine, the effect of metformin treatment on the growth of MCF7, alongside another sensitive cell line MDA-MB-468, was potentiated, while no appreciable effect was observed in the resistant MDA-MB-231 cell line. The effect of metformin on glutamine pool size was not assessed.

^{14}C-FACBC uptake was assessed in the sensitive MDA-MB-468 and MCF7, and resistant MDA-MB-231 after 48 hours of metformin treatment. Based on prior work in our group, a working concentration of 2mM metformin was used. The effect of metformin on growth of these cell lines over 5 days confirmed MDA-MB-468 to be the most sensitive cell line (55 ± 2% of control), followed by MCF7 (82 ± 2% of control), as well as the resistance of MDA-MB-231 (96 ± 2% of control) (Figure 5.8). At the 48-hour timepoint of assessing ^{14}C-FACBC uptake, there was no significant difference in growth between control and metformin treated groups in MCF7 and MDA-MB-231, with a relatively small albeit significant difference in MDA-MB-468 (76 ± 4% of control).

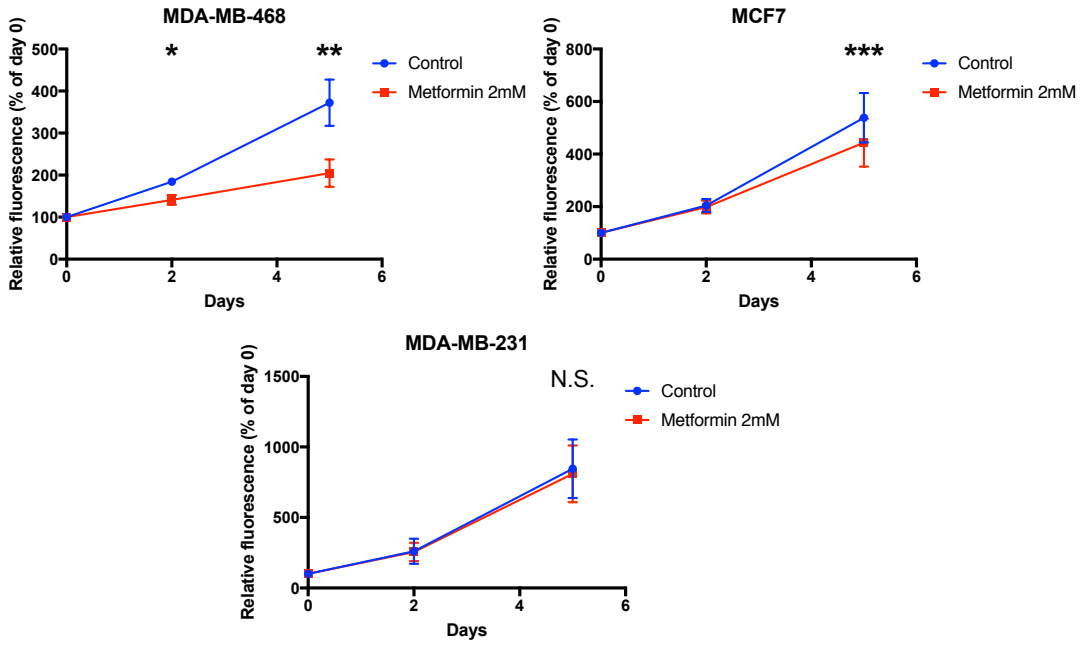

Figure 5.8: Growth of MDA-MB-468, MCF7 and MDA-MB-231 treated with metformin over 5 days, in DMEM containing 5 mM glucose and 1 mM glutamine. Data represented as mean ± SD (*=p<0.05, **=p≤0.01, ***=p≤0.001) (N=3).

In the most sensitive cell line MDA-MB-468, ^{14}C-FACBC uptake in metformin-treated cells decreased to 64 ± 11% of control (p=0.01). A difference was also observed in MCF7 where ^{14}C-FACBC uptake was 79 ± 8% of control (p=0.02). These results were commensurate with the aforementioned degree of growth inhibition at 5 days, using this concentration of metformin (MDA-MB-468 55% of control, MCF7 82% of control). There was no significant change in ^{14}C-FACBC uptake with metformin treatment of MDA-MB-231 (90 ± 8% of control).

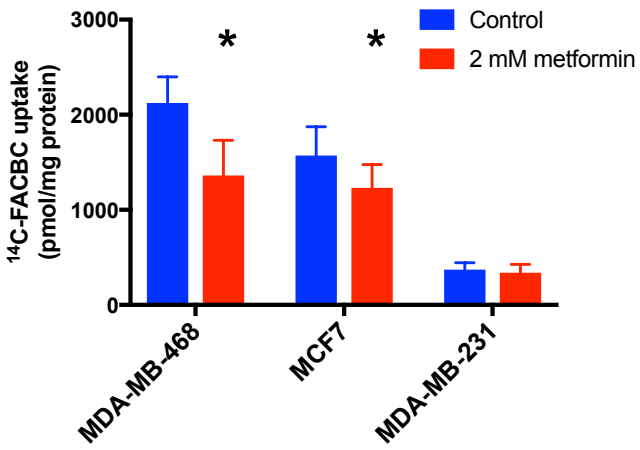

Figure 5.9: ^{14}C-FACBC uptake after 2 days of metformin treatment. There was a decrease in uptake in the sensitive cell lines, highest in MDA-MB-468. Data represented as mean ± SD (*=p<0.05) (N=4).

These results strengthened the postulation that fluciclovine was indeed acting as a surrogate of intracellular glutamine levels, which in this case could be used to predict subsequent response to metformin.

5.3.3 Baseline fluciclovine uptake potentially predicts response to metformin at the outset

In addition to these pertinent findings, it was noted that the sensitive cell lines in this experiment had relatively higher ^{14}C-FACBC uptake at baseline, compared to the resistant MDA-MB-231 cell line (Figure 5.9). Here, ^{14}C-FACBC uptake was 4.1-fold higher in MDA-MB-468, and 3.9-fold higher in MCF7. This prompted exploration of whether baseline fluciclovine uptake could in fact predict sensitivity to metformin.

A panel of 7 breast cancer cell lines representative of the main molecular subtypes (TN: MDA-MB-231, MDA-MB-468, HCC1806; ER+: MCF7, T47D; HER2+: BT474, SKBR3) were treated with increasing doses of metformin (1, 2, 5, 10mM). Intra-molecular subtype heterogeneity of sensitivity to metformin was demonstrated, with MDA-MB-468, T47D and BT474 appearing to be the most sensitive cell lines of each molecular subtype across the range of concentrations (Figure 5.10). Derivation of IC_{50}, to correlate with baseline ^{14}C-FACBC uptake, could not be performed reliably as growth inhibition in excess of 50% was not uniformly achieved. Instead, baseline ^{14}C-FACBC uptake of these 7 cell lines was correlated with the degree of growth with 2mM, 5mM and 10mM metformin. Across these concentrations, 6 out of the 7 cell lines (with BT474 as the outlier) appeared to conform to a linear pattern of negative correlation (Figure 5.11). The overall pattern rendered low correlation coefficients across the board and did not bear statistical significance.

However, as described in the prior chapter, ASCT2 and LAT1 expression is extremely low in BT474, and baseline fluciclovine uptake is the lowest amongst the cell lines evaluated. The clinical relevance of this is that tumours exhibiting low / negative tracer uptake on PET scans would not be suitable for imaging assessment response, where positive response involves demonstrating decrease in tracer uptake. When BT474 was excluded, and the analysis repeated on cell lines with relatively higher baseline uptake, a statistically significant negative correlation was found between baseline ^{14}C-FACBC uptake and growth inhibition with 10mM metformin (r=-0.92, p=0.010), with trends towards significance using 2mM and 5mM metformin (r=-0.83, p=0.058; r=-0.75, p=0.087 respectively) (Figure 5.11).

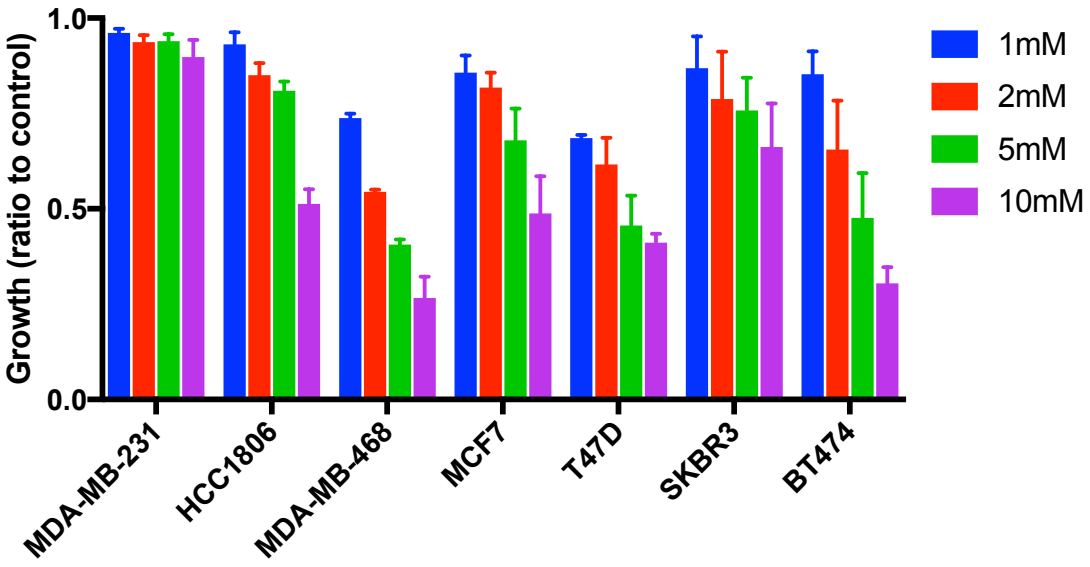

Figure 5.10: Growth of a panel of breast cancer cell lines cell lines treated with a range of concentrations of metformin. Data represented as mean ± SD (N=3).

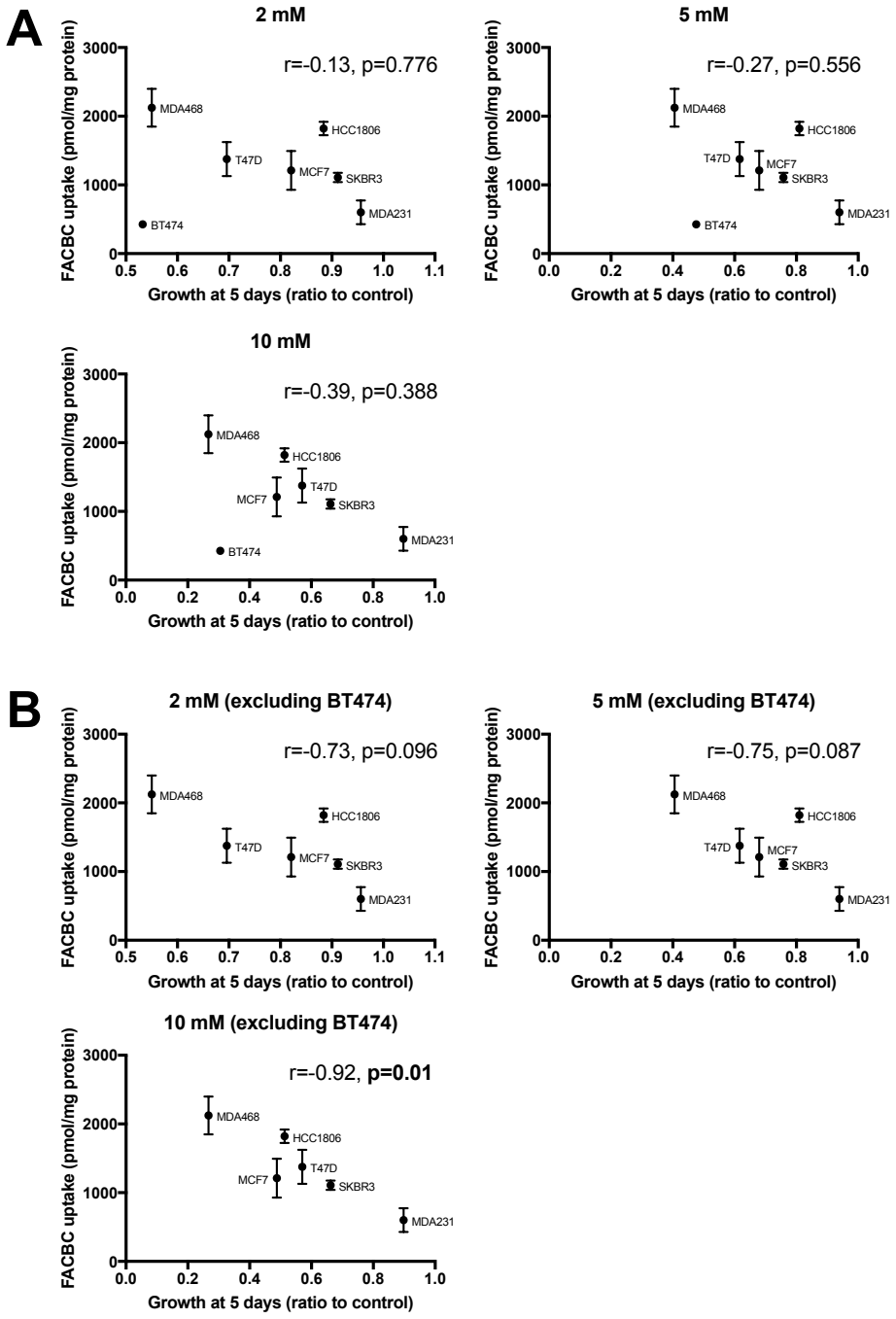

Figure 5.11: Correlation of ^{14}C-FACBC uptake with growth effect of metformin. (A) Baseline ^{14}C-FACBC uptake does not correlate with growth effect across 7 cell lines, with BT474 being a consistent outlier. (B) Repeat analysis was performed excluding BT474, on the rationale that tumours exhibiting low tracer uptake would be unsuitable for imaging response in the clinical setting. This demonstrated stronger correlations between baseline ^{14}C-FACBC and growth effect of metformin, statistically significant at 10 mM. Correlation coefficients were calculated for each indicated dose of metformin. Data represented as mean ± SD (N=3).

5.3.4 Early changes in ^{18}F-fluciclovine uptake predicts sensitivity to metformin in vivo

Following the encouraging *in vitro* results obtained with changes in fluciclovine uptake with metformin, steps were taken to replicate the findings *in vivo*. MDA-MB-468 and HCC1806 xenografts were chosen for this experiment, as they demonstrate similarly high levels of fluciclovine uptake *in vitro*, and had differential response to metformin *in vitro*. The mice underwent ^{18}F-fluciclovine PET/CT at baseline before commencement of treatment, and had a repeat scan after one week of treatment.

In the sensitive MDA-MB-468 xenografts, there was a significant difference in ^{18}F-fluciclovine uptake ratios (Day 7: Day 0) between the control and metformin-treated groups (1.24 ± 0.17 vs 0.84 ± 0.29, p=0.025), in keeping with the working hypothesis (Figure 5.12A, Figure 5.14). In the relatively resistant HCC1806 xenografts, there was no significant difference between the control and metformin-treated groups (0.94 ± 0.14 vs 0.78 ± 0.23, p=0.174) (Figure 5.12B). Tumour volumes between the groups were not significantly different at the outset (MDA-MB-468 control 30 ± 7 mm^3 v 28 ± 6 mm^3; HCC1806 GMD control 65 ± 23 mm^3 v treatment 68 ± 8 mm^3), nor at the 1-week timepoint (MDA-MB-468 control 35 ± 10 mm^3 v 25 ± 13 mm^3; HCC1806 GMD control 172 ± 64 mm^3 v treatment 193 ± 44 mm^3) (Figure 5.13). Commensurate with the *in vitro* growth data, there was a subsequent response to metformin in the MDA-MB-468 xenografts shortly after the scan (10 days into treatment), while the HCC1806 xenografts remained resistant to treatment through to endpoint (Figure 5.13).

As the aforementioned *in vitro* data were based on metformin exposure for 2 days, ^{14}C-FACBC uptake was measured *in vitro* in both cell lines following exposure to metformin for the same length of time as in the *in vivo* experiment, to verify the results. The decrease in uptake in the MDA-MB-468 cell line was remarkably similar to the results from the *in vivo* experiment (70 ± 8% of control, p=0.029) (Figure 5.12C). A marginal decrease, albeit statistically significant, in ^{14}C-FACBC uptake was observed in the HCC1806 cell line, (88 ± 3% of control, p=0.031) (Figure 5.12D) again similar to results from the *in vivo* experiment.

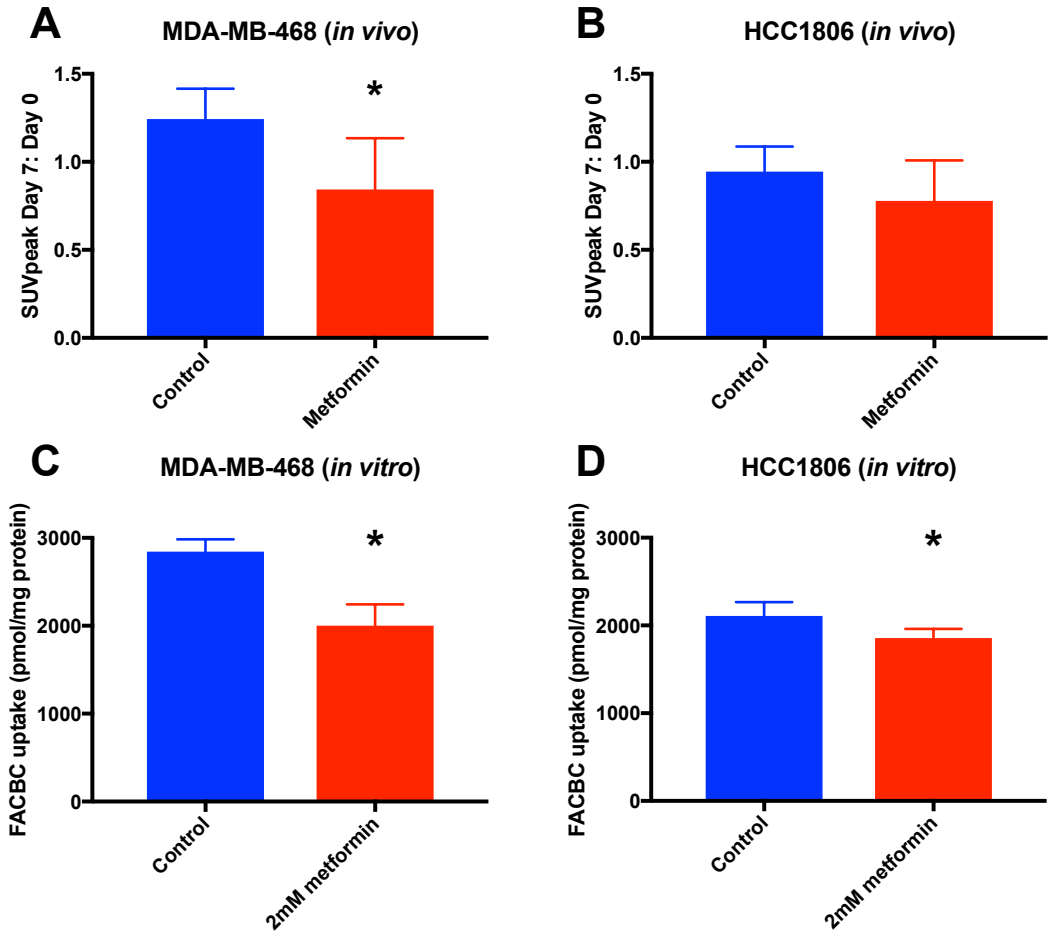

Figure 5.12: ^{18}F-Fluciclovine uptake ratios in sensitive MDA-MB-468 xenografts compared to relatively resistant HCC1806 xenografts (top row). The trends

demonstrated *in vivo* were replicated *in vitro* following metformin treatment of both cell lines matching the timeline of *in vivo* imaging (bottom row). Data represented as mean ± SD (*=p<0.05) (N=5-6 *in vivo*, N=3 *in vitro*).

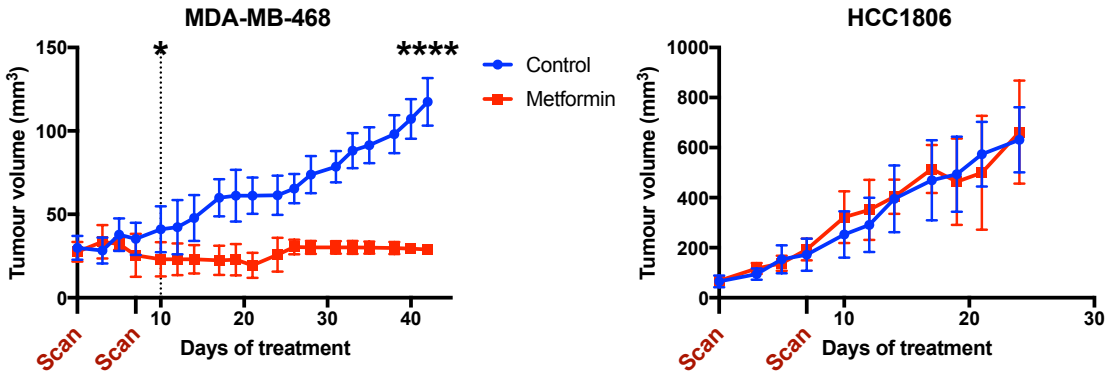

Figure 5.13: *In vivo* response to metformin in sensitive MDA-MB-468 and resistant HCC1806 xenografts. There was no significant difference in xenograft volume between the treatment and control groups at both scanning timepoints (indicated on the horizontal axis of the growth chart). A statistically significant difference in growth was demonstrated in MDA-MB-468 shortly after the second scan (dotted line). Data represented as mean ± SD (*=p<0.05, ****=p≤0.0001) (N=6).

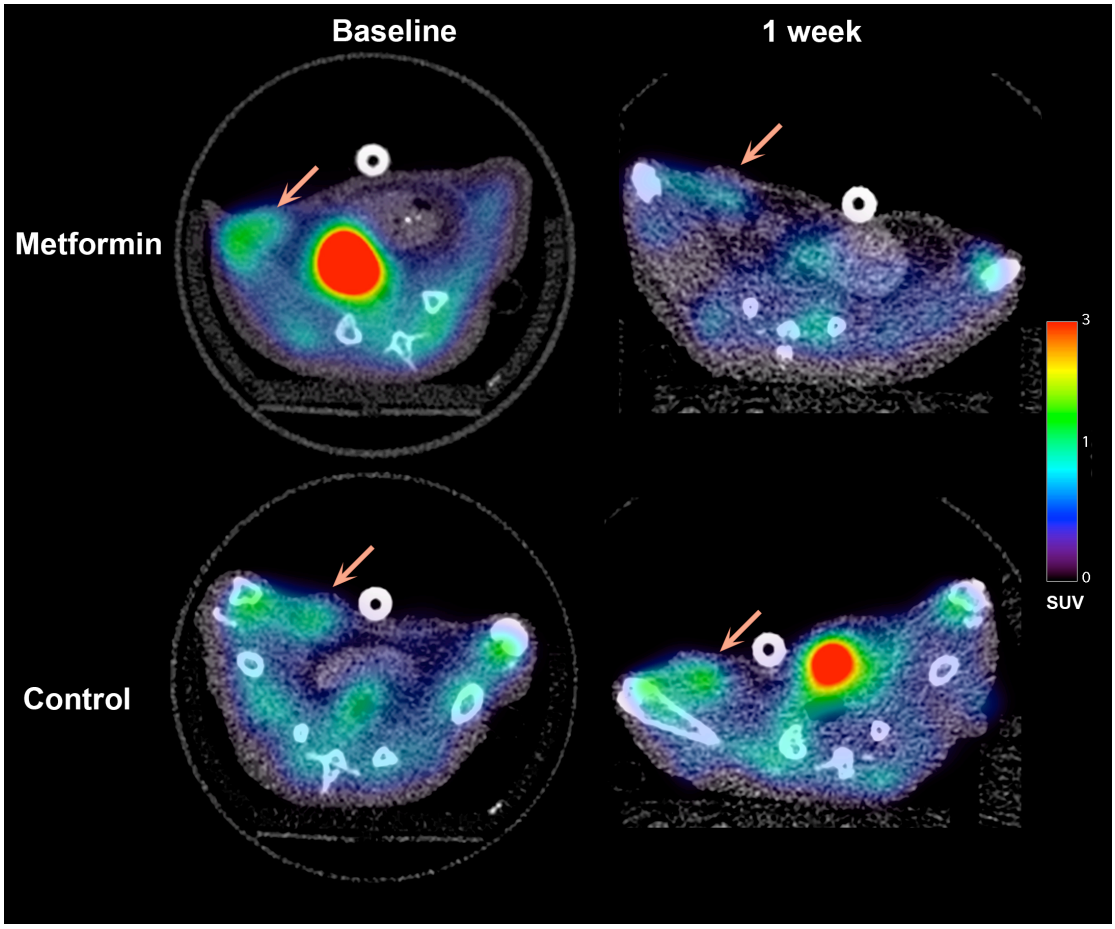

Figure 5.14: Representative ^{18}F-Fluciclovine PET/CT axial images of CD1-nude mice bearing MDA-MB-468 xenografts from the control and metformin treatment groups. ^{18}F-Fluciclovine uptake ratio in the metformin treated xenograft was 0.53 (SUV_{peak} 1.5 at baseline, 0.8 at 1 week), compared to a ratio of 1.29 in the control xenograft (SUV_{peak} 1.4 at baseline, 1.8 at 1 week).

5.3.5 Bithionol treatment of breast cancer cell lines are associated with decreased fluciclovine uptake in vivo

Having evaluated the use of fluciclovine in the setting of glutaminase inhibition with CB-839, the next step was to investigate whether, and how, fluciclovine could inform on effects of inhibiting other steps of glutamine metabolism downstream to glutaminase. As mentioned in the Introduction, bithionol is a glutamate dehydrogenase inhibitor and our group has shown that treatment of breast cancer cell lines results in increased glutamine anaplerosis with

consequent reduction in intracellular glutamine levels, and inhibits breast cancer xenograft growth *in vivo* (manuscript in preparation). In line with the observations with metformin treatment, it was postulated that decrease in fluciclovine uptake should serve as a biomarker of response to bithionol treatment.

Having optimised *in vivo* imaging with ^{18}F-fluciclovine, and established familiarity with using bithiniol *in vivo*, the decision was undertaken to assess the effect of bithionol on xenograft uptake of ^{18}F-fluciclovine. Based on our group's prior studies, bithionol's effect on tumour growth tends to reveal itself after approximately 10 days of treatment. Guided by this, ^{18}F-fluciclovine scans were performed on CD1-nude mice bearing mammary fat pad HCC1806 xenografts before commencing bithionol treatment, and one week into treatment. This was to evaluate whether a change in ^{18}F-fluciclovine uptake, in this case an anticipated decrease, would indeed precede growth effect.

After 7 days of treatment, ^{18}F-fluciclovine uptake ratios were significantly lower in the treatment group (control 0.81 ± 0.21 vs treatment 0.44 ± 0.08, p=0.035) (Figure 5.15), complementary to the working hypothesis. There was no significant difference in tumour volumes between the control and treatment group at either time point (baseline: control 31 ± 13 mm^3, treatment 44 ± 13 mm^3; 1-week: control 82 ± 35 mm^3; treatment 76 ± 33 mm^3), with the subsequent inhibitory effect demonstrated at the experiment endpoint of 3 weeks (Figure 5.15).

This result was recapitulated *in vitro*. HCC1806 cells treated with two concentrations of bithionol also resulted in a decrease in ^{14}C-FACBC uptake (1μM 74 ± 5%; 10μM 75 ± 1%) compared to control (Figure 5.17).

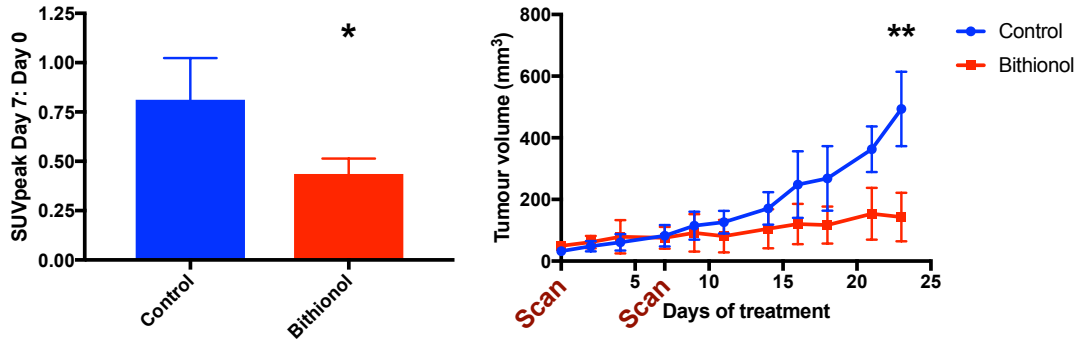

Figure 5.15: Decrease in ^{18}F-Fluciclovine uptake ratios after a short course of bithionol treatment predicts subsequent response in HCC1806 xenografts. There was no significant difference in xenograft volume between the groups at both scanning timepoints (indicated on the horizontal axis of the growth chart). Data represented as mean ± SD (*=p<0.05, **=p≤0.01) (N=4).

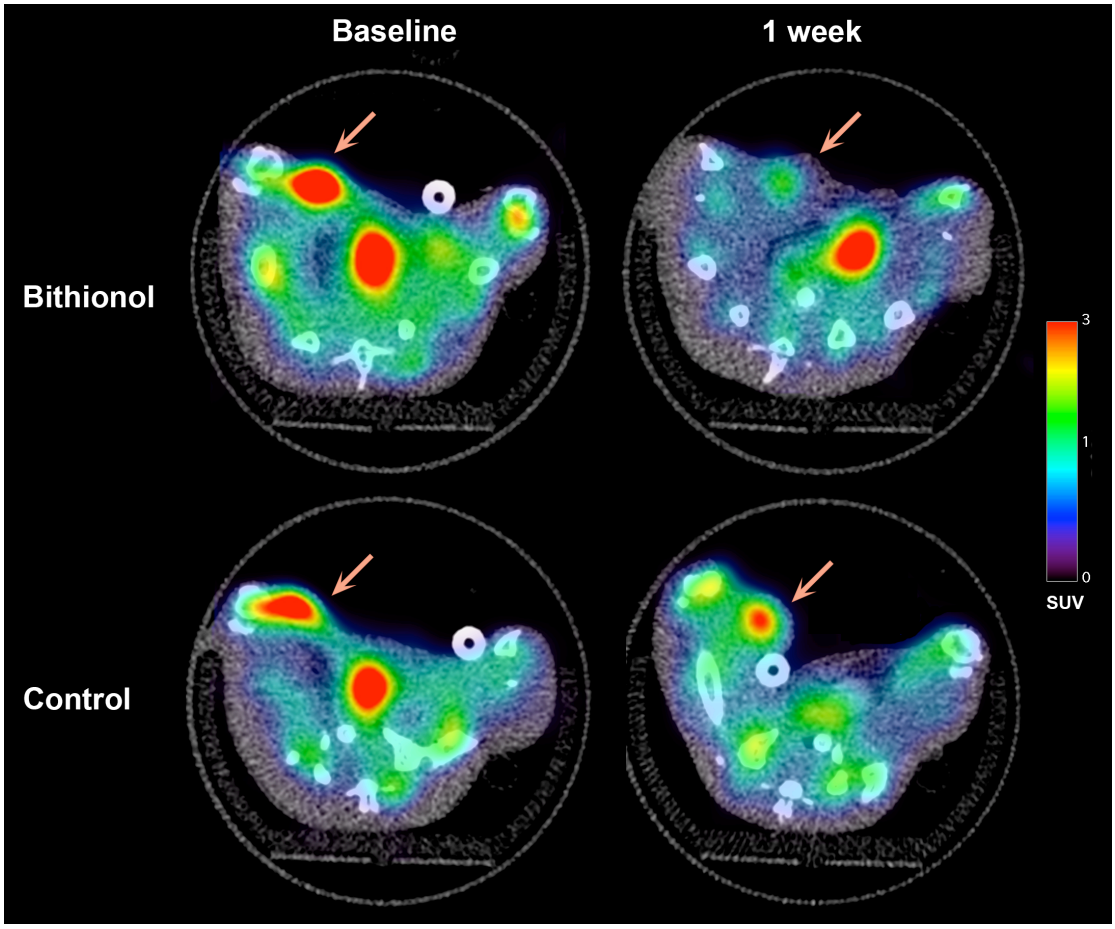

Figure 5.16: Representative ^{18}F-Fluciclovine PET/CT axial images of CD1-nude mice bearing HCC1806 xenografts from the control and bithionol treatment groups. ^{18}F-Fluciclovine uptake ratio in the bithionol treated xenograft was 0.38 (SUV_{peak} 4.5 at baseline, 1.7 at 1 week), compared to a ratio of 0.84 in the control xenograft (SUV_{peak} 3.2 at baseline, 2.7 at 1 week).

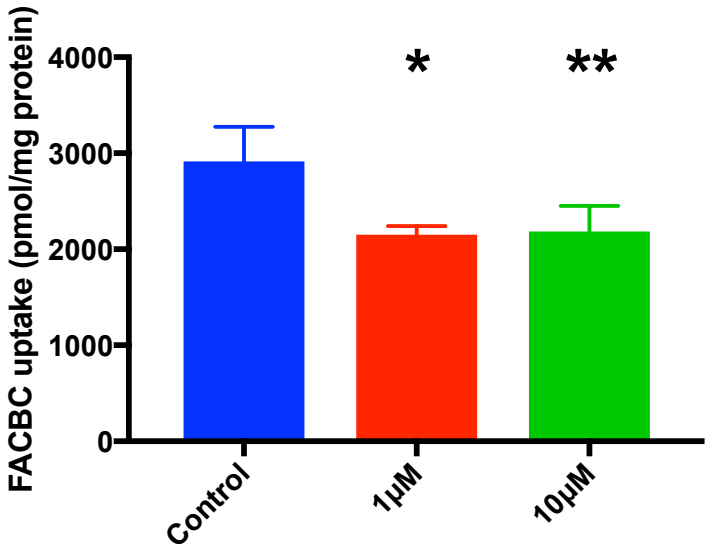

Figure 5.17: ^{14}C-FACBC uptake in the HCC1806 cell line after 7 days of bithionol treatment, matching the timeline of *in vivo* imaging. The decrease in uptake was similar to results from the *in vivo* experiment. Data represented as mean ± SD (*=p<0.05, **=p≤0.01) (N=3).

5.3.6 mTORC1 inhibition does not alter fluciclovine uptake

The implication of ASCT2 and LAT1 in the cascade of signalling to mTORC1 raises the possibility that activity of these transporters characterised by fluciclovine may be used as a surrogate for early treatment response to mTORC1 inhibition. To evaluate this, ^{14}C-FACBC uptake was evaluated in the three representative breast cancer cell lines after 48 hours of everolimus (RAD001) treatment.

The effect of everolimus on growth of these cell lines over 5 days confirmed MCF7 and BT474 to be sensitive cell lines (33 ± 2% and 36 ± 4% of control, p=0.027 and p=0.006 respectively), while HCC1806 was relatively resistant (69 ± 5% of control, p=0.021) (Figure 5.18). At the 48-hour timepoint of assessing ^{14}C-FACBC uptake, while a decrease in uptake was observed in all

cell lines, this was not discriminatory of sensitivity to everolimus. In the relatively resistant HCC1806 cell line, ^{14}C-FACBC uptake was 89 ± 6% of control (p=0.045) and this was similar to that of MCF7 (85 ± 9%). BT474, which is equally sensitive to MCF7, demonstrated a moderate decrease in ^{14}C-FACBC uptake (64 ± 14% of control, p=0.048) (Figure 5.18).

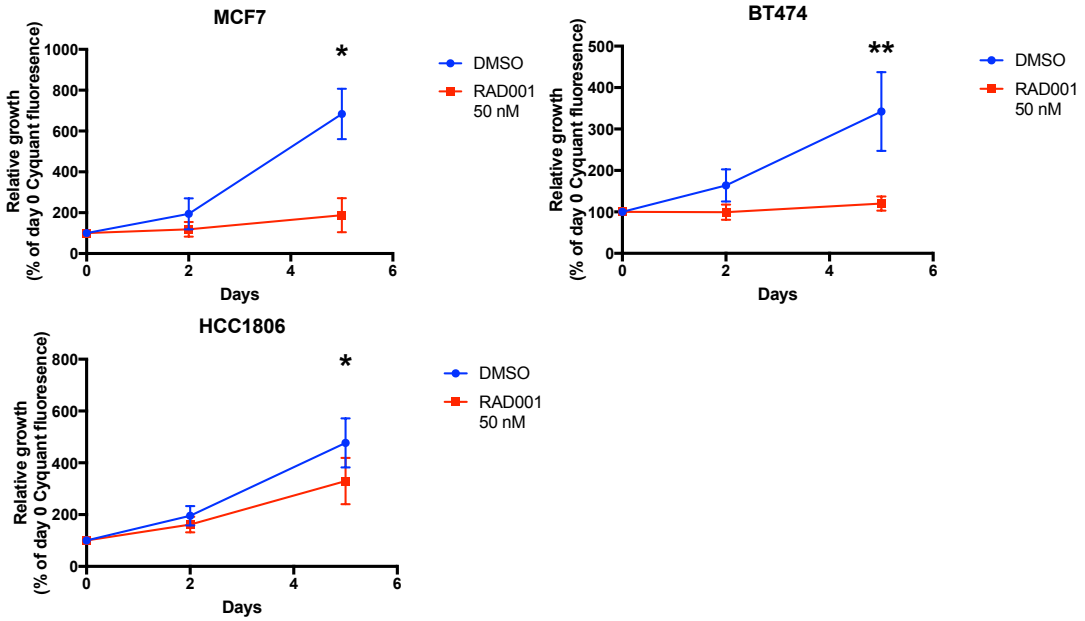

Figure 5.18: Growth of MCF7, BT474 and HCC1806 treated with everolimus over 5 days. Data represented as mean ± SD (*=p<0.05, **=p≤0.01) (N=3).

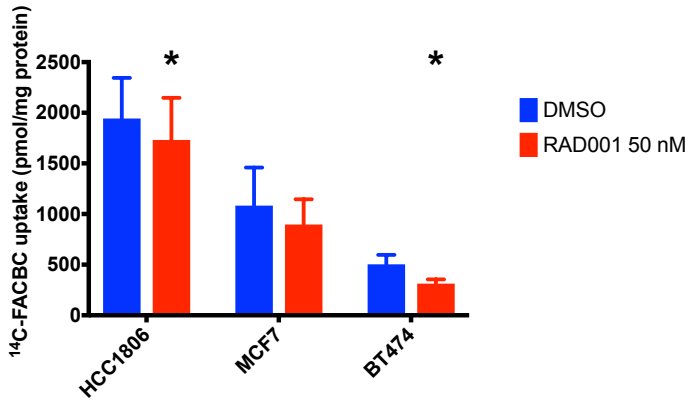

Figure 5.19: ^{14}C-FACBC uptake after 2 days of everolimus treatment. There was minor decrease in all the cell lines, non-discriminatory of sensitivity. Data represented as mean ± SD (*=p<0.05) (N=4).

Separate to this negative result, the involvement of ASCT2 in the cascade of signalling to mTORC1 also raised the possibility that activity of this transporters characterised by fluciclovine may be used as a readout of mTORC1 activity, with potential implications for patient selection for related therapies. To investigate this, pS6, as a marker of mTORC1 activity, was correlated to ^{14}C-FACBC in baseline conditions across a panel of 6 breast cancer cell lines. This demonstrated a distinct heterogeneity of pS6 activity across the cell lines, which bore no correlation to ^{14}C-FACBC uptake (Figure 5.20).

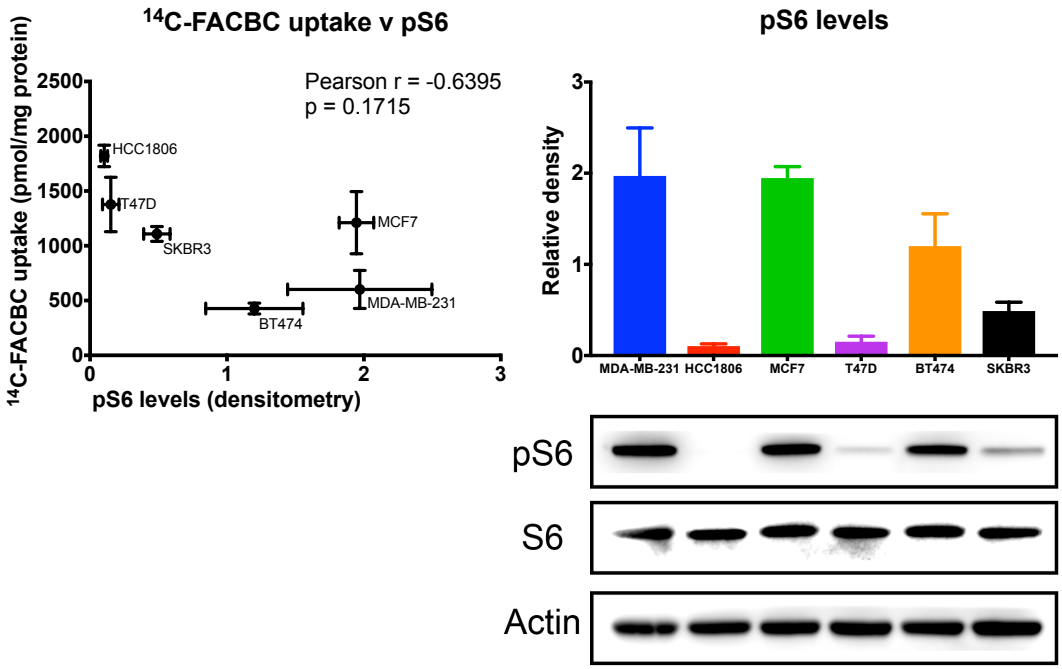

Figure 5.20: pS6 does not correlate to ^{14}C-FACBC uptake. The data represents activity at baseline conditions (5 mM glucose DMEM, 48 h, normoxia, N=3).

5.3.7 Fluciclovine uptake is non-predictive of sensitivity to, and unaltered following glutamine deprivation

As ASCT2 is a high-affinity glutamine transporter, investigation was undertaken to examine whether fluciclovine could serve as an imaging biomarker of glutamine dependence.

Firstly, the effects of glutamine deprivation on growth were examined in a panel of 6 breast cancer cell lines over 5 days. An anti-proliferative effect was observed across the panel (Figure 5.21), highlighting the overarching importance of glutamine in supporting growth in this wide range of cell lines.

To characterise sensitivity to glutamine deprivation in each cell line, the difference in fold change in proliferation from the start and end of experiment between the control and glutamine deprived groups was derived (Δ_{fc}). Both

TN cell lines MDA-MB-231 and HCC1806, and MCF7, were more sensitive to glutamine deprivation (Δ_{fc} 3.1-3.6), compared to T47D and the two HER2+ cell lines SKBR3 and BT474 (Δ_{fc} 1.0-1.6) (Figure 5.21).

The potential for fluciclovine both as a predictor of glutamine dependence and in assessment of early response to glutamine deprivation was evaluated. For the former, baseline levels of ^{14}C-FACBC uptake in these cell lines were correlated with sensitivity to glutamine deprivation. There was no statistically significant correlation (r=0.26, p=0.66) (Figure 5.22) between these two entities.

To assess early response to glutamine deprivation, ^{14}C-FACBC uptake was measured in the cell line panel 48 hours after glutamine deprivation. At this timepoint, there was no statistically significant difference in growth between the control and glutamine deprived groups in most of the cell lines, with exception of HCC1806 (Figure 5.21). After 48 hours of glutamine deprivation, there was no statistically significant difference in ^{14}C-FACBC uptake compared to controls in 4 out of the 6 cell lines. In the other 2 cell lines, T47D and SKBR3, there was a minor increase in uptake (119 ± 6%, p=0.013 and 112± 2%, p=0.019 of control respectively). Accordingly, there was no significant correlation between relative ^{14}C-FACBC uptake following glutamine deprivation, and sensitivity to glutamine deprivation.

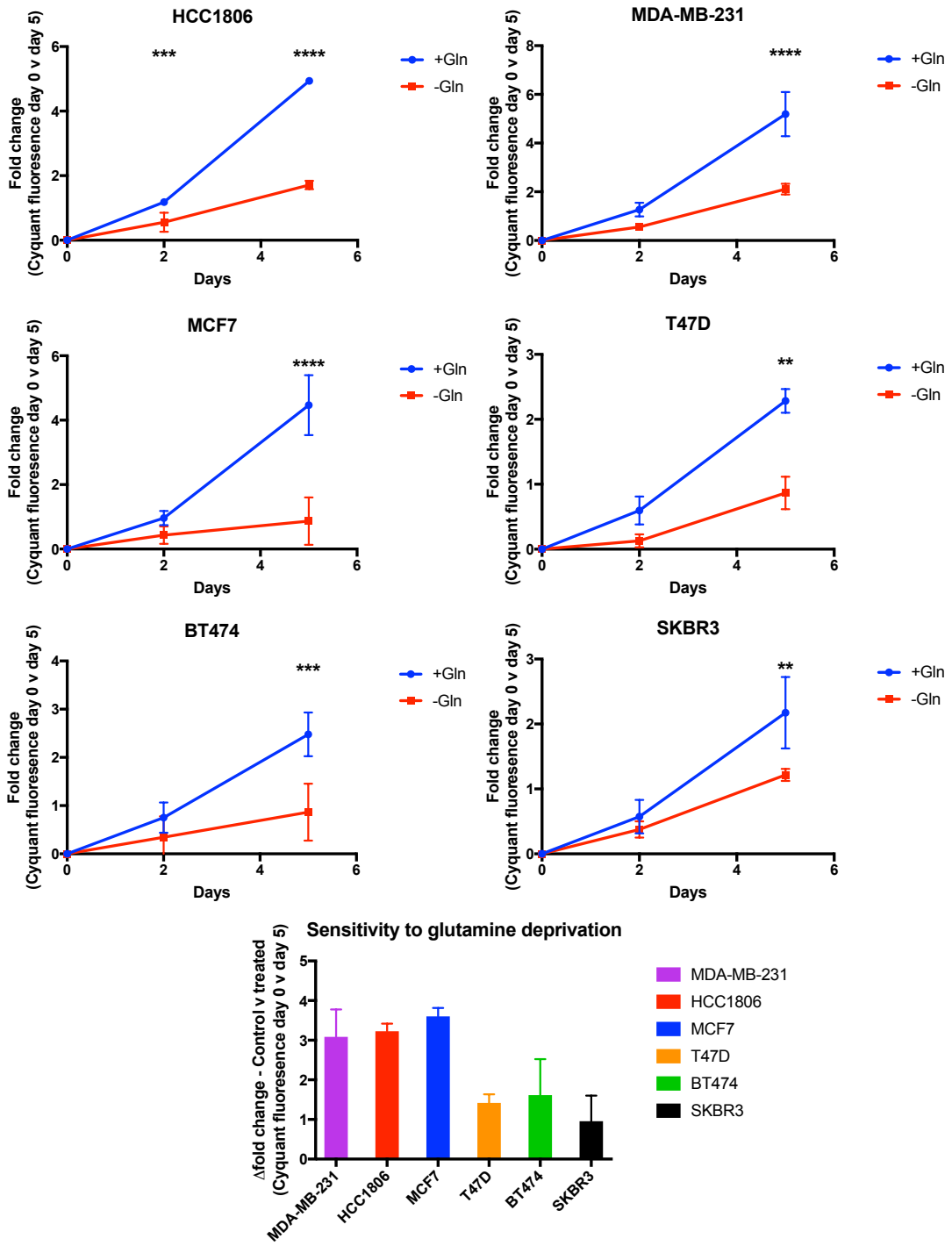

Figure 5.21: Effect of glutamine deprivation on proliferation of the breast cancer cell line panel. Data represented as mean ± SD (*=p<0.05, **=p≤0.01, ***=p≤0.001, ****=p≤0.0001) (N=3).

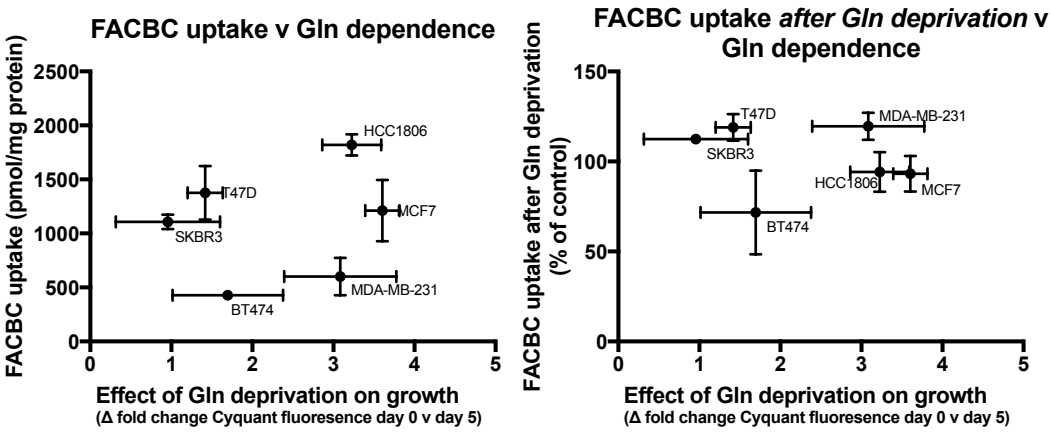

Figure 5.22: ^{14}C-FACBC uptake at neither baseline nor following glutamine deprivation correlate with sensitivity to glutamine deprivation. Data represented as mean ± SD (N=3).

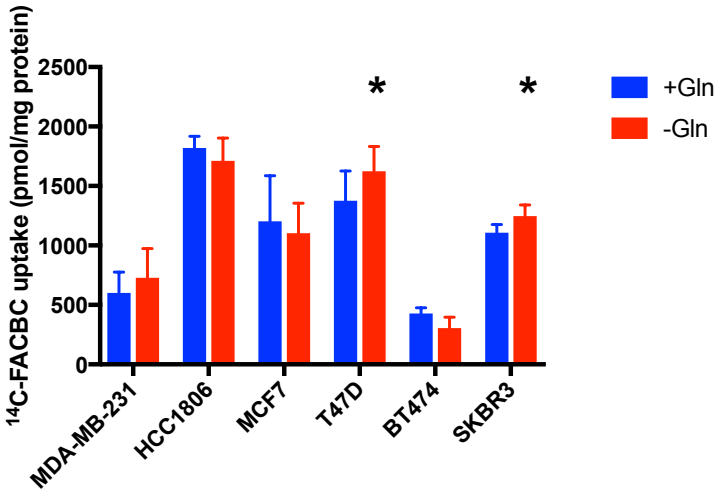

Figure 5.23: ^{14}C-FACBC uptake after 2 days of glutamine deprivation. There were only statistically significant differences in uptake in 2 of the 6 cell lines, non-discriminatory of sensitivity to glutamine deprivation. Data represented as mean ± SD (*=p<0.05) (N=4).

5.3.8 Fluciclovine uptake is unaltered in hypoxia

As described in the *Introduction*, the metabolic response to hypoxia constitutes in part, an increase in utilisation of amino acids and AAT expression particularly SNAT2 and LAT1. Based on this, it was hypothesised

that fluciclovine uptake would be relatively increased by tumour cells under hypoxic stress. If validated, this would potentially afford the means to interrogate metabolic shifts in amino acid utilisation / AAT expression, particularly in research therapeutic settings involving modulation of the hypoxic tumour microenvironment. Furthermore, there was the potential to repurpose fluciclovine as an imaging biomarker of tumour hypoxia, in lieu of the current hypoxia PET tracers such as ^{18}F-fluoromisonidazole / ^{18}F-fluoroazomycinarabinofuranoside, which require protracted imaging timepoints of up to 4 hours following tracer administration.

To test this hypothesis, ^{14}C-FACBC uptake was evaluated in the three representative breast cancer cell lines after 48 hours exposure to both 1% and 0.1% oxygen levels. Our group has shown that SNAT2 is massively upregulated, and to a lesser extent LAT1, in MCF7 and HCC1806 cell lines under these conditions (manuscript in preparation). Despite this, there was no significant difference in ^{14}C-FACBC uptake between normoxia and either degree of hypoxia across the 3 cell lines (Figure 5.24).

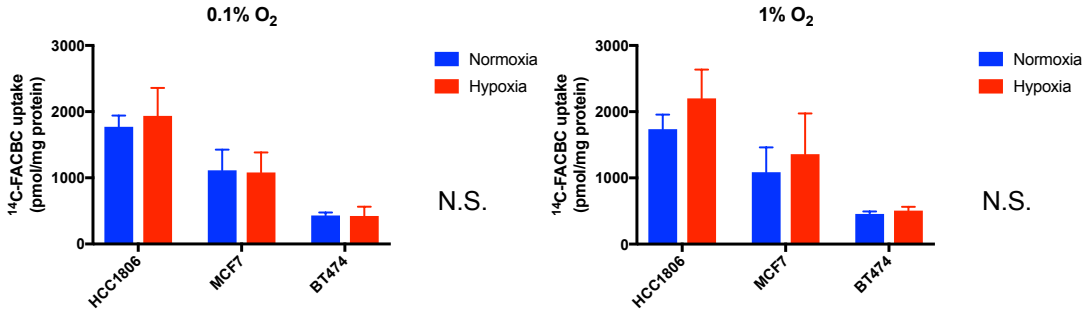

Figure 5.24: Effect of different levels of hypoxia on ^{14}C-FACBC uptake across three representative breast cancer cell lines. Cells were exposed to respective oxygenation conditions for 48 hours prior to the uptake assay (N=4-6). Data represented as mean ± SD.

Having previously demonstrated ASCT2 to be the dominant transporter of fluciclovine in these cell lines, it was postulated that while the net uptake of fluciclovine was unchanged under hypoxia, the contribution of SNAT2 to net uptake could be higher commensurate with its massive upregulation under hypoxia. To evaluate this, competitive inhibition of ^{14}C-FACBC uptake by MeAIB and GPNA was performed under hypoxia. As demonstrated under normoxic conditions in the prior section, there was no significant inhibition of ^{14}C-FACBC uptake by MeAIB under hypoxia, while GPNA caused significant reduction in ^{14}C-FACBC uptake in all 3 cell lines (Figure 5.25). While refuting this hypothesis, the observation lends weight to the major role of ASCT2 in fluciclovine transport in these breast cancer cell lines.

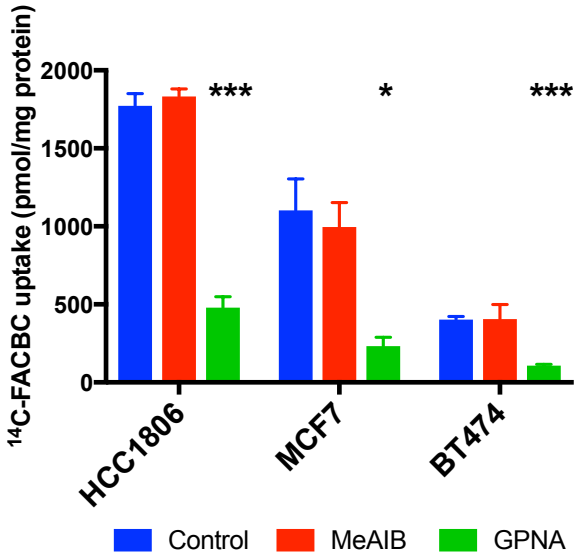

Figure 5.25: Competitive inhibition of ^{14}C-FACBC uptake by MeAIB compared to GPNA. Cells were exposed to 0.1% oxygen levels for 48 hours prior to the uptake assay (N=3). Statistical comparisons made to control. Data represented as mean ± SD (*=p<0.05, **=p≤0.01, ***=p≤0.001) (N=3).

5.4 Discussion

This aspect of the project focused on exploring the utility of fluciclovine in early assessment of response to treatments of related metabolic and biological targets. Therapies and pathways evaluated included those augmenting glutamine metabolism, mTORC1 inhibition, hypoxia and characterisation of glutamine dependence.

The results demonstrated increased fluciclovine uptake in cell lines sensitive to glutaminase inhibition with CB-839 (which is known to result in build-up of intra-cellular glutamine); and the opposite with bithionol and metformin treatment which are known to reduce intra-cellular glutamine (Figure 5.26). The latter observations were recapitulated in animal models, and collectively raise the potential for fluciclovine to be used as an imaging biomarker of glutamine pool, in addition to early response assessment in therapies augmenting glutamine metabolism.

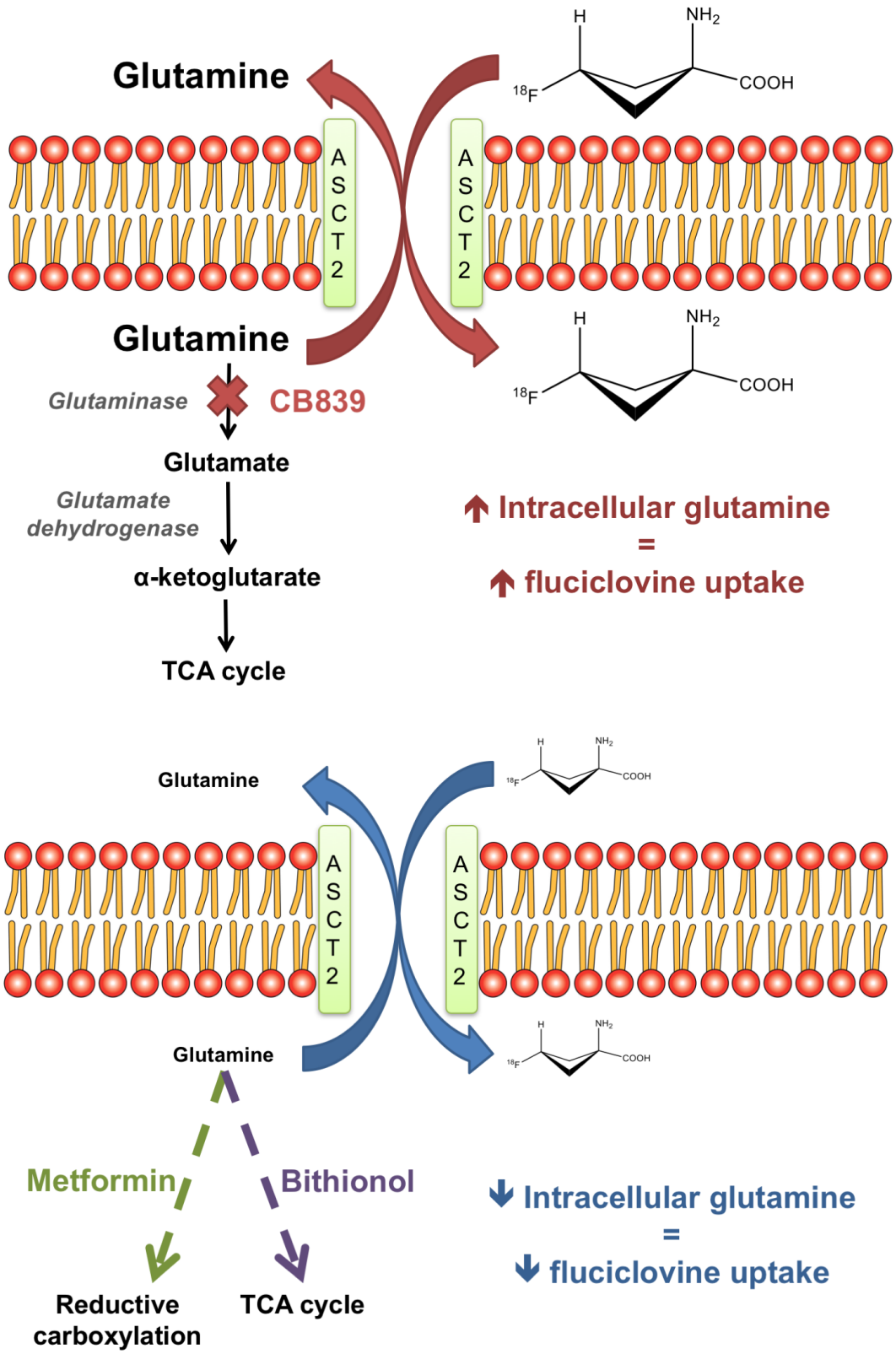

Figure 5.26: Proposed schematic of fluciclovine as an imaging biomarker of intracellular glutamine levels, based on the results presented in this thesis.

During the course of this project, the prospect of using ^{18}F(2S,4R)4-fluoroglutamine PET as a biomarker of glutamine pool size, to assess the pharmacodynamic effect of glutaminase inhibition in breast cancer, was described by Zhou et al. [136]. The authors reported *in vitro* results complementary to ours in that following a short course of CB-839 treatment, uptake of fluoroglutamine was significantly increased in HCC1806 cell line, and only to a minor extent in MCF7. The authors evaluated the intra-cellular glutamine levels in these conditions and demonstrated matching trends – with high intra-cellular glutamine in HCC1806 following glutaminase inhibition compared to MCF7. These findings were validated in animal models, and the collective findings were also supported by working knowledge of distinct differences in glutaminase activity between the two cell lines (high in HCC1806 and low in MCF7).

The differences between Zhou et al's work and ours is underpinned by the focus the authors placed on imaging the immediate pharmacodynamic effect of glutaminase inhibition, and as such, correlation with downstream phenotypic response was not studied. Here, tumour size was only evaluated for up to 3 days on treatment. Indeed, our results demonstrate MCF7 is still sensitive to CB-839 *in vitro*, albeit to a lesser extent, and is consistent with other literature [88]. This suggests that while both fluciclovine and fluoroglutamine indeed provides an estimate of *biochemical* response to glutaminase inhibition, the positive predictive value and sensitivity for subsequent phenotypic response may be lower.

With specific context of developing an imaging biomarker of tumour response to glutaminase inhibition, the collective results highlight the need for more work. This is especially because having a higher false positive rate in this setting, is more acceptable than false negative findings which may lead to premature withdrawal of potentially effective treatment. This of course has to be balanced against treatment toxicity and other patient factors. The relatively lower sensitivity of MCF7 to glutaminase inhibition also draws attention to the opportunity of concurrent targeting of cancer metabolism with other therapies to achieve synthetic lethality (as described in the Introduction). In this context, the potential of an imaging agent like fluciclovine to detect early response will need to be clearly characterised and re-defined, as the sensitivity and positive predictive value for this may swing in either direction depending on the combined effect of the treatments on tumoural amino acid pool.

The aforementioned results contributed to the stronger and more immediate focus we placed on using fluciclovine for imaging the reverse phenomenon of glutamine depletion, and tying it into treatment response. Collectively, the metformin and bithionol experimental results are highly encouraging in this respect, particularly with the distinction demonstrated between the metformin-sensitive and metformin-resistant cell lines *in vivo*. The translational implications extend to other treatments that not only target glutamine metabolism directly, but as a bystander or secondary effect, as long as this biochemical shift can be accurately correlated to clinical outcome.

The results with metformin are also significant in light of other work our group has done in assessing the biological response of breast cancer to metformin therapy [137]. On the premise that metformin increases glycolysis in cancer cells by inhibiting oxidative phosphorylation [138], ^{18}F-FDG was selected as an ideal imaging biomarker to characterise tumour glucose utilisation in this window-of-opportunity clinical study. Metformin-sensitive tumours demonstrated increased ^{18}F-FDG flux, a parameter derived from dynamic PET data. With the added tier of complexities that come with dynamic PET data analysis, future clinical adoption of ^{18}F-FDG in assessing response to metformin may be limited. Conversely, the results with ^{18}F-fluciclovine, borne out of static measures of uptake, suggest it could be a more appropriate imaging biomarker as static measures of PET uptake form part of routine clinical imaging practice. This will require clinical validation.

Along with the wave of interest in targeting glutamine metabolism in cancer, other means beyond the intra-cellular compartment have been explored, namely at the transporter level. Compounds such as benzylserine and GPNA inhibit ASCT2 activity [139], and monoclonal antibodies against ASCT2 have been recently described [140]. It has been shown that targeting ASCT2 transporter activity using GPNA or gene silencing in triple-negative breast cancer has an anti-tumour effect both *in vitro* and *in vivo* [84]. This is in addition to work in other tumour sites including prostate [139], endometrial [141], gastric [140] and skin [87]. Findings on the predominant ASCT2-mediated uptake mechanism of fluciclovine therefore raises the potential for application in guiding development of ASCT2-targeted therapies, particularly

in the clinical research setting. Here, unlike our negative findings for predicting response glutamine deprivation, imaging ASCT2 expression would anticipatedly have a direct role for pre-treatment selection of patients / clinical trial participants, and response prediction for therapies targeting ASCT2 directly.

A further result borne out of the initial optimisation work is that fasting improves tumour uptake of ^{18}F-fluciclovine *in vivo*. In the context of heterogeneous practice of patient preparation for amino acid PET, this finding is important for validating current clinical practice, and informs the use of ^{18}F-fluciclovine in future research. During the course of this project, another group published similar work in this regard [142]. Here, ^{14}C-FACBC autoradiography was performed in a rat breast cancer bone metastasis model, either with or without an overnight fast. In the fasted rats, ^{14}C-FACBC uptake was found to be significantly higher in both osteolytic and osteoblastic bone metastases (by 64% and 88% respectively), compared to non-fasted rats. Our findings are complementary in that similar effects on fluciclovine uptake were demonstrated in a different model using inframammary fat pad tumours. Furthermore, our results provide a natural progression towards translation, having been produced using the actual ^{18}F-labelled compound, and with imaging technology more analogous to clinical PET.

In consideration of future work, the *in vitro* results with CB-839 should be validated *in vivo*. This should facilitate integration of meaningful imaging endpoints into studies as this and similar treatments progress through clinical

development. Despite the negative results *in vitro*, it would be worth investigating if ^{18}F-fluciclovine could be used for assessing early response to mTOR inhibition using everolimus *in vivo*. While there has been good overall concordance between *in vitro* and *in vivo* results in this project, effects of therapy on the xenograft tumour microenvironment may alter AAT activity. For instance, a low pH microenvironment would increase the activity of LAT1 and its other system L counterparts [143], and decrease activity of SNAT2 and other system N transporters [144]. Compounded with the known effects of hypoxia on AAT expression, it may well be that changes in the tumour microenvironment in early treatment with everolimus, would impact on the imaging phenotype of tumours *in vivo*, and potentially render a different result.

The oncogenic transcription factor Myc is a master regulator of cell proliferation and metabolism [145], and has been implicated in the development of endocrine-resistance in ER-positive breast cancer [146, 147]. Myc activation results in a state of glutamine addiction, supported by transcriptional activation of genes involved in glutamine uptake and metabolism, such as those encoding for ASCT2 and glutaminase [82]. Another avenue for future work may be to evaluate how ^{18}F-fluciclovine may be used to capitalise on this metabolic signature and detect early development of endocrine resistance in ER-positive breast cancer.

The overarching hope is that imaging is considered early on in the development pipeline of glutamine / cancer metabolism targeting treatments, and as stressed throughout the Discussion, focus on understanding the flux of

relevant imaging metabolites and underlying biology specific to each treatment / treatment combination, will help to guide choice of imaging agent and future clinical interpretation. This ultimately necessitates direct correlation of imaging to these aspects of tumour behavior in the clinical setting, which is what we sought to address in the next chapter.

Chapter 6 : Initial insights from FRONTIER: A clinical study to characterise ^{18}F-fluciclovine uptake in breast cancer

Declaration of work

E.J. Teoh was primary author of the FRONTIER study protocol, with intellectual direction and input from Prof. Adrian Harris, and statistical input from Dr. Syed Haider and Prof. Francesca Buffa. Regulatory applications for the study were jointly written by E.J. Teoh and the Oncology Clinical Trials Office.

E.J. Teoh collated and analysed the FRONTIER clinical and imaging data presented. Participant recruitment and sample collections were performed by the Surgical Research Team and E.J. Teoh. Identification of suitable participants and intra-operative biopsies were supported by the breast surgical team of Mr. Dennis Remoundous, Mrs. Gael Maclean and Mrs. Pankaj Roy.

6.1 Introduction

As described in the first chapter, there has been very limited experience with using ^{18}F-fluciclovine for imaging breast cancer in the clinical setting, with only two groups having published their experience only during the course of this project [112, 114, 115]. The focus of these works has been predominantly on disease detection, and in this respect the potential for ^{18}F-fluciclovine to be used in staging in lobular carcinoma, in addition / as an alternative to ^{18}F-FDG, has been raised. Across the published work, there has been a paucity of data on patterns of ^{18}F-fluciclovine uptake across molecular subtypes and other histopathological / biological parameters. With clinical evidence that breast cancers exhibit positive ^{18}F-fluciclovine uptake, building this knowledgebase is now the next step to form an essential cornerstone for translating the use of ^{18}F-fluciclovine into future clinical research and practice.

To address this, a single centre open-labelled clinical study (FRONTIER) was set up, where ^{18}F-fluciclovine PET/CT would be performed in breast cancer patients due for surgery, with subsequent analyses on tumour tissue samples retrieved during surgery. The primary objective was to characterise ^{18}F-fluciclovine uptake in different breast cancer subtypes. The secondary objectives were to correlate ^{18}F-fluciclovine uptake with breast cancer AAT expression, expression of related growth pathways, and tumour metabolites. This chapter presents primary endpoint data on the entire cohort to date, and secondary endpoint data on the first subset of patients, where secondary analyses were performed as per study protocol.

6.2 Patients

At time of writing, 14 patients have been recruited into FRONTIER. One patient did not undergo the research scan, leaving 13 participants with evaluable primary endpoint data. Key patient demographics are summarised in .

Table 6.1: Demographics of FRONTIER participants.

Parameter	Value
Age *(years, median and range)*	63 years (52-81 years)
Tumour size (longest diameter measured on conventional imaging, median and range)	25 mm (20-70 mm)
Grade	Grade 1: 8% (1/13) Grade 2: 54% (7/13) Grade 3: 38% (5/13)
Molecular type	ER+ (HER2-): 54% (7/13) HER2+: 23% (3/13) TN: 23% (3/13)

Twelve out of 13 patients had invasive ductal carcinoma. One patient who had been diagnosed with invasive ductal carcinoma on initial biopsy, then had a revised diagnosis of invasive lobular carcinoma on histopathological assessment of the resected tumour.

6.3 Definition of ^{18}F-fluciclovine tumour uptake

To determine the optimum time point for defining ^{18}F-fluciclovine tumour uptake, tumour time activity curves of the first 5 participants were evaluated. In 4 out of the 5 cases, both tumour SUV_{peak} and SUV_{max} were the highest in the second (5-10 minute) time frame (Figure 6.1). In the remaining case (participant 106), SUVs were highest in the third (10-15 minute) frame. In all cases, beyond the first time frame, SUV_{peak} were within 90.1-98.9% of the

highest value, and SUV_{max} within 84.2-99.1% of the highest value, indicating a gradual washout (Figure 6.1).

Based on this, SUV_{peak} at the 5-10 minute time frame was selected as the primary metric for tumour ^{18}F-fluciclovine uptake. SUV_{peak} was chosen as it is regarded as a more reliable parameter than SUV_{max}, and is the metric recommended in assessing tumour response in clinical ^{18}F-FDG PET using the PERCIST criteria [148].

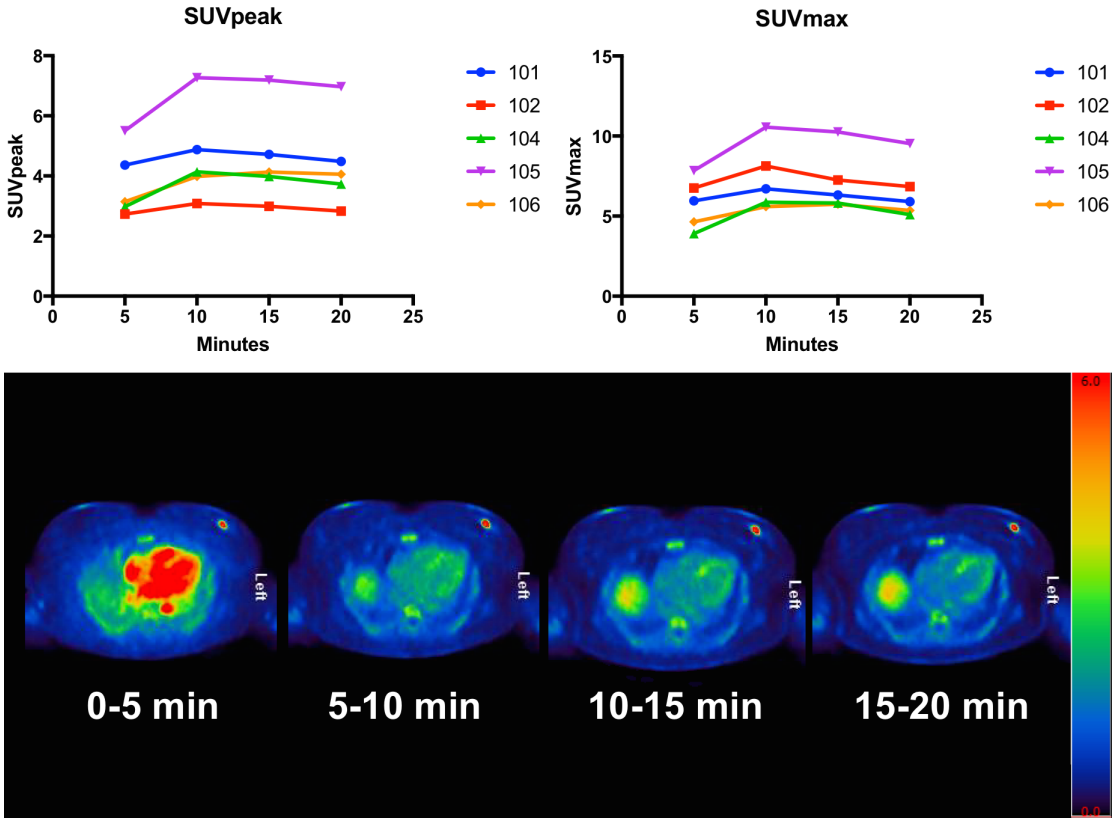

Figure 6.1: ^{18}F-Fluciclovine breast tumour uptake in the first 5 FRONTIER participants over time, indicating peak activity to be in the 5-10 minute time frame in majority of cases (top row). Representative axial ^{18}F-fluciclovine PET images of participant 105, who had the highest ^{18}F-fluciclovine uptake (in this analysis) within a left breast cancer, are demonstrated in the bottom row.

6.4 ^{18}F-Fluciclovine uptake stratified by molecular type and grade

When categorised by molecular type, ^{18}F-fluciclovine uptake was highest in TN tumours (n=3, mean SUV_{peak} 6.6 ± 1.0), followed by ER+ HER2- (n=7, SUV_{peak} 6.0 ± 2.0), then HER2+ tumours (n=3, mean SUV_{peak} 3.9 ± 0.4). This trend matched that reported in the 13-patient cohort from Emory University published during the course of this project [115]. ^{18}F-Fluciclovine uptake appeared to be higher in grade 2 and 3 tumours (mean SUV_{peak} 5.9 ± 2.1 and 5.4 ± 1.7 respectively) compared to grade 1 (SUV_{peak} 4.7).

Interestingly, there was a bi-modal distribution of ^{18}F-fluciclovine uptake in the 7 ER+ tumours contributing to a relatively wide spread of data. Further analysis of the clinical demographics of these patients was undertaken to explore possible explanations for this distribution. Comparing the 4 lower uptake ER+ tumours (SUV_{peak} 3.1-5.8) to 3 higher uptake ER+ tumours (SUV_{peak} 7.3-9.0), 3 out of 4 (75%) lower uptake tumours had associated DCIS (all intermediate grade), compared to 1 out of the 3 (33%) higher uptake tumours which had associated DCIS (also intermediate grade). Two out of the 3 (67%) higher uptake tumours had axillary nodal disease confirmed on histology, compared to 1 out of the 4 (25%) lower uptake tumours.

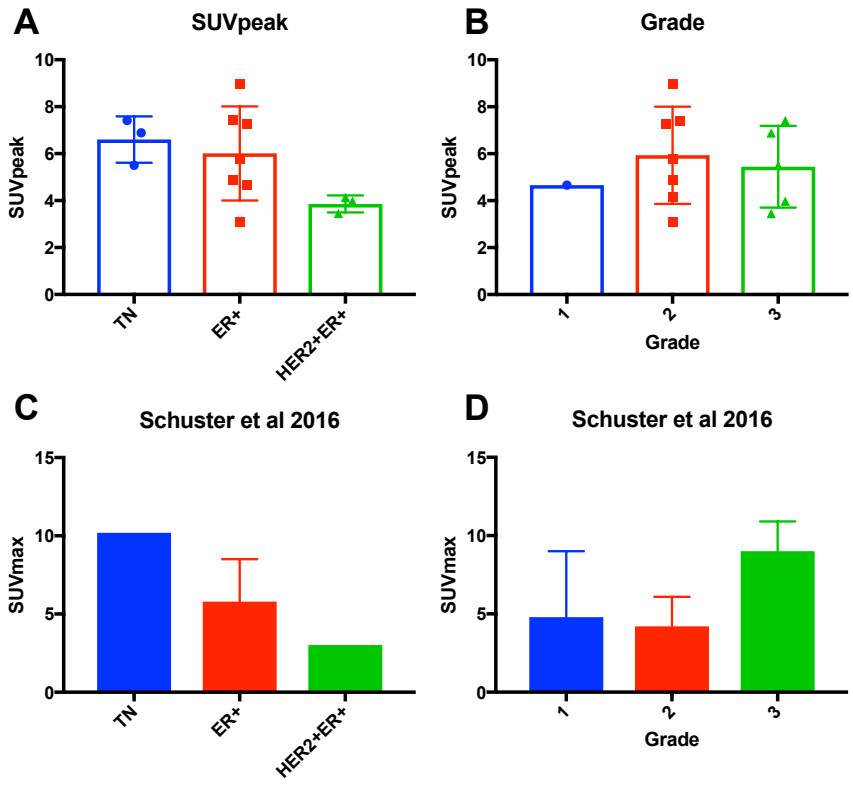

Figure 6.2: ^{18}F-Fluciclovine breast cancer uptake in the FRONTIER cohort (n=10), stratified by molecular type (A) and Nottingham grade (B). Trends based on molecular type were similar to the only other published dataset in existence (C), albeit disparate when stratified by grade. Data represented as mean (± SD where number of patients in category ≥3).

6.5 Initial metabolomics insights

Metabolite analysis was performed on the first 4 analysable paired samples (tumour and adjacent stroma), with the primary purpose of ensuring the processes for extraction and analysis were smooth and no changes to sample collection or processing were required.

Total ion count from the LC/MS analysis demonstrated higher levels in the tumour samples compared to the adjacent stroma in all cases, indicating consistently higher total polar metabolite levels in tumour (Figure 6.3).

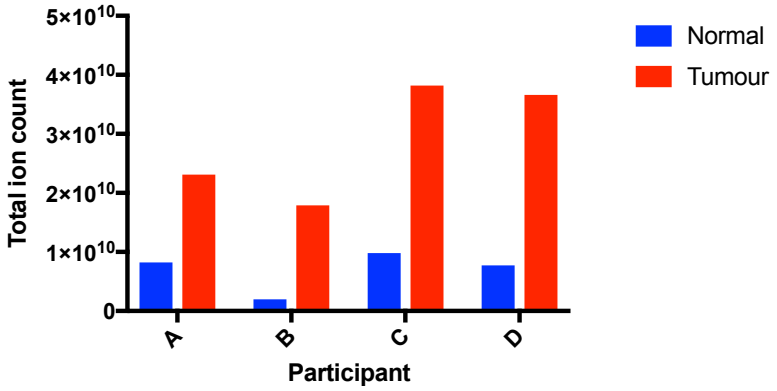

Figure 6.3: Total ion count on LC/MS analysis of tumour and adjacent "normal" stroma samples.

An exploratory analysis of metabolite levels was undertaken, and represents the principles which will be adopted for the final analysis. Here, tumour metabolite levels were correlated to tumour ^{18}F-fluciclovine SUV_{peak}.

In view of the small patient numbers, none of the correlations rendered statistical significance. Nonetheless, considering the relatively strongest correlations, there were positive correlations between tumour ^{18}F-fluciclovine uptake and leucine, glutamate, lysine and taurine (ρ=1.0, p=0.08, Figure 6.4). For reference, correlation of ^{18}F-fluciclovine uptake to itself (i.e. SUV_{peak} to SUV_{peak}) in this small sample size, rendered the same correlation coefficient. A further panel of metabolites demonstrated relatively weaker positive correlation (ρ=0.8, p=0.33). These included alanine, arginine, aspartate, glutathione, pyruvate and tryptophan. Glucose was the metabolite with the strongest negative correlation (ρ=0.8, p=0.33). No correlation was observed with glutamine (ρ=0), nor the sum of high-affinity metabolites for ASCT2 (alanine, serine, cysteine, glutamine and threonine) (ρ=0.4) in this small sample size.

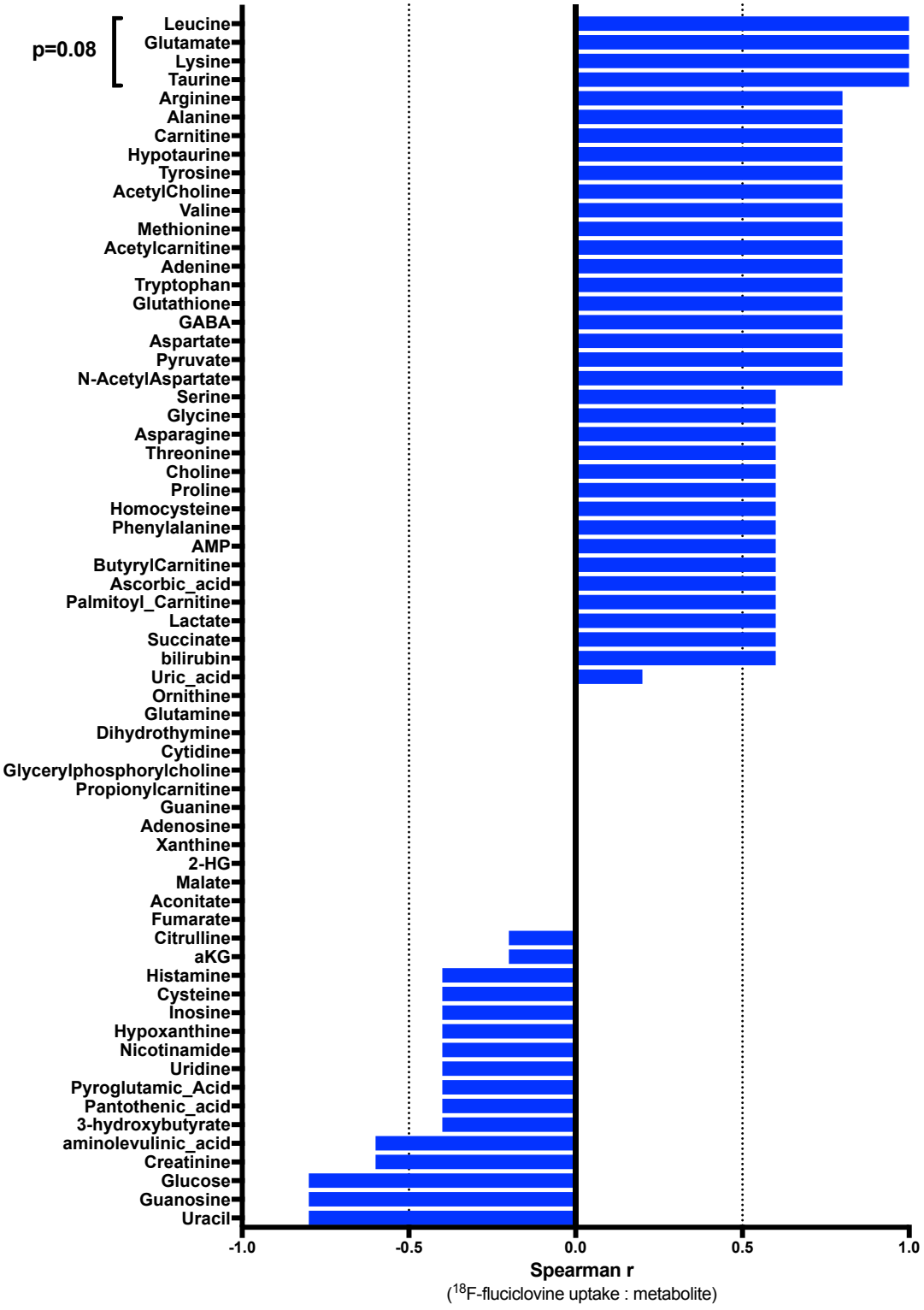

Figure 6.4: Coefficients of correlation between tumour ^{18}F-fluciclovine uptake and metabolites.

6.6 Axillary lymph node involvement

Out of the 13 participants who had a ^{18}F-fluciclovine scan, 12 went on to have surgery. One participant was deemed to be unfit for surgery only after the research scan due to pre-existing co-morbidities. Of the 12 patients, 6 had increased ^{18}F-fluciclovine axillary nodal uptake, of which 5 had histopathological confirmation of axillary nodal disease. In the one patient with negative histopathology, the degree of increased ^{18}F-fluciclovine uptake was faint, SUV_{max} 2.0. There was one false-negative case, where a 0.5mm deposit of micrometastasis was found in 1 axillary node. When considering diagnostic performance for axillary node detection at a patient level, this produced a sensitivity of 83% (95% CI 71-96%), specificity of 83% (95% CI 71-96%) and positive predictive value of 83% (95% CI 71-96%).

Amongst the 12 patients, two had resection of surgical level II axillary nodes. This allowed evaluation of diagnostic performance based on surgical levels. In a total of 14 stations were sampled, 7 were positive on histopathology, 6 with increased ^{18}F-fluciclovine uptake (the false negative case here being the same as mentioned in the previous paragraph). This produced a sensitivity of 86% (95% CI 74-97%), specificity of 86% (95% CI 74-97%) and positive predictive value of 86% (95% CI 74-97%).

Table 6.2: Diagnostic performance of ^{18}F-fluciclovine for detection of axillary nodal involvement on a patient-based and surgical level-based analysis in this small cohort. Parentheses depict 95% confidence intervals.

Diagnostic performance parameter	Patient (N=9)	Surgical level (N=11)
Sensitivity	83% (71-96%)	86% (74-97%)
Specificity	83% (71-96%)	86% (74-97%)
Positive Predictive Value	83% (71-96%)	86% (74-97%)
Negative Predictive Value	83% (71-96%)	86% (74-97%)
Accuracy	83% (74-92%)	86% (78-94%)

6.7 Discussion

The FRONTIER study was designed to establish how ^{18}F-fluciclovine can be used to characterise breast cancer and its underlying biology. The preliminary results are encouraging in that all of the invasive cancers have demonstrated increased ^{18}F-fluciclovine uptake, and in the relatively larger ER+ group, intra-group variation in activity is observed. As more patients are recruited, it would be interesting to see how underlying clinical and biological characteristics influence this variation of ^{18}F-fluciclovine uptake.

The primary endpoint of characterisation of ^{18}F-fluciclovine uptake in different molecular types was driven by our observations of differential LAT1 expression across these groups in the METABRIC cohort (described in Introduction), and initial working hypothesis that LAT1 would be the dominant transporter of ^{18}F-fluciclovine in breast cancer. Subsequent publication of

results from Emory University demonstrating a trend of highest uptake in TN, followed by ER+ then HER2+ tumours [115], have complemented our expectations, as well as the *in vitro* results presented in the previous chapter. It was most encouraging to see a similar trend emergent from the preliminary results.

An attempt was made to explain an apparent bi-modal distribution of ^{18}F-fluciclovine uptake in the 7 ER+ tumours contributing to a relatively wide spread of data. While a higher proportion of axillary nodal involvement and lower proportion of associated DCIS was observed in the higher uptake tumours, the subject numbers remain relatively low and no firm conclusions can be made. In addition to clinico-pathological variables, it would be interesting to see if specific metabolite profiles contribute to this distinction in the ER+ patients, which may then inform future targeting of metabolism in this prevalent group of breast cancer.

A subset of samples were processed for metabolomics analysis primary for technical validation. The findings of consistently higher total polar metabolite levels in tumour (Figure 6.3) were assuring of the success of this exercise, being in keeping with the predominantly fat composition of the patients in the sampled age range (median 63 years, range 60-81 years). The remainder of these samples and that of the other participants will be processed and analysed together at the end of the study, to minimise batch-to-batch variation.

Analysis of the metabolomic data as presented in this chapter was undertaken primarily to demonstrate principles which will be adopted for the final analysis. Therefore, interpretation of this analysis is highly speculative due to the small sample size. Nonetheless, the trends are potentially intriguing, particularly if sustained or reinforced with increasing numbers. Of the 4 metabolites demonstrating the strongest positive correlations with ^{18}F-fluciclovine uptake, leucine and glutamate are particularly noteworthy.

Leucine is a high-affinity substrate of LAT1, and maintenance of an intra-cellular pool by working in concert with ASCT2 (which transports glutamine into the cell which LAT1 utilises to exchange with leucine), contributes to mTORC1 signalling as described in the Introduction chapter. Subject to further validation in the final analysis, it may be postulated that this may represent a link between mTORC1 activity and ^{18}F-fluciclovine uptake, reviving one of the hypotheses we sought to investigate at the outset. Here, increased ASCT2-mediated amino acid transport supports increased LAT1-mediated leucine influx and therefore mTORC1 activation via the aforementioned pathway, and ^{18}F-fluciclovine uptake functions as a direct readout of ASCT2-mediated transport. This would be in keeping with our initial hypothesis, despite the negative results from the *in vitro* experiments discussed in the previous chapter which does not account for potential effects of the tumour microenvironment *in vivo*. Accordingly, the positive correlation with leucine could also be a manifestation of shift of transporter affinity, given that the activity of system L transporters which transport leucine with high affinity, increase in low pH conditions [143], a common feature of the tumour

microenvironment [149]. Correlation with pS6 and LAT1 levels on immunohistochemistry, supported with trends from the rest of the metabolite profile (e.g. arginine also contributes to mTORC1 activation [150]) and the tumour transcriptome on RNA-sequencing, will be pivotal for validating these proposed mechanisms.

As described in the Introduction chapter, glutamate is central to glutamine metabolism, being converted from glutamine by glutaminase, prior to diverse biological fates, spanning utilitsation in the TCA cycle, reductive carboxylation, contribution to nucleotide and glutathione biosynthesis. Therefore, the positive correlation of glutamate levels with ^{18}F-fluciclovine could tie in well with the overarching depiction of aggressive tumour biology, and may also support the predominantly ASCT2-mediated mechanism of transport demonstrated *in vivo*, given its precursor glutamine. The absence of correlation with glutamine in itself, in this small sample, is of indeterminate significance and requires verification in the final analysis. If this trend (of no correlation) remains, it may be possible that reliance on glutamine or degree of metabolism is depicted more by its downstream metabolites, particularly glutamate. Here, levels of the other TCA cycle metabolites, nucleotides and glutathione, will all have to be considered in the final analysis, aside from being of interest in their own right. Alternatively (in considering the absence of correlation to glutamine), as postulated above, other transporter systems, could have a more dominant role in the tumour microenvironment.

The data accumulated to date also allowed assessment of diagnostic performance of ^{18}F-fluciclovine in assessing axillary nodal status. The relatively high performance, particularly in positive predictive value, is encouraging in this respect, and may be of future use in re-purposing of ^{18}F-fluciclovine for staging in breast cancer. While it is unlikely to eclipse the mainstay of surgical management with sentinel node biopsy, it may serve its purpose as an adjunct diagnostic in whole body staging with indeterminate conventional imaging or ^{18}F-FDG-negative disease, particularly in lobular carcinoma. In respect of the use of PET, consideration has to be borne to the fact that even the use of ^{18}F-FDG in whole body staging of breast cancer is limited at this point in time [151].

6.8 Conclusion

Increased ^{18}F-fluciclovine uptake has been demonstrated in primary breast cancers in the FRONTIER study, with a trend of differential uptake between molecular subtypes and supportive of the primary objective. Initial insights from a small subset, of possible correlations between tumour metabolites and ^{18}F-fluciclovine uptake, will be intriguing if corroborated in final analyses. Recruitment is ongoing and targeted to be complete by November 2018.

Chapter 7 : Final discussion

7.1 Overview

The overall aims of this DPhil project were to:

1. set up a multicentre clinical trial to investigate the impact of ^{18}F-fluciclovine imaging on clinical management of men with BCR of prostate cancer and factors influencing scan positivity, and optimise its application with modern PET image reconstruction technology as a substudy;
2. establish the transport mechanisms of fluciclovine in breast cancer;
3. explore the utility of fluciclovine in early assessment of response to treatments of related metabolic and biological targets;
4. set up a clinical study to investigate how ^{18}F-fluciclovine uptake can be used to characterise breast cancer biology.

7.2 The positive impact of ^{18}F-fluciclovine PET/CT in management of recurrent prostate cancer

As part of this project, the UK multicentre FALCON trial was established to evaluate the impact of ^{18}F-fluciclovine imaging on the management of patients with BCR being considered for radical salvage therapy. The pre-planned interim analysis demonstrated overwhelming effectiveness with 61% (52/85) of participants having revised management following the scan, leading to early termination of recruitment [119]. The significance of the result is raised by the predominantly low PSA across the cohort (median 0.63 ng/mL). The described results from the Oxford site, which made a significant contribution to the study by exceeding its recruitment target, demonstrate that 44% of a post-prostatectomy, lower PSA cohort (median 0.37 ng/mL) had their intended management plan revised. A trend of relatively higher short-term response

rates to fluciclovine-guided salvage radiotherapy compared to standard salvage radiotherapy was also observed, and it will be exciting to see how this compares to the outcomes from across the trial.

What remains to be established is the impact of image-guided management on long term outcomes. There is opportunity to address this in a follow-up study to FALCON, as well as in a "sister" study LOCATE in the USA, which has also recently completed recruitment (NCT02680041). The burgeoning use of PSMA-targeted imaging over the course of this project cannot be ignored, and recent work demonstrates similar rates in change of management influenced by such imaging. Ultimately, the focus also has to be re-aligned to evaluating the impact on long term outcomes.

7.3 The potential implications of ASCT2-mediated transport of ^{18}F-fluciclovine in breast cancer

Described results from a range of *in vitro* experiments point towards the predominant contribution of ASCT2, a high-affinity glutamine transporter, to fluciclovine transport in breast cancer. We were then able to demonstrate that fluciclovine could be used to interrogate early response to therapies targeting / augmenting glutamine metabolism, both *in vitro* and *in vivo*. We propose the mechanism of action for this is by exchange of intra-cellular glutamine with extra-cellular ^{18}F-fluciclovine via ASCT2, providing a direct readout of intra-cellular glutamine levels. There is ample room for further pre-clinical work, to ratify the proposed mechanism.

The results as they stand present an opportunity to translate this into companion imaging for future clinical research of glutamine modulating cancer therapeutics. The most immediate opportunity in this regard is glutaminase inhibitor CB-839 which is undergoing active evaluation in early phase clinical trials (NCT02071862, NCT02771626). Outside of the potential for imaging in future clinical research of treatments modulating glutamine metabolism, the central role of ASCT2 also raises the potential for ^{18}F-fluciclovine in guiding development of ASCT2-targeted therapies.

In such future work, prospective comparison with other PET tracers will be important to see if different therapies produce different imaging endpoints that are predictive of outcome. For example, early response to inhibitors of intermediary metabolism may be appropriately characterised by a metabolite-based tracer such as ^{18}F-fluciclovine. Conversely, the proliferation tracer ^{18}F-fluorothymidine may provide different or additional information, particularly when such inhibitors are tested in combination with cytotoxic drugs or cell cycle inhibition.

Parallel to this, imaging biomarker development in the burgeoning field of cancer immunotherapy could be complemented with the use of ^{18}F-fluciclovine. Several radiotracers specific for immunotherapy markers have been described [152, 153], and it has been postulated that ^{18}F-fluciclovine may be able to selectively image T-cell modulation in the tumour microenvironment [154]. This is based on reports that unlike ^{18}F-FDG, which undergoes indiscriminate uptake following activation of either innate or

adaptive immune response components, fluciclovine uptake is specifically increased in activation of T- and B-cells, but not granulocytes and macrophages [130].

7.4 Characterising tumour biology with ^{18}F-fluciclovine: the tasks ahead

Accompanying the insights borne from pre-clinical investigations, correlation of imaging to tumour biology in the clinical setting is pivotal to guide translational work. During this project, the FRONTIER study was set up to gain insights into how ^{18}F-fluciclovine uptake can be used to characterise underlying biology of primary invasive ductal breast cancers.

To date, 35% recruitment has been achieved and the study will remain open beyond the timelines of this project. The data so far demonstrate that all tumours have increased ^{18}F-fluciclovine uptake, a testament to the increased amino acid demand in cancer. A trend of highest ^{18}F-fluciclovine uptake in TN, followed by ER+ then HER2+ tumours has emerged, complementing our *in vitro* results and that of another clinical study [115], published during the course of the project.

Initial metabolomic results from technical validation of a small subset of samples suggest positive correlations of ^{18}F-fluciclovine uptake with leucine and glutamate, metabolites instrinsic to several arms of aggressive tumour biology. With greater sample numbers, realising the significant opportunity for non-invasive interrogation of tumour behaviour linked to these pathways will

require integration of the data from rest of the metabolome, protein expression (optimised as part of the project), RNA-sequencing of the tumour transcriptome and imaging. With respect to imaging, the dynamic PET data will also be explored and may add an extra dimension with information on tracer influx and efflux, of direct relevance to the antiporter mechanism of ASCT2 and LAT1.

The resultant compendium of data should serve well in informing the application and interpretation of ^{18}F-fluciclovine in future clinical research and practice in this prevalent cancer.

REFERENCES

1. Shoup TM, Olson J, Hoffman JM, Votaw J, Eshima D, Eshima L, et al. Synthesis and evaluation of [18F]1-amino-3-fluorocyclobutane-1-carboxylic acid to image brain tumors. J Nucl Med. 1999;40(2):331-38.
2. Okudaira H, Shikano N, Nishii R, Miyagi T, Yoshimoto M, Kobayashi M, et al. Putative transport mechanism and intracellular fate of trans-1-amino-3-18F-fluorocyclobutanecarboxylic acid in human prostate cancer. J Nucl Med. 2011;52(5):822-29.
3. Sorensen J, Owenius R, Lax M, Johansson S. Regional distribution and kinetics of [18F]fluciclovine (anti-[18F]FACBC), a tracer of amino acid transport, in subjects with primary prostate cancer. Eur J Nucl Med Mol Imaging. 2013;40(3):394-402.
4. Oka S, Okudaira H, Yoshida Y, Schuster DM, Goodman MM, Shirakami Y. Transport mechanisms of trans-1-amino-3-fluoro[1-(14)C]cyclobutanecarboxylic acid in prostate cancer cells. Nucl Med Biol. 2012;39(1):109-19.
5. FDA approves new diagnostic imaging agent to detect recurrent prostate cancer. U.S. Food and Drug Administration website. Available from: https://www.fda.gov/NewsEvents/Newsroom/PressAnnouncements/ucm503920.htm. Accessed 19 May 2017.
6. CHMP summary of positive opinion for Axumin. European Medicines Agency website. Available from: http://www.ema.europa.eu/ema/index.jsp?curl=pages/medicines/human/medicines/004197/smops/Positive/human_smop_001110.jsp&mid=WC0b01ac058001d127. Accessed 19 May 2017.
7. Okudaira H, Nakanishi T, Oka S, Kobayashi M, Tamagami H, Schuster DM, et al. Kinetic analyses of trans-1-amino-3-[18F]fluorocyclobutanecarboxylic acid transport in Xenopus laevis oocytes expressing human ASCT2 and SNAT2. Nucl Med Biol. 2013;40(5):670-5.
8. Office for National S. Cancer Registration Statistics, England, 20162018 Contract No.: Report.
9. Cancer Research UK. Cancer Stats report - Prostate Cancer. 2016.
10. Punnen S, Cooperberg MR, D'Amico AV, Karakiewicz PI, Moul JW, Scher HI, et al. Management of biochemical recurrence after primary treatment of prostate cancer: a systematic review of the literature. Eur Urol. 2013;64(6):905-15.
11. Force USPST. Screening for prostate cancer: US preventive services task force recommendation statement. JAMA. 2018;319(18):1901-13.
12. Mottet N, Bellmunt J, Bolla M, Briers E, Cumberbatch MG, De Santis M, et al. EAU-ESTRO-SIOG guidelines on prostate cancer. Part 1: Screening, diagnosis, and local treatment with curative intent. Eur Urol. 2017;71(4):618-29.
13. Roach M, 3rd, Hanks G, Thames H, Jr., Schellhammer P, Shipley WU, Sokol GH, et al. Defining biochemical failure following radiotherapy with or without hormonal therapy in men with clinically localized prostate cancer:

recommendations of the RTOG-ASTRO Phoenix Consensus Conference. Int J Radiat Oncol Biol Phys. 2006;65(4):965-74.
14. National Institute for Clinical Excellence. Prostate cancer: diagnosis and treatment. NICE clinical guideline 175. 2014.
15. Heidenreich A, Bastian PJ, Bellmunt J, Bolla M, Joniau S, van der Kwast T, et al. EAU guidelines on prostate cancer. Part II: Treatment of advanced, relapsing, and castration-resistant prostate cancer. Eur Urol. 2014;65(2):467-79.
16. Rouviere O, Vitry T, Lyonnet D. Imaging of prostate cancer local recurrences: why and how? Eur Radiol. 2010;20(5):1254-66.
17. Beresford MJ, Gillatt D, Benson RJ, Ajithkumar T. A systematic review of the role of imaging before salvage radiotherapy for post-prostatectomy biochemical recurrence. Clin Oncol. 2010;22(1):46-55.
18. Kane CJ, Amling CL, Johnstone PA, Pak N, Lance RS, Thrasher JB, et al. Limited value of bone scintigraphy and computed tomography in assessing biochemical failure after radical prostatectomy. Urology. 2003;61(3):607-11.
19. McArthur C, McLaughlin G, Meddings RN. Changing the referral criteria for bone scan in newly diagnosed prostate cancer patients. Br J Radiol. 2012;85(1012):390-4.
20. Johnstone PA, Tarman GJ, Riffenburgh R, Rohde DC, Puckett ML, Kane CJ. Yield of imaging and scintigraphy assessing biochemical failure in prostate cancer patients. Urol Oncol. 1997;3(4):108-12.
21. Hovels AM, Heesakkers RA, Adang EM, Jager GJ, Strum S, Hoogeveen YL, et al. The diagnostic accuracy of CT and MRI in the staging of pelvic lymph nodes in patients with prostate cancer: a meta-analysis. Clin Radiol. 2008;63(4):387-95.
22. Powles T, Murray I, Brock C, Oliver T, Avril N. Molecular positron emission tomography and PET/CT imaging in urological malignancies. Eur Urol. 2007;51(6):1511-20; discussion 20-1.
23. Effert PJ, Bares R, Handt S, Wolff JM, Bull U, Jakse G. Metabolic imaging of untreated prostate cancer by positron emission tomography with 18fluorine-labeled deoxyglucose. J Urol. 1996;155(3):994-98.
24. Ramirez de Molina A, Rodriguez-Gonzalez A, Gutierrez R, Martinez-Pineiro L, Sanchez J, Bonilla F, et al. Overexpression of choline kinase is a frequent feature in human tumor-derived cell lines and in lung, prostate, and colorectal human cancers. Biochem Biophys Res Commun. 2002;296(3):580-83.
25. Haroon A, Zanoni L, Celli M, Zakavi R, Beheshti M, Langsteger W, et al. Multicenter study evaluating extraprostatic uptake of 11C-choline, 18F-methylcholine, and 18F-ethylcholine in male patients: physiological distribution, statistical differences, imaging pearls, and normal variants. Nucl Med Commun. 2015;36(11):1065-75.
26. Evangelista L, Cervino A, Burei M, Gregianin M, Saladini G, Marzola M, et al. Comparative studies of radiolabeled choline positron emission tomography, histology of primary tumor and other imaging modalities in prostate cancer: a systematic review and meta-analysis. Clin Transl Imaging. 2013;1(2):99-109.
27. von Eyben FE, Kairemo K. Meta-analysis of (11)C-choline and (18)F-choline PET/CT for management of patients with prostate cancer. Nucl Med Commun. 2014;35(3):221-30.

28. Giovacchini G, Picchio M, Briganti A, Cozzarini C, Scattoni V, Salonia A, et al. (11C)choline positron emission tomography/computerized tomography to restage prostate cancer cases with biochemical failure after radical prostatectomy and no disease evidence on conventional imaging. J Urol. 2010;184(3):938-43.
29. Ceci F, Herrmann K, Castellucci P, Graziani T, Bluemel C, Schiavina R, et al. Impact of C-choline PET/CT on clinical decision making in recurrent prostate cancer: results from a retrospective two-centre trial. Eur J Nucl Med Mol Imaging. 2014.
30. Schiavina R, Martorana G. The promise of choline-PET/CT in the detection of recurrent prostate cancer: what are the limits of our investigation? Eur Urol. 2013;63(5):797-99.
31. Evangelista L, Guttilla A, Zattoni F, Muzzio PC, Zattoni F. Utility of choline positron emission tomography/computed tomography for lymph node involvement identification in intermediate- to high-risk prostate cancer: a systematic literature review and meta-analysis. Eur Urol. 2013;63(6):1040-48.
32. Husarik DB, Miralbell R, Dubs M, John H, Giger OT, Gelet A, et al. Evaluation of [(18)F]-choline PET/CT for staging and restaging of prostate cancer. Eur J Nucl Med Mol Imaging. 2008;35(2):253-63.
33. Castellucci P, Fuccio C, Nanni C, Santi I, Rizzello A, Lodi F, et al. Influence of trigger PSA and PSA kinetics on 11C-Choline PET/CT detection rate in patients with biochemical relapse after radical prostatectomy. J Nucl Med. 2009;50(9):1394-400.
34. Rinnab L, Mottaghy FM, Simon J, Volkmer BG, de Petriconi R, Hautmann RE, et al. 11C]Choline PET/CT for targeted salvage lymph node dissection in patients with biochemical recurrence after primary curative therapy for prostate cancer. Preliminary results of a prospective study. Urol Int. 2008;81(2):191-97.
35. Sutinen E, Nurmi M, Roivainen A, Varpula M, Tolvanen T, Lehikoinen P, et al. Kinetics of [(11)C]choline uptake in prostate cancer: a PET study. Eur J Nucl Med Mol Imaging. 2004;31(3):317-24.
36. Schiavina R, Scattoni V, Castellucci P, Picchio M, Corti B, Briganti A, et al. 11C-choline positron emission tomography/computerized tomography for preoperative lymph-node staging in intermediate-risk and high-risk prostate cancer: comparison with clinical staging nomograms. Eur Urol. 2008;54(2):392-401.
37. Beheshti M, Imamovic L, Broinger G, Vali R, Waldenberger P, Stoiber F, et al. 18F choline PET/CT in the preoperative staging of prostate cancer in patients with intermediate or high risk of extracapsular disease: a prospective study of 130 patients. Radiology. 2010;254(3):925-33.
38. Juweid ME, Cheson BD. Positron-emission tomography and assessment of cancer therapy. N Engl J Med. 2006;354(5):496-507.
39. Beheshti M, Vali R, Waldenberger P, Fitz F, Nader M, Hammer J, et al. The use of F-18 choline PET in the assessment of bone metastases in prostate cancer: correlation with morphological changes on CT. Mol Imaging Biol. 2009;11(6):446-54.
40. Murphy RC, Kawashima A, Peller PJ. The utility of 11C-choline PET/CT for imaging prostate cancer: a pictorial guide. AJR Am J Roentgenol. 2011;196(6):1390-98.

41. Schillaci O, Calabria F, Tavolozza M, Ciccio C, Carlani M, Caracciolo CR, et al. 18F-choline PET/CT physiological distribution and pitfalls in image interpretation: experience in 80 patients with prostate cancer. Nucl Med Commun. 2010;31(1):39-45.
42. Stephenson AJ, Scardino PT, Kattan MW, Pisansky TM, Slawin KM, Klein EA, et al. Predicting the outcome of salvage radiation therapy for recurrent prostate cancer after radical prostatectomy. J Clin Oncol. 2007;25(15):2035-41.
43. Rigatti P, Suardi N, Briganti A, Da Pozzo LF, Tutolo M, Villa L, et al. Pelvic/retroperitoneal salvage lymph node dissection for patients treated with radical prostatectomy with biochemical recurrence and nodal recurrence detected by [11C]choline positron emission tomography/computed tomography. Eur Urol. 2011;60(5):935-43.
44. Jilg CA, Rischke HC, Reske SN, Henne K, Grosu AL, Weber W, et al. Salvage lymph node dissection with adjuvant radiotherapy for nodal recurrence of prostate cancer. J Urol. 2012;188(6):2190-97.
45. Alongi F, Fogliata A, Clerici E, Navarria P, Tozzi A, Comito T, et al. Volumetric modulated arc therapy with flattening filter free beams for isolated abdominal/pelvic lymph nodes: report of dosimetric and early clinical results in oligometastatic patients. Radiat Oncol. 2012;7:204-717X-7-204.
46. Berkovic P, De Meerleer G, Delrue L, Lambert B, Fonteyne V, Lumen N, et al. Salvage stereotactic body radiotherapy for patients with limited prostate cancer metastases: deferring androgen deprivation therapy. Clin Genitourin Cancer. 2013;11(1):27-32.
47. Jereczek-Fossa BA, Beltramo G, Fariselli L, Fodor C, Santoro L, Vavassori A, et al. Robotic image-guided stereotactic radiotherapy, for isolated recurrent primary, lymph node or metastatic prostate cancer. Int J Radiat Oncol Biol Phys. 2012;82(2):889-97.
48. Petrylak DP. Risk Factors for the Development of Bone Metastases in Prostate Cancer. Eur Urol Suppl. 2007;6(11):677-82.
49. Schuster DM, Votaw JR, Nieh PT, Yu W, Nye JA, Master V, et al. Initial experience with the radiotracer anti-1-amino-3-18F-fluorocyclobutane-1-carboxylic acid with PET/CT in prostate carcinoma. J Nucl Med. 2007;48(1):56-63.
50. Osborne JR, Akhtar NH, Vallabhajosula S, Anand A, Deh K, Tagawa ST. Prostate-specific membrane antigen-based imaging. Urol Oncol. 2013;31(2):144-54.
51. Schuster DM, Nieh PT, Jani AB, Amzat R, Bowman FD, Halkar RK, et al. Anti-3-[(18)F]FACBC positron emission tomography-computerized tomography and (111)In-capromab pendetide single photon emission computerized tomography-computerized tomography for recurrent prostate carcinoma: results of a prospective clinical trial. J Urol. 2014;191(5):1446-53.
52. Nanni C, Schiavina R, Brunocilla E, Boschi S, Borghesi M, Zanoni L, et al. 18F-Fluciclovine PET/CT for the detection of prostate cancer relapse: a comparison to 11C-choline PET/CT. Clin Nucl Med. 2015;40(8):e386-91.
53. Nanni C, Schiavina R, Brunocilla E, Borghesi M, Ambrosini V, Zanoni L, et al. 18F-FACBC compared with 11C-choline PET/CT in patients with biochemical relapse after radical prostatectomy: a prospective study in 28 patients. Clin Genitourin Cancer. 2014;12(2):106-10.

54. Pano B, Sebastia C, Bunesch L, Mestres J, Salvador R, Macias NG, et al. Pathways of lymphatic spread in male urogenital pelvic malignancies. Radiographics. 2011;31(1):135-60.
55. Teoh EJ, McGowan DR, Bradley KM, Belcher E, Black E, Gleeson FV. Novel penalised likelihood reconstruction of PET in the assessment of histologically verified small pulmonary nodules. Eur Radiol. 2016;26(2):576-84.
56. Adams MC, Turkington TG, Wilson JM, Wong TZ. A systematic review of the factors affecting accuracy of SUV measurements. AJR Am J Roentgenol. 2010;195(2):310-20.
57. Tong S, Alessio AM, Kinahan PE. Image reconstruction for PET/CT scanners: past achievements and future challenges. Imaging Med. 2010;2(5):529-45.
58. Alessio AM, Stearns CW, Tong S, Ross SG, Kohlmyer S, Ganin A, et al. Application and evaluation of a measured spatially variant system model for PET image reconstruction. IEEE Trans Med Imaging. 2010;29(3):938-49.
59. Teoh EJ, McGowan DR, Macpherson RE, Bradley KM, Gleeson FV. Phantom and clinical evaluation of the Bayesian penalized likelihood reconstruction algorithm Q.Clear on an LYSO PET/CT system. J Nucl Med. 2015;56(9):1447-52.
60. Teoh EJ, McGowan DR, Bradley KM, Belcher E, Black E, Moore A, et al. 18F-FDG PET/CT assessment of histopathologically confirmed mediastinal lymph nodes in non-small cell lung cancer using a penalised likelihood reconstruction. Eur Radiol. 2016;26(11):4098-106.
61. Parvizi N, Franklin JM, McGowan DR, Teoh EJ, Bradley KM, Gleeson FV. Does a novel penalized likelihood reconstruction of 18F-FDG PET-CT improve signal-to-background in colorectal liver metastases? Eur J Radiol. 2015;84(10):1873-8.
62. Rowley LM, Bradley KM, Boardman P, Hallam A, McGowan DR. Optimization of image reconstruction for 90Y selective internal radiotherapy on a lutetium yttrium orthosilicate PET/CT System using a Bayesian penalized likelihood reconstruction algorithm. J Nucl Med. 2017;58(4):658-64.
63. Cancer registration statistics, England ... : newly registered cases of cancer by type (area of the body affected), sex, age and regional variations.
64. Cancer Research UK. Breast cancer incidence (invasive) statistics. Available from: http://www.cancerresearchuk.org/health-professional/cancer-statistics/statistics-by-cancer-type/breast-cancer/incidence-invasive. Accessed 23 December 2017.
65. Cancer Research UK. Breast cancer survival statistics. Available from: http://www.cancerresearchuk.org/health-professional/cancer-statistics/statistics-by-cancer-type/breast-cancer/survival. Accessed 23 December 2017.
66. Cancer Research UK. Breast cancer statistics. Available from: https://www.cancerresearchuk.org/health-professional/cancer-statistics/statistics-by-cancer-type/breast-cancer. Accessed 23 December 2017.
67. Colleoni M, Sun Z, Price KN, Karlsson P, Forbes JF, Thurlimann B, et al. Annual hazard rates of recurrence for breast cancer during 24 years of follow-up: results from the International Breast Cancer Study Group trials I to V. J Clin Oncol. 2016;34(9):927-35.

68. Furuya M, Horiguchi J, Nakajima H, Kanai Y, Oyama T. Correlation of L-type amino acid transporter 1 and CD98 expression with triple negative breast cancer prognosis. Cancer Sci. 2012;103(2):382-89.
69. Liang Z, Cho HT, Williams L, Zhu A, Liang K, Huang K, et al. Potential biomarker of L-type amino acid transporter 1 in breast cancer progression. Nucl Med Biol. 2011;45(2):93-102.
70. Kaira K, Oriuchi N, Imai H, Shimizu K, Yanagitani N, Sunaga N, et al. l-type amino acid transporter 1 and CD98 expression in primary and metastatic sites of human neoplasms. Cancer Sci. 2008;99(12):2380-86.
71. Shennan DB, Thomson J, Gow IF, Travers MT, Barber MC. L-leucine transport in human breast cancer cells (MCF-7 and MDA-MB-231): kinetics, regulation by estrogen and molecular identity of the transporter. Biochim Biophys Acta. 2004;1664(2):206-16.
72. Shennan DB, Thomson J. Inhibition of system L (LAT1/CD98hc) reduces the growth of cultured human breast cancer cells. Oncol Rep. 2008;20(4):885-89.
73. Soulez M, Parker MG. Identification of novel oestrogen receptor target genes in human ZR75-1 breast cancer cells by expression profiling. J Mol Endocrinol. 2001;27(3):259-74.
74. Mihaly Z, Kormos M, Lanczky A, Dank M, Budczies J, Szasz MA, et al. A meta-analysis of gene expression-based biomarkers predicting outcome after tamoxifen treatment in breast cancer. Breast Cancer Res Treat. 2013;140(2):219-32.
75. Ring BZ, Seitz RS, Beck R, Shasteen WJ, Tarr SM, Cheang MC, et al. Novel prognostic immunohistochemical biomarker panel for estrogen receptor-positive breast cancer. J Clin Oncol. 2006;24(19):3039-47.
76. Ross DT, Kim CY, Tang G, Bohn OL, Beck RA, Ring BZ, et al. Chemosensitivity and stratification by a five monoclonal antibody immunohistochemistry test in the NSABP B14 and B20 trials. Clin Cancer Res. 2008;14(20):6602-09.
77. Hosios AM, Hecht VC, Danai LV, Johnson MO, Rathmell JC, Steinhauser ML, et al. Amino acids rather than glucose account for the majority of cell mass in proliferating mammalian cells. Dev Cell. 2016;36(5):540-9.
78. Moreadith RW, Lehninger AL. The pathways of glutamate and glutamine oxidation by tumor cell mitochondria. Role of mitochondrial NAD(P)+-dependent malic enzyme. J Biol Chem. 1984;259(10):6215-21.
79. Altman BJ, Stine ZE, Dang CV. From Krebs to clinic: glutamine metabolism to cancer therapy. Nat Rev Cancer. 2016;16(10):619-34.
80. Lane AN, Fan TW. Regulation of mammalian nucleotide metabolism and biosynthesis. Nucleic Acids Res. 2015;43(4):2466-85.
81. White MA, Lin C, Rajapakshe K, Dong J, Shi Y, Tsouko E, et al. Glutamine transporters are targets of multiple oncogenic signaling pathways in prostate cancer. Mol Cancer Res. 2017;15(8):1017-28.
82. Wise DR, DeBerardinis RJ, Mancuso A, Sayed N, Zhang XY, Pfeiffer HK, et al. Myc regulates a transcriptional program that stimulates mitochondrial glutaminolysis and leads to glutamine addiction. Proc Natl Acad Sci U S A. 2008;105(48):18782-7.

83. Gao P, Tchernyshyov I, Chang TC, Lee YS, Kita K, Ochi T, et al. c-Myc suppression of miR-23a/b enhances mitochondrial glutaminase expression and glutamine metabolism. Nature. 2009;458(7239):762-5.
84. van Geldermalsen M, Wang Q, Nagarajah R, Marshall AD, Thoeng A, Gao D, et al. ASCT2/SLC1A5 controls glutamine uptake and tumour growth in triple-negative basal-like breast cancer. Oncogene. 2016;35(24):3201-8.
85. Bensaad K, Harris AL. Cancer metabolism as a therapeutic target: metabolic synthetic lethality. Oncology. 2013;27(5):467, 73-4.
86. Hassanein M, Hoeksema MD, Shiota M, Qian J, Harris BK, Chen H, et al. SLC1A5 mediates glutamine transport required for lung cancer cell growth and survival. Clin Cancer Res. 2013;19(3):560-70.
87. Wang Q, Beaumont KA, Otte NJ, Font J, Bailey CG, van Geldermalsen M, et al. Targeting glutamine transport to suppress melanoma cell growth. International journal of cancer. 2014;135(5):1060-71.
88. Gross MI, Demo SD, Dennison JB, Chen L, Chernov-Rogan T, Goyal B, et al. Antitumor activity of the glutaminase inhibitor CB-839 in triple-negative breast cancer. Mol Cancer Ther. 2014;13(4):890-901.
89. Xiang Y, Stine ZE, Xia J, Lu Y, O'Connor RS, Altman BJ, et al. Targeted inhibition of tumor-specific glutaminase diminishes cell-autonomous tumorigenesis. J Clin Invest. 2015;125(6):2293-306.
90. Ayyagari VN, Brard L. Bithionol inhibits ovarian cancer cell growth in vitro - studies on mechanism(s) of action. BMC Cancer. 2014;14:61.
91. Jin L, Li D, Alesi GN, Fan J, Kang HB, Lu Z, et al. Glutamate dehydrogenase 1 signals through antioxidant glutathione peroxidase 1 to regulate redox homeostasis and tumor growth. Cancer Cell. 2015;27(2):257-70.
92. Braddock D. Small molecule inhibitors of autotaxin and methods of use. Google Patents; 2011.
93. Nicklin P, Bergman P, Zhang B, Triantafellow E, Wang H, Nyfeler B, et al. Bidirectional transport of amino acids regulates mTOR and autophagy. Cell. 2009;136(3):521-34.
94. Vicier C, Dieci MV, Arnedos M, Delaloge S, Viens P, Andre F. Clinical development of mTOR inhibitors in breast cancer. Breast Cancer Res. 2014;16(1):203.
95. Qiu GZ, Jin MZ, Dai JX, Sun W, Feng JH, Jin WL. Reprogramming of the tumor in the hypoxic niche: the emerging concept and associated therapeutic strategies. Trends Pharmacol Sci. 2017;38(8):669-86.
96. Schito L, Semenza GL. Hypoxia-inducible factors: master regulators of cancer progression. Trends Cancer. 2016;2(12):758-70.
97. Soh H, Wasa M, Fukuzawa M. Hypoxia upregulates amino acid transport in a human neuroblastoma cell line. J Pediatr Surg. 2007;42(4):608-12.
98. Elorza A, Soro-Arnaiz I, Melendez-Rodriguez F, Rodriguez-Vaello V, Marsboom G, de Carcer G, et al. HIF2alpha acts as an mTORC1 activator through the amino acid carrier SLC7A5. Mol Cell. 2012;48(5):681-91.
99. von Minckwitz G, Blohmer JU, Costa SD, Denkert C, Eidtmann H, Eiermann W, et al. Response-guided neoadjuvant chemotherapy for breast cancer. J Clin Oncol. 2013;31(29):3623-30.
100. Coudert B, Pierga JY, Mouret-Reynier MA, Kerrou K, Ferrero JM, Petit T, et al. Use of [(18)F]-FDG PET to predict response to neoadjuvant

trastuzumab and docetaxel in patients with HER2-positive breast cancer, and addition of bevacizumab to neoadjuvant trastuzumab and docetaxel in [(18)F]-FDG PET-predicted non-responders (AVATAXHER): an open-label, randomised phase 2 trial. Lancet Oncol. 2014;15(13):1493-502.
101. Smith IC, Heys SD, Hutcheon AW, Miller ID, Payne S, Gilbert FJ, et al. Neoadjuvant chemotherapy in breast cancer: significantly enhanced response with docetaxel. J Clin Oncol. 2002;20(6):1456-66.
102. Mghanga FP, Lan X, Bakari KH, Li C, Zhang Y. Fluorine-18 fluorodeoxyglucose positron emission tomography-computed tomography in monitoring the response of breast cancer to neoadjuvant chemotherapy: a meta-analysis. Clin Breast Cancer. 2013;13(4):271-79.
103. Humbert O, Berriolo-Riedinger A, Riedinger JM, Coudert B, Arnould L, Cochet A, et al. Changes in 18F-FDG tumor metabolism after a first course of neoadjuvant chemotherapy in breast cancer: influence of tumor subtypes. Ann Oncol. 2012;23(10):2572-77.
104. Keam B, Im SA, Koh Y, Han SW, Oh DY, Cho N, et al. Early metabolic response using FDG PET/CT and molecular phenotypes of breast cancer treated with neoadjuvant chemotherapy. BMC cancer. 2011;11:452-2407-11-452.
105. Schwarz-Dose J, Untch M, Tiling R, Sassen S, Mahner S, Kahlert S, et al. Monitoring primary systemic therapy of large and locally advanced breast cancer by using sequential positron emission tomography imaging with [18F]fluorodeoxyglucose. J Clin Oncol. 2009;27(4):535-41.
106. Humbert O, Cochet A, Coudert B, Berriolo-Riedinger A, Kanoun S, Brunotte F, et al. Role of positron emission tomography for the monitoring of response to therapy in breast cancer. Oncologist. 2015;20(2):94-104.
107. Groheux D, Majdoub M, Sanna A, de Cremoux P, Hindie E, Giacchetti S, et al. Early metabolic response to neoadjuvant treatment: FDG PET/CT criteria according to breast cancer subtype. Radiology. 2015:141638.
108. Koolen BB, Pengel KE, Wesseling J, Vogel WV, Vrancken Peeters MJ, Vincent AD, et al. FDG PET/CT during neoadjuvant chemotherapy may predict response in ER-positive/HER2-negative and triple negative, but not in HER2-positive breast cancer. Breast. 2013;22(5):691-97.
109. Groheux D, Giacchetti S, Hatt M, Marty M, Vercellino L, de Roquancourt A, et al. HER2-overexpressing breast cancer: FDG uptake after two cycles of chemotherapy predicts the outcome of neoadjuvant treatment. Br J Cancer. 2013;109(5):1157-64.
110. Smith TA, Appleyard MV, Sharp S, Fleming IN, Murray K, Thompson AM. Response to trastuzumab by HER2 expressing breast tumour xenografts is accompanied by decreased Hexokinase II, glut1 and [18F]-FDG incorporation and changes in 31P-NMR-detectable phosphomonoesters. Cancer Chemother Pharmacol. 2013;71(2):473-80.
111. Oka S, Kanagawa M, Doi Y, Schuster DM, Goodman MM, Yoshimura H. PET tracer 18F-fluciclovine can detect histologically proven bone metastatic lesions: a preclinical study in rat osteolytic and osteoblastic bone metastasis models. Theranostics. 2017;7(7):2048-64.
112. Ulaner GA, Goldman D, Gonen M, Pham H, Castillo R, Lyashchenko S, et al. Initial results of a prospective clinical trial of 18F-Fluciclovine PET/CT in newly diagnosed invasive ductal and invasive lobular breast cancers. J Nucl Med. 2016.

113. Hogan MP, Goldman DA, Dashevsky B, Riedl CC, Gonen M, Osborne JR, et al. Comparison of 18F-FDG PET/CT for systemic staging of newly diagnosed invasive lobular carcinoma versus invasive ductal carcinoma. J Nucl Med. 2015;56(11):1674-80.
114. Ulaner GA, Goldman DA, Corben A, Lyashchenko SK, Gonen M, Lewis JS, et al. Prospective clinical trial of 18F-fluciclovine PET/CT for determining the response to neoadjuvant therapy in invasive ductal and invasive lobular breast cancers. J Nucl Med. 2017;58(7):1037-42.
115. Tade FI, Cohen MA, Styblo TM, Odewole OA, Holbrook AI, Newell MS, et al. Anti-3-18F-FACBC (18F-Fluciclovine) PET/CT of breast cancer: an exploratory study. J Nucl Med. 2016;57(9):1357-63.
116. McConathy J, Voll RJ, Yu W, Crowe RJ, Goodman MM. Improved synthesis of anti-[18F]FACBC: improved preparation of labeling precursor and automated radiosynthesis. Appl Radiat Isot. 2003;58(6):657-66.
117. Mackay GM, Zheng L, van den Broek NJ, Gottlieb E. Analysis of cell metabolism using LC-MS and isotope tracers. Methods Enzymol. 2015;561:171-96.
118. Lord SR. 'Effect of metformin on breast cancer metabolism', DPhil thesis. University of Oxford, Oxford, UK, 2014.
119. Teoh E, Bottomley D, Scarsbrook A, Payne H, Afaq A, Bomanji J, et al. Impact of 18F-fluciclovine PET/CT on clinical management of patients with recurrent prostate cancer: results from the phase 3 FALCON trial. Int J Radiat Oncol Biol Phys. 2017;99(5):1316-17.
120. Rajasekaran AK, Anilkumar G, Christiansen JJ. Is prostate-specific membrane antigen a multifunctional protein? Am J Physiol Cell Physiol. 2005;288(5):C975-81.
121. Castanares MA, Mukherjee A, Chowdhury WH, Liu M, Chen Y, Mease RC, et al. Evaluation of prostate-specific membrane antigen as an imaging reporter. J Nucl Med. 2014;55(5):805-11.
122. Fendler WP, Eiber M, Beheshti M, Bomanji J, Ceci F, Cho S, et al. (68)Ga-PSMA PET/CT: Joint EANM and SNMMI procedure guideline for prostate cancer imaging: version 1.0. Eur J Nucl Med Mol Imaging. 2017;44(6):1014-24.
123. Szabo Z, Mena E, Rowe SP, Plyku D, Nidal R, Eisenberger MA, et al. Initial evaluation of [(18)F]DCFPyL for prostate-specific membrane antigen (PSMA)-targeted PET imaging of prostate cancer. Mol Imaging Biol. 2015;17(4):565-74.
124. Kesch C, Vinsensia M, Radtke JP, Schlemmer HP, Heller M, Ellert E, et al. Intraindividual comparison of (18)F-PSMA-1007 PET/CT, multiparametric MRI, and radical prostatectomy specimens in patients with primary prostate cancer: a retrospective, proof-of-concept study. J Nucl Med. 2017;58(11):1805-10.
125. Perera M, Papa N, Christidis D, Wetherell D, Hofman MS, Murphy DG, et al. Sensitivity, specificity, and predictors of positive (68)Ga-prostate-specific membrane antigen positron emission tomography in advanced prostate cancer: a systematic review and meta-analysis. Eur Urol. 2016;70(6):926-37.
126. Bach-Gansmo T, Nanni C, Nieh PT, Zanoni L, Bogsrud TV, Sletten H, et al. Multisite experience of the safety, detection rate and diagnostic performance of fluciclovine (18F) positron emission tomography/computerized

tomography imaging in the staging of biochemically recurrent prostate cancer. J Urol. 2017;197(3 Pt 1):676-83.
127. Roach PJ, Francis R, Emmett L, Hsiao E, Kneebone A, Hruby G, et al. The impact of (68)Ga-PSMA PET/CT on management intent in prostate cancer: results of an Australian prospective multicenter study. J Nucl Med. 2017.
128. Teoh EJ, McGowan DR, Schuster DM, Tsakok MT, Gleeson FV, Bradley KM. Bayesian penalised likelihood reconstruction (Q.Clear) of (18)F-fluciclovine PET for imaging of recurrent prostate cancer: semi-quantitative and clinical evaluation. Br J Radiol. 2018:20170727.
129. Miller MP, Kostakoglu L, Pryma D, Yu JQ, Chau A, Perlman E, et al. Reader training for the re-staging of biochemically recurrent prostate cancer using fluciclovine (18F) PET/CT. J Nucl Med. 2017.
130. Oka S, Okudaira H, Ono M, Schuster DM, Goodman MM, Kawai K, et al. Differences in transport mechanisms of trans-1-amino-3-[18F]fluorocyclobutanecarboxylic acid in inflammation, prostate cancer, and glioma cells: comparison with L-[methyl-11C]methionine and 2-deoxy-2-[18F]fluoro-D-glucose. Mol Imaging Biol. 2014;16(3):322-9.
131. Amzat R, Taleghani P, Miller DL, Beitler JJ, Bellamy LM, Nye JA, et al. Pilot study of the utility of the synthetic PET amino-acid radiotracer anti-1-amino-3-[(18)F]fluorocyclobutane-1-carboxylic acid for the noninvasive imaging of pulmonary lesions. Mol Imaging Biol. 2013;15(5):633-43.
132. Isohashi K, Shimosegawa E, Kato H, Kanai Y, Naka S, Fujino K, et al. Optimization of [11C]methionine PET study: appropriate scan timing and effect of plasma amino acid concentrations on the SUV. EJNMMI Res. 2013;3(1):27.
133. Stegink LD, Filer LJ, Jr., Brummel MC, Baker GL, Krause WL, Bell EF, et al. Plasma amino acid concentrations and amino acid ratios in normal adults and adults heterozygous for phenylketonuria ingesting a hamburger and milk shake meal. Am J Clin Nutr. 1991;53(3):670-5.
134. Ito H, Hatazawa J, Murakami M, Miura S, Iida H, Bloomfield PM, et al. Aging effect on neutral amino acid transport at the blood-brain barrier measured with L-[2-18F]-fluorophenylalanine and PET. J Nucl Med. 1995;36(7):1232-7.
135. Lahoutte T, Caveliers V, Camargo SM, Franca R, Ramadan T, Veljkovic E, et al. SPECT and PET amino acid tracer influx via system L (h4F2hc-hLAT1) and its transstimulation. J Nucl Med. 2004;45(9):1591-6.
136. Zhou R, Pantel AR, Li S, Lieberman BP, Ploessl K, Choi H, et al. [(18)F](2S,4R)4-Fluoroglutamine PET detects glutamine pool size changes in triple-negative breast cancer in response to glutaminase inhibition. Cancer Res. 2017;77(6):1476-84.
137. Lord S, Liu D, Cheng W-C, Haider S, Gaude E, Teoh E, et al. Metformin increases 18F-FDG flux and inhibits fatty acid oxidation at clinical doses in breast cancer: Results of a phase 0 clinical trial. Eur J Surg Oncol. 2016;42(11):S230.
138. Javeshghani S, Zakikhani M, Austin S, Bazile M, Blouin MJ, Topisirovic I, et al. Carbon source and myc expression influence the antiproliferative actions of metformin. Cancer Res. 2012;72(23):6257-67.

139. Wang Q, Hardie RA, Hoy AJ, van Geldermalsen M, Gao D, Fazli L, et al. Targeting ASCT2-mediated glutamine uptake blocks prostate cancer growth and tumour development. J Pathol. 2015;236(3):278-89.
140. Kasai N, Sasakawa A, Hosomi K, Poh TW, Chua BL, Yong WP, et al. Anti-tumor efficacy evaluation of a novel monoclonal antibody targeting neutral amino acid transporter ASCT2 using patient-derived xenograft mouse models of gastric cancer. Am J Transl Res. 2017;9(7):3399-410.
141. Marshall AD, van Geldermalsen M, Otte NJ, Lum T, Vellozzi M, Thoeng A, et al. ASCT2 regulates glutamine uptake and cell growth in endometrial carcinoma. Oncogenesis. 2017;6(7):e367.
142. Oka S, Kanagawa M, Doi Y, Schuster DM, Goodman MM, Yoshimura H. Fasting enhances the contrast of bone metastatic lesions in (18)F-fluciclovine-pet: preclinical study using a rat model of mixed osteolytic/osteoblastic bone metastases. Int J Mol Sci. 2017;18(5).
143. Shotwell MA, Jayme DW, Kilberg MS, Oxender DL. Neutral amino acid transport systems in Chinese hamster ovary cells. J Biol Chem. 1981;256(11):5422-7.
144. Mackenzie B, Erickson JD. Sodium-coupled neutral amino acid (System N/A) transporters of the SLC38 gene family. Pflugers Arch. 2004;447(5):784-95.
145. Dang CV. MYC, microRNAs and glutamine addiction in cancers. Cell Cycle. 2009;8(20):3243-5.
146. Miller TW, Balko JM, Ghazoui Z, Dunbier A, Anderson H, Dowsett M, et al. A gene expression signature from human breast cancer cells with acquired hormone independence identifies MYC as a mediator of antiestrogen resistance. Clin Cancer Res. 2011;17(7):2024-34.
147. Shajahan-Haq AN, Cook KL, Schwartz-Roberts JL, Eltayeb AE, Demas DM, Warri AM, et al. MYC regulates the unfolded protein response and glucose and glutamine uptake in endocrine resistant breast cancer. Mol Cancer. 2014;13:239.
148. Wahl RL, Jacene H, Kasamon Y, Lodge MA. From RECIST to PERCIST: Evolving Considerations for PET response criteria in solid tumors. J Nucl Med. 2009;50 Suppl 1:122S-50S.
149. Kato Y, Ozawa S, Miyamoto C, Maehata Y, Suzuki A, Maeda T, et al. Acidic extracellular microenvironment and cancer. Cancer Cell Int. 2013;13(1):89.
150. Wang S, Tsun ZY, Wolfson RL, Shen K, Wyant GA, Plovanich ME, et al. Metabolism. Lysosomal amino acid transporter SLC38A9 signals arginine sufficiency to mTORC1. Science. 2015;347(6218):188-94.
151. Barter SB, P. Recommendations for cross-sectional imaging in cancer management, Second edition. London: The Royal College of Radiologists, 2014.
152. Chatterjee S, Lesniak WG, Gabrielson M, Lisok A, Wharram B, Sysa-Shah P, et al. A humanized antibody for imaging immune checkpoint ligand PD-L1 expression in tumors. Oncotarget. 2016;7(9):10215-27.
153. Gonzalez Trotter DE, Meng X, McQuade P, Rubins D, Klimas M, Zeng Z, et al. In vivo imaging of the programmed death ligand 1 by (18)F PET. J Nucl Med. 2017;58(11):1852-57.

154. Teoh EJ, Tsakok MT, Bradley KM, Hyde K, Subesinghe M, Gleeson FV. Recurrent malignant melanoma detected on 18F-fluciclovine PET/CT imaging for prostate cancer. Clin Nucl Med. 2017;42(10):803-04.